AD-A181 316 PHYSICAL CHEMISTRY OF ENERGETIC NITRIDES(U) DENVER UNIV 1/1
COLO DEPT OF CHEMISTRY R D COOMBE 28 MAY 87
AFOSR-TR-87-0773 AFOSR-84-0031

UNCLASSIFIED F/G 7/4 NL

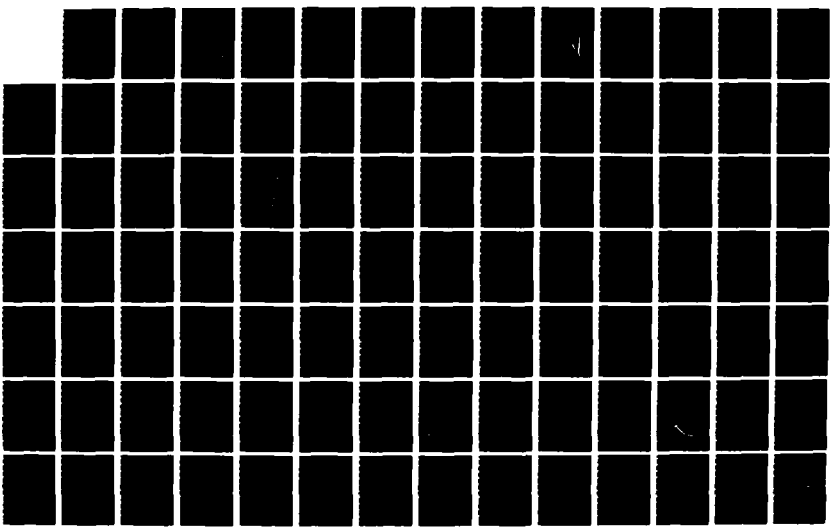

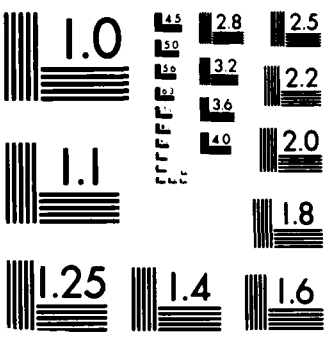
1.0
1.1
1.25
1.4
1.6
1.8
2.0
2.2
2.5
2.8
3.2
3.6
4.0
4.5
5.0
5.6
6.3

UNCLASSIFIED

ECURITY CLASSIFICATION OF THIS PAGE

REPORT DOCUMENTATION PAGE

1a. REPORT SECURITY CLASSIFICATION: Unclassified	1b. RESTRICTIVE MARKINGS
2a. SECURITY CLASSIFICATION AUTHORITY	3. DISTRIBUTION/AVAILABILITY OF REPORT: Approved for public release; Distribution unlimited
2b. DECLASSIFICATION/DOWNGRADING SCHEDULE	
4. PERFORMING ORGANIZATION REPORT NUMBER(S)	5. MONITORING ORGANIZATION REPORT NUMBER(S): AFOSR-TR 87-0773

6a. NAME OF PERFORMING ORGANIZATION: Department of Chemistry, University of Denver	6b. OFFICE SYMBOL (If applicable): CH	7a. NAME OF MONITORING ORGANIZATION: AFOSR/NC
6c. ADDRESS (City, State and ZIP Code): Denver, Colorado 80208		7b. ADDRESS (City, State and ZIP Code): Bolling Air Force Base DC, 20332 Bldg 410
8a. NAME OF FUNDING/SPONSORING ORGANIZATION: AFOSR	8b. OFFICE SYMBOL (If applicable): NC	9. PROCUREMENT INSTRUMENT IDENTIFICATION NUMBER: AFOSR-84-0031
8c. ADDRESS (City, State and ZIP Code): Building 410 Bolling AFB DC 20332		10. SOURCE OF FUNDING NOS.

PROGRAM ELEMENT NO.	PROJECT NO.	TASK NO.	WORK UNIT NO.
61102F	2303	B1	

11. TITLE (Include Security Classification): Physical Chemistry of Energetic Nitrides

12. PERSONAL AUTHOR(S): Coombe, Robert D.

13a. TYPE OF REPORT	13b. TIME COVERED	14. DATE OF REPORT (Yr., Mo., Day)	15. PAGE COUNT
Final report	FROM 83 Nov 1 TO 87 Ap 30		94

16. SUPPLEMENTARY NOTATION

17. COSATI CODES			18. SUBJECT TERMS (Continue on reverse if necessary and identify by block number)
FIELD	GROUP	SUB. GR.	azides, isocyanates, amines, nitrenes, metastables, photodissociation, reactions, excited states, lasers.

19. ABSTRACT (Continue on reverse if necessary and identify by block number)

This program has addressed a number of aspects of the chemistry of energetic nitrogen-based compounds. Topics investigated include the photochemistry of halogen isocyanates and halogen amines, radiative and collisional relaxation processes in electronically excited halogen nitrenes, the mechanisms of collisional decomposition of halogen azides, and the production of excited metastable nitrogen molecules (in azide-based reactions) for the collisional excitation of laser candidate species. The data obtained offer insight into the storage of energy in metastable halogen azides, halogen isocyanates, and halogen amines, and the mechanisms by which this energy is released when these molecules are stimulated by photolysis or undergo chemical reactions.

(Keywords!)

20. DISTRIBUTION/AVAILABILITY OF ABSTRACT	21. ABSTRACT SECURITY CLASSIFICATION
UNCLASSIFIED/UNLIMITED ☒ SAME AS RPT. ☐ DTIC USERS ☐	Unclassified

22a. NAME OF RESPONSIBLE INDIVIDUAL	22b. TELEPHONE NUMBER (Include Area Code)	22c. OFFICE SYMBOL
Wodarczyk, F.J.	(202)-767-4963	NC

DD FORM 1473, 83 APR EDITION OF 1 JAN 73 IS OBSOLETE

AFOSR-TR- 87-0773

CONTENTS

I INTRODUCTION

Energetic nitrogen-based compounds have fascinated chemists for centuries. The ability of these molecules to liberate large amounts of energy (explosively or otherwise) has generally been assumed to be linked tc the eventual production of molecular nitrogen, although detailed mechanisms for the energy release have been rarely (if ever) determined. Typical information found in the literature is often limited to classical thermodynamic properties, explosion limits, and similar parameters. It has become apparent in recent years, however, that more thorough analysis of the pathways for energy flow in these systems is required by the needs of both the scientific community and the department of defense. This understanding must rest on detailed knowledge of decomposition mechanisms stimulated by various methods of initiation. For compounds with small numbers of atoms, the individual reactions involved in the energy release are often strongly constrained (e.g., by spin and orbital angular momentum correlations) to generate excited products. Because these reactions are constrained, they may hold promise as mechanisms for either energy storage in or pumping of new UV-visible laser systems. Finally, since the molecules decompose to nitrogen-based fragments, their chemistry is often useful in understanding energetic phenomena in the atmosphere.

This document reports information obtained from the program "Physical Chemistry of Energetic Nitrides" (AFOSR grant No. AFOSR-84-0031), which has addressed a number of these specific needs. The program has focussed mainly on the chemistry of metastable halogen azides, halogen isocyanates, and halogen amines. Such small nitrogen-halogen species are of particular interest because (1) they are metastables which carry very large amounts

of energy, and (2) the radical fragments, in particular N_3, NCO, and NX_2 radicals, undergo reactions which are strongly constrained to generate excited metastable products.

The metastability of halogen azides and halogen isocyanates arises from the perturbation of the π electron cloud of the N_3 or NCO chain by the filled p atomic orbitals of the halogen atom, whose directional character enhances this interaction. The molecules are thus "energized" to the extent that they are metastable with respect to dissociation to $NX+N_2$ (or NX+CO), and in some cases with respect to dissociation to N_3+X.[1,2,3] We have investigated the means by which this stored energy is released when these species are photodissociated or they undergo reaction with atoms or radicals.

Photochemical excitation of the singlet ground states of the molecular azides generates singlet excited states which can dissociate to singlet, doublet, or triplet fragments:

$$RN_3(X^1A') \xrightarrow{h\nu} RN_3^*(^1A'') \begin{cases} \longrightarrow NR^*(\text{singlets})+N_2(X^1\,\Sigma_g^+) & \text{(1a)} \\ \longrightarrow R(\text{doublets})+N_3(^2\Pi_g) & \text{(1b)} \\ \searrow NR(\text{triplets})+ \\ \quad N_2^*(A^3\Sigma_u^+, B^3\Pi_g, \text{ etc.}) & \text{(1c)} \end{cases}$$

Because the energy released is the <u>sum</u> of the photon energy $h\nu$ plus the energy initially borne by the molecule, high energy channels such as (1c) become accessible at rather long photolysis wavelengths. For example, we have found that $N_2(A^3\,\Sigma_u^+)$ metastables are produced from photolysis of BrN_3 at wavelengths as long as 308 nm,[1] and from ClN_3 at 249 nm.[4] These metastables are formed with a quantum yield[3] of less than 5%, yet play an important role in the overall energy release since they carry subsequent chain reactions which can completely remove the available azide. The production of excited nitrenes NR (channel 1a) has been found to be

important in the photodissociation of ClN_3,[4,5], FN_3[6], and BrN_3,[7] with quantum yields on the order of 10 to 20%. We have used pulsed photolysis methods to study the radiative and collisional decay rates[7,8,9] of excited singlets of the halogen nitrenes, which are of considerable interest because they are isolectronic to the group VI diatomics, and are a rather clear-cut case of the influence of increasing spin-orbit coupling in the F, Cl, Br series. Channel 1b, allowed dissociation to doublet fragments, does not appear to be important in the azides, but may well be in the isocyanates. Early photolysis experiments with HNCO by Wooley and Back[10] suggested that the quantum yield for NCO production at 206 nm may be as high as that for production of NH+CO. We have performed experiments[11] involving photolysis of ClNCO and BrNCO. The photodissociation produces intense blue NCO $A \rightarrow X$ emission in both cases. The excited NCO(A) is a direct fragment of the photodissociation of BrNCO, and is formed with considerable vibrational excitation. From its time profile, the NCO(A) observed in the ClNCO experiments is not a direct photofragment, but rather is made by reaction of a fragment with the parent molecule. This fragment was identified as excited $N(^2D)$ atoms, likely generated by pre-dissociation of an excited NCO. These results surely indicate operation of the doublet channel in the photodissociation process, and suggest the possible action of metastable nitrogen atoms in the collisional decomposition of azides and isocyanates.

These photochemical experiments have served in the main to establish the thermodynamics (heats of formation) of the halogen azides and ClNCO, and the amounts of energy liberated by various reaction paths. Such information was extracted largely from the maximum excitation observed in photofragments and from the nature of spontaneous reactions occurring

subsequent to the photolysis. Table I below presents a summary of this information.

Table I. Thermodynamics of XN_3 and XNCO Compounds (a)

Molecule	$\Delta H_{f,298}$	D_o, X-N	D_o, N-N or N-C
FN_3[6]	120 to 130		-60 to -75
ClN_3[4]	93	25	-30
BrN_3[1,2]	131	0	-60
ClNCO[11]	53		-8
BrNCO	44		

(a) All values are Kcal $mole^{-1}$

Note that even though the N-C bond in isocyanates is typically much stronger than the analogous N-N bond in azides (hence the greater stability of these species), the perturbation of the NCO chain by the chlorine atom is so great as to still render ClNCO a metastable species with respect to dissociation to NCl+CO.

A second part of this program has addressed the energy release in reactions of metastable azides and isocyanates with atomic species. Because of the weakness of the bonds in these compounds, such reactions can be extremely exothermic. Further, the reactions of N_3 and NCO radicals are often strongly constrained by angular momentum conservation rules to produce electronically excited products. For example, N_3 radicals have been found to often behave as $N(^2D)$ atoms weakly bound to ground state N_2 (the $^2\Pi_g$ ground state of N_3 correlates to $N(^2D)+N_2(^1\Sigma^+_g)$). Hence, $R+N_3$ reactions tend to produce excited nitrenes NR correlating to $R+N(^2D)$. In effect, the ground state entry valley of the RN_3 potential energy surface correlates to an excited state surface in the exit valley. A qualitative

potential energy surface for a metastable RN_3 molecule is shown in Figure 1. For species R in which the spin-orbit coupling is weak the probability of the system hopping to the lower energy product surface is small. An excellent example is the reaction of $N(^4S)$ atoms with $N_3(^2\Pi_g)$ radicals to form two N_2 molecules.[12] Spin conservation would suggest that excited triplet or quintet states of N_2 might be formed (the other product being ground state N_2). Orbital correlations would select those states correlating to $N(^4S)+N(^2D)$, i.e., the $B^3\Pi_g$ and $W^3\Delta_u$ states. In fact, this reaction is extremely rapid and produces a very nigh yield of $N_2(B^3\Pi_g)$.[12,13] No evidence for the direct formation of other triplet states was found. As a part of this AFOSR-funded program and related programs sponsored in our laboratory by the Air Force Weapons Laboratory and SDIO (Los Alamos National Laboratory), we have determined rate constants and excited products for a number of $R+N_3$ reactions. These data are collected in Table II.

Table II. Chemiluminescent Reactions of N_3 Radicals

Reaction	k (cm^3s^{-1})	Excited Products
$H+N_3$[14]	$3.8 \pm 0.8X10^{-12}$	-----
$C+N_3$[14]	-----	$CN(B^2\Sigma^+, A^2\Pi)$
$N+N_3$[13]	$1.4 \pm 0.4X10^{-10}$	$N_2(B^3\Pi_g, W^3\Delta_u)$
$O+N_3$[14,15]	$1.0 \pm 0.5X10^{-11}$	$NO\ (A^2\Sigma^+)$
$F+N_3$[16,13]	$1.8 \pm 0.2X10^{-12}$	$NF(a^1\Delta)$
$P+N_3$[17]	$4.7 \pm 0.4X10^{-11}$	$PN(a^3\Pi$ or $a^3\Sigma^+, A^1\Pi)$
$Cl+N_3$[18]	$1.0 \pm 0.2X10^{-11}$	$NCl\ (a^1\Delta, b^1\Sigma^+)$
$Br+N_3$[19]	$1.0 \pm 0.5X10^{-11}$	$NBr(a^1\Delta, b^1\Sigma^+)$

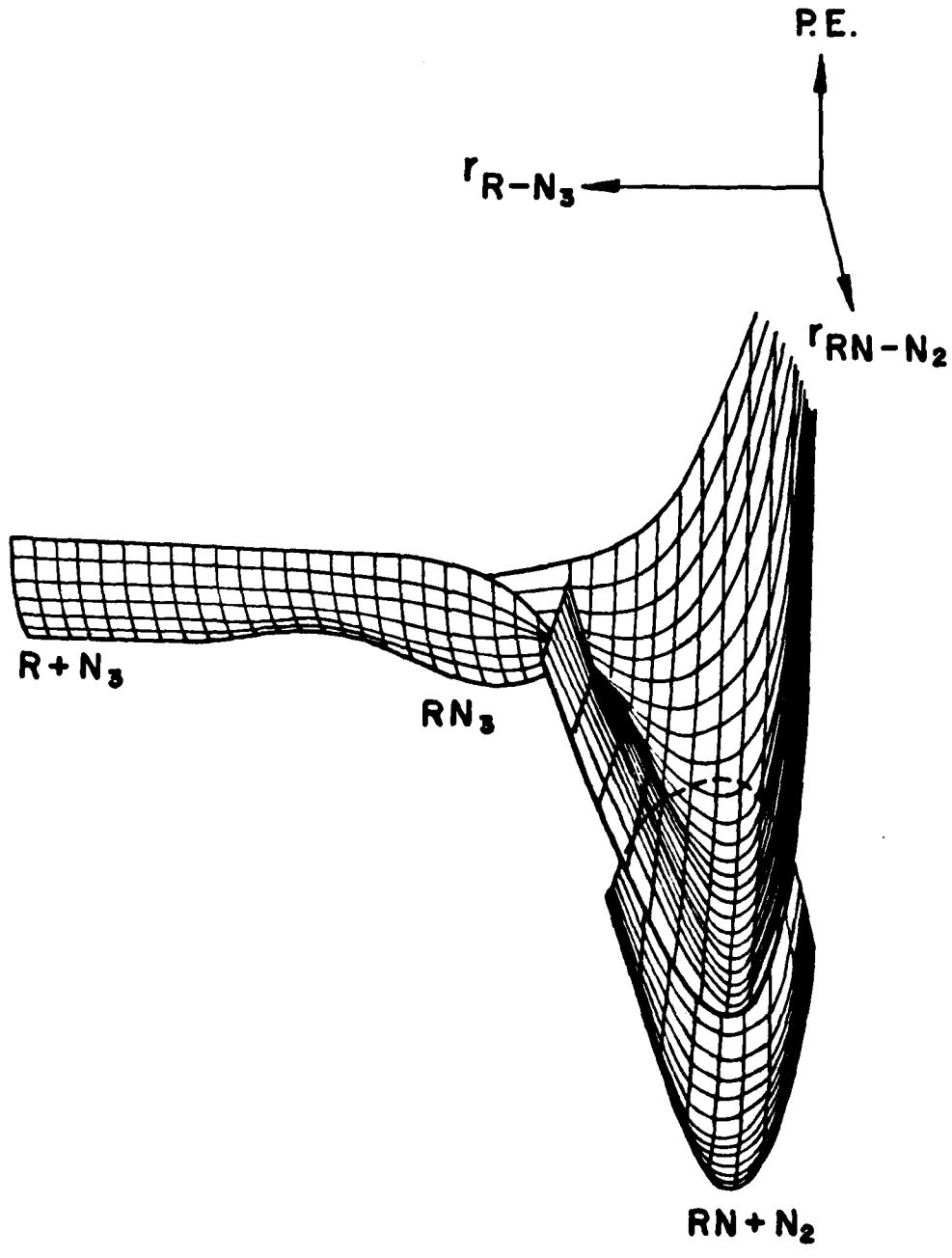

Figure 1. Qualitative potential energy surfaces for the R + N_3 reaction, where R is an atom or radical.

Many of the excited products shown in this table are metastable species which can suffer further collisions with parent molecular azides, dissociating them to form new reactive species. Hence, chain processes occur readily in these systems, and can be the principal mechanism for energy release. We have investigated the chain decomposition of ClN_3 and BrN_3, the latter case in some detail. For BrN_3, chain decomposition can be initiated by creation of bromine atoms, N_3 radicals, or triplet N_2 metastables, all of which act as intermediate chain carriers. Based on a variety of experimental observations, a model was constructed for the chain decomposition of BrN_3 which adequately predicts the results of both continuous discharge-flow and pulsed photolysis experiments.[20]

Apart from their role in liberating the energy stored in azide systems, reactions such as those shown in Table II are clearly of interest with respect to the development of chemically pumped lasers operating on transitions in the visible or UV. Indeed, optically pumped lasers have been demonstrated[21,22] on transitions in CN and NO (the products of $C+N_3$ and $O+N_3$, respectively), and $N_2(A)$-IF and NF(a)-BiF energy transfer systems[23,24] are under development at the present time in this and other laboratories. In particular, we have recently developed pulsed methods for operating chemically pumped N_3-based systems.[25] These pulsed methods allow for operation of these chemical systems at densities significantly higher than those typical of discharge-flow chemiluminescence experiments, and hence offer insight into the possible utility of these systems as short wavelength chemical lasers.

In recent months, we have expanded the program to include studies of halogen amines, in particular NCl_3. This energetic compound has been known since original studies of its explosive nature by DuLong (1811) and Davy

(1813).[26] Although a number of researchers have investigated its properties over the ensuing 175 years, its heat of formation and bond strengths are not well known, and the collisional decomposition mechanism has not been well established. We have studied the photochemistry of NCl_3 in pulsed photolysis experiments, and the collisional reaction chemistry of the molecule in a continuous discharge-flow reactor. These experiments have produced a wealth of new information concerning the excited state chemistry of NCl_3 and its dissociation mechanisms.

II PHOTOCHEMISTRY OF HALOGEN ISOCYANATES AND HALOGEN AMINES

Photochemistry of Halogen Isocyanates

1. Preparation of ClNCO and BrNCO

Flowing streams of gaseous ClNCO and BrNCO were prepared by using the method outlined by Frost and co-workers.[27] In brief, streams of Cl_2 or Br_2 heavily diluted in N_2 (e.g., Cl_2:N_2=1:28) were passed slowly over solid AgNCO suspended on glass wool, in an oven held at 423 K. The AgNCO was prepared by precipitation from aqueous $AgNO_3$ and KOCN solutions. The total pressure in the generator was typically about 60 Torr. The effluent from the generator was analyzed by infrared spectroscopy, which indicated that no significant IR active impurities were present. During experiments, relative amounts of the isocyanates were monitored by on-line measurement of the absorption intensity of the NCO asymmetric stretching vibration near 2200 cm^{-1}. UV and vacuum UV absorption spectra were also measured on-line with the generator flow, by using an Acton Research VM-502 spectrometer modified to include a 4 cm long absorption cell. For the conditions employed, continuous absorptions by Cl_2 or Br_2 were not evident in the UV spectra, suggesting a high yield of the isocyanates as found[27] by Frost, et. al.

2. Photochemistry of ClNCO

The UV-VUV absorption spectrum recorded for gaseous ClNCO is shown in Figure 2. The longest wavelength feature in the spectrum is a continuous, nearly symmetrical band centered near 250nm. Assuming 100% yield of ClNCO from the Cl_2 flow entering the generator, the extinction coefficient (decadic) at 250nm was determined to be ϵ_{250}=460 l $mole^{-1}cm^{-1}$. A second strong absorption begins near 210nm, rising to a shoulder at about 180nm.

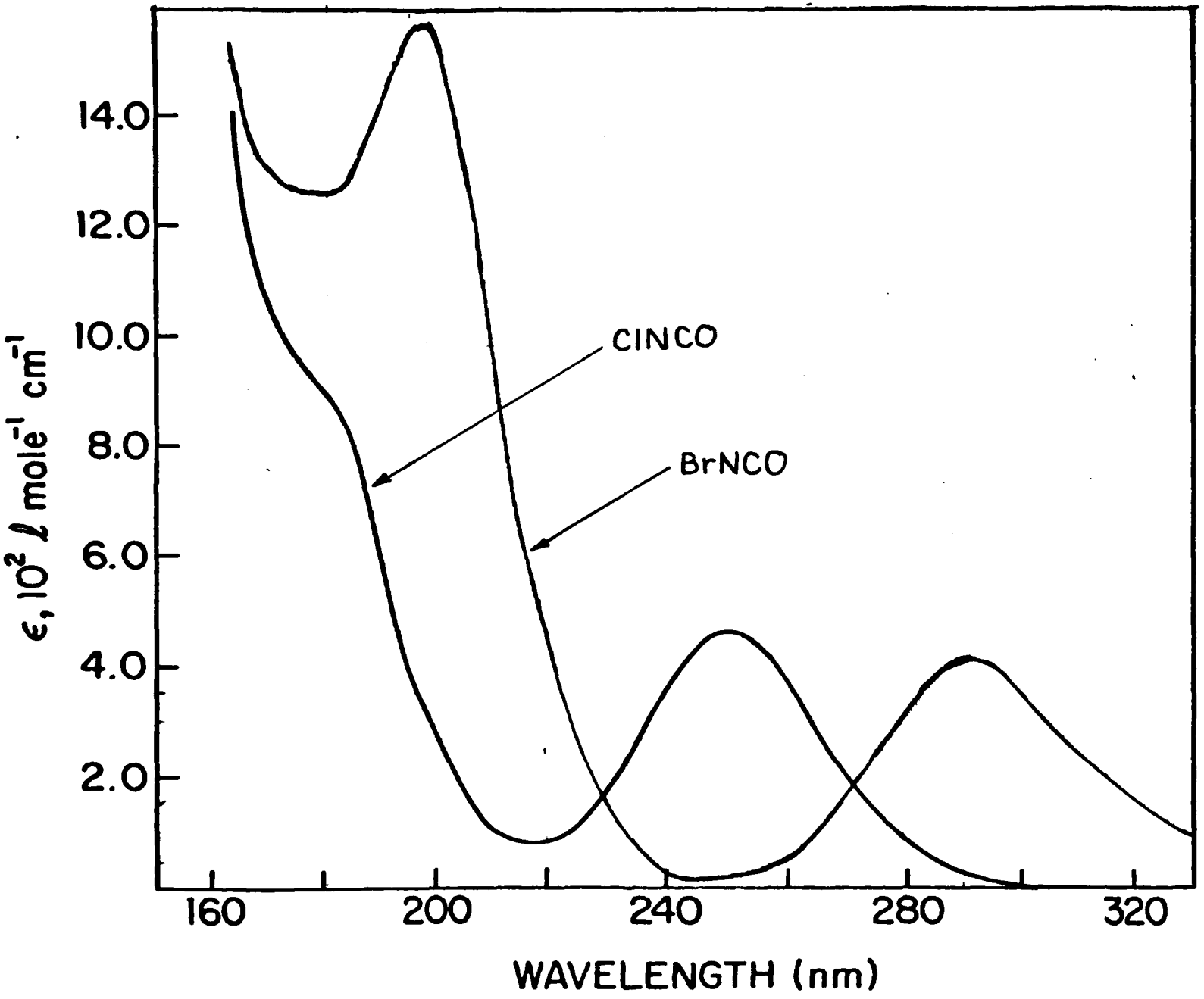

Figure 2. Absorption spectra of ClNCO and BrNCO.

The ClNCO absorption below ~170nm was very strong. The continuous nature of these absorption features suggests that ClNCO can be conveniently photodissociated by irradiation with KrF and ArF excimer lasers at 249nm and 193nm, respectively.

KrF laser photolysis of a $ClNCO/N_2$ mixture (~3.5% ClNCO) at 4.0 Torr produced a deep blue emission visible to the eye. A spectrum of the emission was recorded with a 0.25m scanning monochromator and a cooled GaAs photomultiplier tube. The response of the PMT was amplified and analyzed with a gated integration system. The most intense portion of the spectrum is shown in Figure 3, for a gate extending from 0.5 to 50 μs after the laser pulse. This emission is identified as bands of the $A^2\Sigma^+ \rightarrow X^2\Pi$ transition in NCO. Its intensity was observed to vary linearly with the fluence of the photolysis pulse. The NCO $A \rightarrow X$ emission was the only emitter found over the region of sensitivity of the PMT; we note, however, that the reset pulse of the gated integrator "blinded" the first 0.5 μs after the laser pulse, such that rapid emitters produced directly by the photodissociation (e.g., NCO ($B^2\Pi$)) would not have been seen. Longer-lived excited species (e.g., NCl ($b^1\Sigma^+$)) would have been observed if produced, however.

The time profile of the NCO $A \rightarrow X$ emission was measured by amplifying the PMT response at a particular wavelength (e.g., 438nm), conversion of the analog signal to digital data and signal averaging over a number of successive laser pulsed. Digitizing and averaging was accomplished with a Nicolet 1270 interfaced to an IBM-PC. The PC acted as a terminal and intermediate storage station for a VAX 780 mainframe computer. The time profiles recorded in this manner were fround to exhibit an electronics limited rise (~400ns) followed by a decay over several μs. In

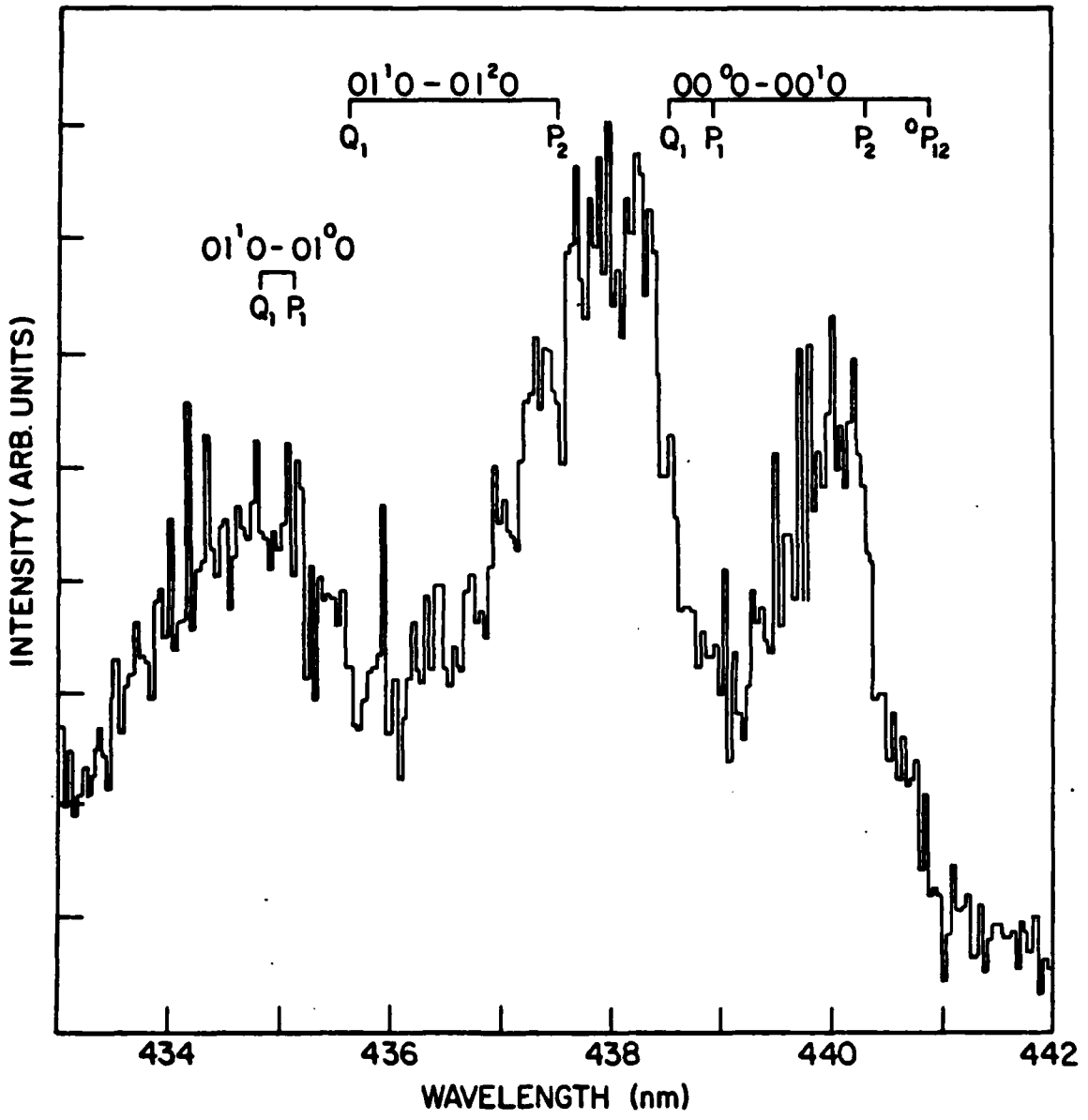

Figure 3. A portion of the spectrum of emission produced by photodissociation of ClNCO at 249 nm. Features of the $A^2\Sigma^+ \rightarrow X^2\Pi$ transition in NCO are indicated.

view of the radiative lifetime of the NCO(A) state,[28] 320ns, the time decay is indicative of the rate of a collisional process which produces NCO(A). The decay rate (s^{-1}) was observed to vary in proportion to the ClNCO flow. This result, in combination with the fluence data noted above, indicates the reaction in question to involve an initial one-photon photofragment and the parent ClNCO. The identity of the fragment, necessarily a metastable in order to suffer collisions with ClNCO, was established by admission of a flow of N_2O to the system. This resulted in complete quenching of the NCO $A \rightarrow X$ emission and production of the spectrum shown in Figure 4. The major features of this spectrum are easily identified as bands of the $B^2\Pi \rightarrow X^2\Sigma^+$ transition in NO, as shown in the figure. These data suggest the metastable precursor of the NCO(A) to be $N(^2D)$ atoms, since production of NO $B \rightarrow X$ emission (the so-called β bands) is characteristic[29] of the $N(^2D)+N_2O$ reaction:

$$N(^2D)+N_2O \rightarrow NO(B^2\Pi)+N_2. \qquad (2)$$

Consequently, $N(^2D)$ must be produced by the initial photodissociation process:

$$ClNCO \xrightarrow[249]{h\nu} Cl+N(^2D)+CO \qquad (3)$$

From the variation of the time decay of the NCO $A \rightarrow X$ emission with the ClNCO density, the rate constant of the subsequent reaction

$$N(^2D)+ClNCO \rightarrow NCl+NCO(A^2\Sigma^+) \qquad (4)$$

was determined to be $k_4=2.1 \pm 0.2 \times 10^{-11} cm^3 s^{-1}$.

From the operation of process (3), a lower limit for the heat of formation of ClNCO is determined to be $\Delta H_f(ClNCO) \geq 52.9$ kcal $mole^{-1}$. This value suggests the molecule to be more stable than ClN_3 (see Table I above) but substantially less stable than HNCO ($\Delta H_f > -14.3$ kcal $mole^{-1}$), in

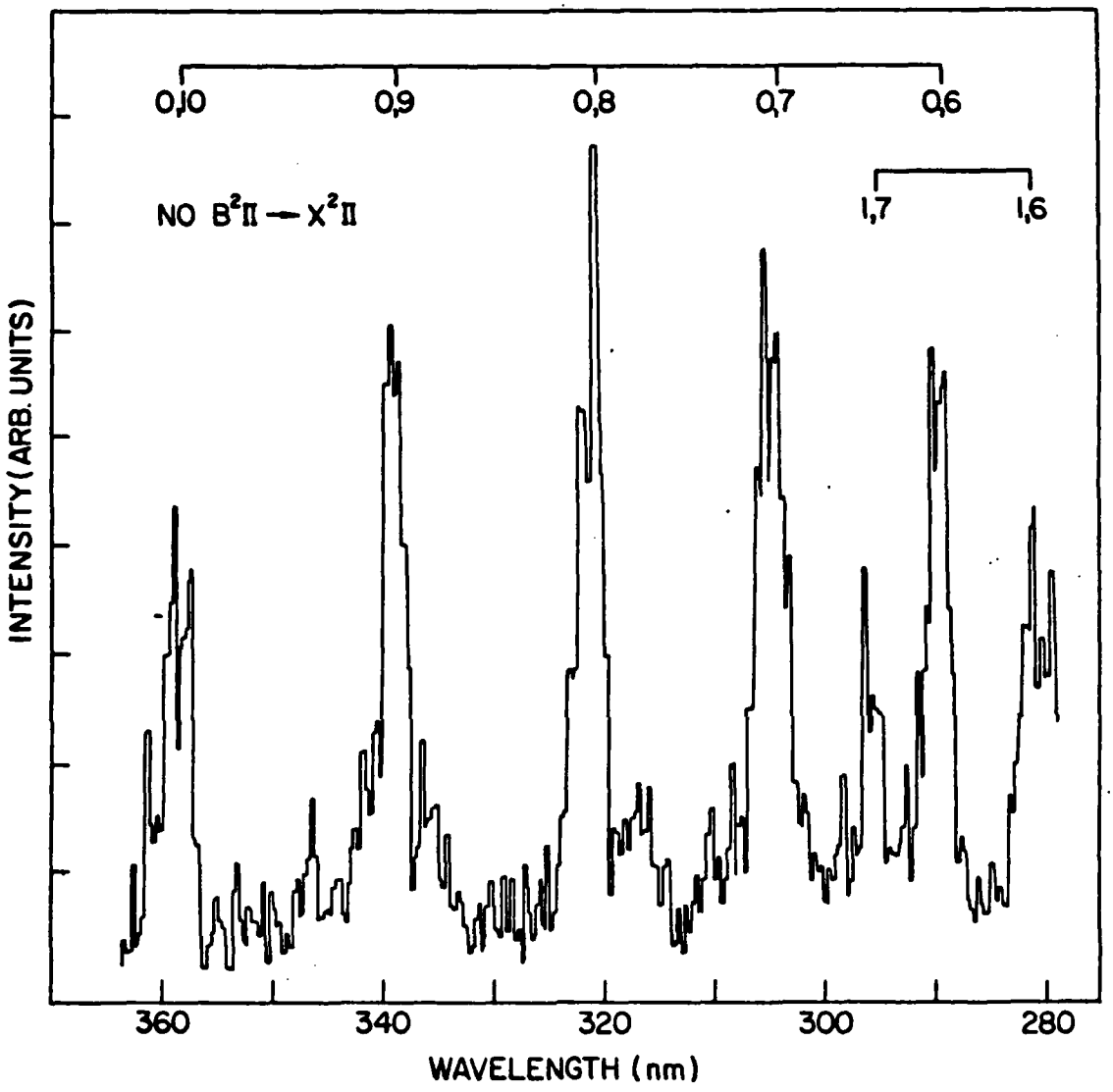

Figure 4. Spectrum of NO β bands produced by photolysis of a $ClNCO/N_2O$ mixture at 249 nm.

evidence of the substantial perturbation on the system by the chlorine atom. Process (3) represents operation of either the allowed singlet or allowed doublet pathways for dissociation of the excited singlet state of ClNCO produced by absorption of the 249nm photon. The singlet channel would generate $CO(X^1\Sigma^+)$ and excited singlet NCl, the latter in a state which might pre-dissociate to $N(^2D)+Cl(^2P)$. We note in this regard that both $NCl(b^1\Sigma^+)$ and $NCl(a^1\Delta)$ dissociate adiabatically to $N(^2D)$. Alternatively, operation of the doublet channel would produce $Cl(^2P)+NCO$ (doublet states). In this case, the NCO fragment might well predissociate to $N(^2D)+CO(X^1\Sigma^+)$.

3. Photochemistry of BrNCO

The UV absorption spectrum recorded for BrNCO is shown in Figure 2. Clearly, the features of the spectrum are very similar to those found for ClNCO, but are shifted about 30nm to the red. The longest wavelength feature is again a symmetrical continuum, for BrNCO centered near 290nm with an extinction coefficient ε_{290} =420 l $mole^{-1}cm^{-1}$. The lower wavelength shoulder noted in the ClNCO spectrum appears near 200nm for BrNCO and is better resolved. This feature is clearly accessible to photolysis with ArF laser radiation at 193nm, where the extinction coefficient is ε = 1500 l $mole^{-1}cm^{-1}$. The longer wavelength absorption feature can be probed with XeCl laser radiation near 308nm, but the extinction coefficient at this wavelength is only ε_{308}=300 l $mole^{-1}cm^{-1}$.

Photolysis of a flowing stream of $BrNCO:N_2$=1:10, at a total pressure near 1.2 Torr, produced a very weak emission which appeared blue-violet to the eye. The spectrum of the emission, recorded with a much faster gated integration system (SRS 235), showed broad features in the general area of

the NCO A →X emission. The intensity was so small as to preclude a definite identification of the emitter, however. In contrast to the behavior observed for the ClNCO system, the time duration of the emission was very short, decaying in less than 0.5 μs.

Much better data was obtained from photolysis of the BrNCO:N_2 flow at 193nm, where the extinction coefficient is much greater. Photolysis at this wavelength produced very intense blue-violet emission. The spectrum of this emission, recorded with a delay of 1ns and a gate width of 1 μs (longer than the time duration of the emission) is shown in Figure 5a. This spectrum is similar to that found from 308nm photolysis, but is much better resolved. It seems very likely that this emission is from excited NCO(A), and some individual features can be assigned. It is apparent, however, that the NCO(A) is highly vibrationally (and perhaps rotationally) excited, giving rise to this very broad spectrum. In contrast, the spectrum shown in Figure 3 from photolysis of ClNCO represents NCO(A) with a fairly cold vibrational distribution. In order to corroborate our identification of the emitter in the BrNCO system as vibrationally excited NCO(A), successively larger flows of SF_6 were added to the system in an effort to vibrationally relax the molecule. These data are shown in Figures 5b-5e. Clearly, the spectrum collapses to one which is dominated by the 000,000 band of NCO A→X near 438nm.

As for photolysis at 308nm, measurement of the time profile of the emission revealed an electronics limited rise (~50ns in this case) followed by a decay over 350ns or less. These data are in accord with the radiative lifetime of NCO(A), 320ns. The dependence of the emission on the incident laser fluence is shown in Figure 6. The plot, obtained for BrNCO:N_2=1:10

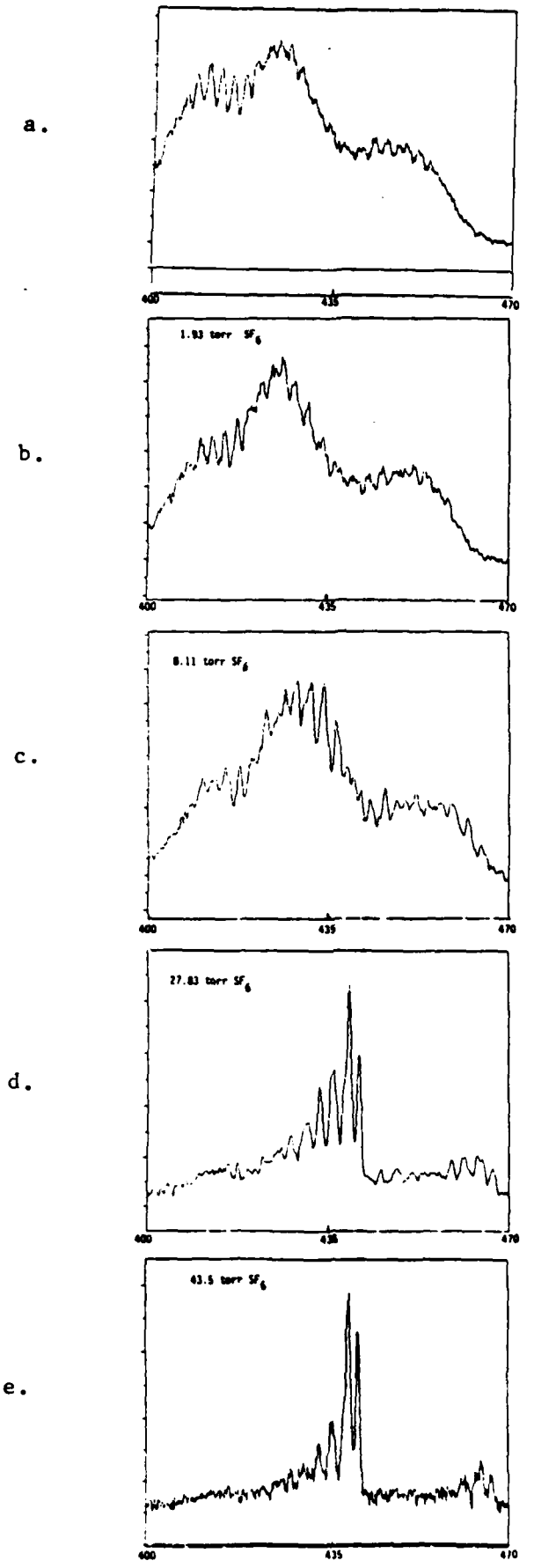

Figure 5. a. Spectrum of emission from 193 nm photolysis of BrNCO.

b-e. Spectra with amounts of SF_6 added as shown. Wavelengths are in nm.

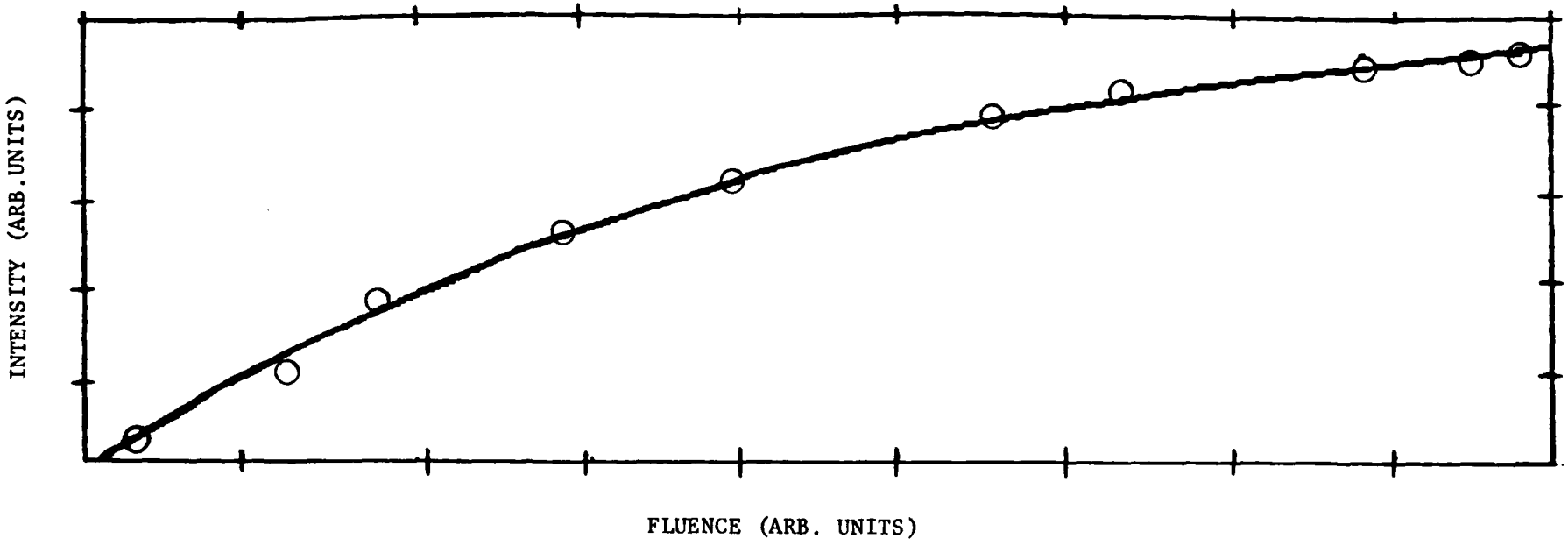

Figure 6. Fluence dependence of the NCO A→X intensity from the photodissociation of BrNCO.

at 1.2 Torr, is linear at low fluence, but clearly levels off at higher fluence, suggesting saturation. The curve was fitted to the relation

$$\text{Intensity}=I_o\left[1-\exp\left(\frac{\sigma E}{h\nu}\right)\right] \qquad (5)$$

where σ is the absorption cross section and E is the fluence. This procedure yielded a value $\sigma = 2.7\times10^{-18}$ cm^2, corresponding to an extinction coefficient $\epsilon_{193} = 1620$ l mole^{-1}cm^{-1}, in very good agreement with the value determined from the absorption spectrum based on the assumption of a 100% yield of BrNCO in the generator.

From these data, it would appear that NCO($A^2\Sigma^+$), in a highly vibrationally excited state, is produced as a direct fragment from the photodissociation of BrNCO at either 193nm or 308nm:

$$\text{BrNCO} \xrightarrow[193,\ 308]{h\nu} \text{Br+NCO}\ (A^2\Sigma^+, v) \qquad (6)$$

From the occurrence of reaction (6), and taking the total excitation of the product NCO as corresponding to the short wavelength limit of the A→X emission near 360nm, a limit on the heat of formation of BrNCO is calculated to be $\Delta H_f \geq 44$ kcal mole^{-1}. In this calculation, the heat of formation of NCO was taken to be 34 kcal mole^{-1} after Okabe.[30] From a more recent value of this parameter reported by Sullivan,[31] et. al., ΔH_f(NCO) >48 kcal mole^{-1}, we find ΔH_f(BrNCO) >58 kcal mole^{-1}. Sullivan's value is the subject of some considerable debate, however. Either limit is likely to be considerably lower than the true value of ΔH_f(BrNCO), however, since BrNCO is expected to be less stable than ClNCO and our experiments with ClNCO established that ΔH_f ClNCO $\geq$53 kcal mole^{-1}.

The vibrational excitation of NCO(A) suggests that the molecule is distorted, likely with an elongated N-C bond, in the dissociative state of

BrNCO produced by the photolysis. Indeed, the perturbation by the bromine atom is expected to weaken this bond substantially in the ground state of the molecule. Franck-Condon excitation would then produce the excited state with this elongated bond. The complexity of the spectrum is so great as to preclude judging the extent of excitation of bending vibrations or rotations, which would indicate a bent dissociative state.

These data for BrNCO surely support the idea that the doublet dissociative channel (Eqn. 1b above) is responsible for the excited state chemistry observed in the halogen isocyanate systems. The observation of excited NCO as a direct photofragment in the BrNCO case indicates that predissociation of NCO is the most probable origin of $N(^2D)$ produced by 249nm photolysis of ClNCO. This behavior is in strong contrast to that observed in the halogen azides, and likely results from the greater strength of the N-C bond in the isocyanates relative to the weak N-N bond in the azides. The production of $N(^2D)$ from the photolysis of ClNCO is a very unique pulsed source of the metastable atoms, which is potentially useful in real time studies of $N(^2D)$ reactions. A number of such reactions have been suggested as possible chemical laser sources.[31]

Photochemistry of Halogen Amines

1. Preparaton of NCl_3

NCl_3 was synthesized using a variation of the method reported by Clark and Clyne.[32] Cl_2 diluted with helium was bubbled through an aqueous solution of ammonium sulfate in 1M sulfuric acid. The product NCl_3 was swept out of the solution with He and was condensed with the excess Cl_2 from the gas stream in a cold trap. The trap was allowed to warm up and any trapped Cl_2 vaporized quickly and was removed by a continuous stream of

helium. NCl_3 vapor was carried in helium through teflon tubing from the trap to the photolysis system.

To verify that we were indeed synthesizing NCl_3 and not measurable amounts of $HNCl_2$ or H_2NCl, a mass spectrum and an IR spectrum of the gas stream were obtained. The mass spectrum agreed with that reported by Clark and Clyne[32] for NCl_3. The IR spectrum showed no evidence of NH stretching vibrations, and was dominated by the strong NCl_3 asymmetric stretch at 640 cm^{-1}.

Stringent safety precautions were taken due to the explosive nature of the condensed liquid. The generator was set up in a hood behind a polycarbonate shield and the glass trap was wrapped in two layers of metal screen. No explosions were experienced during the course of this work, possibly because the pressure above the condensed NCl_3 was never allowed to drop below ambient. There is some evidence that explosions are likely when NCl_3 evaporates in vacuo.

2. Photolysis of NCl_3

The ultraviolet absorption spectrum[32] of gaseous NCl_3 exhibits a continuum peaking near 220nm, with a very long tail extending into the visible. Photolysis of NCl_3 with pulsed radiation at either 248nm (KrF) or 308nm (XeCl) produced a pale yellow glow along the length of the photolysis cell, which was a pyrex tube (2.54cm i.d.) 75cm in length. An NCl_3/He mixture was passed through the cell at a slow flow rate, at a total pressure near 300m mTorr. The spectrum of the emission from 248nm photolysis is shown in Figure 7a. Two components are evident, which are an unresolved emission extending from 476nm to 744nm with a maximum near 546nm, and a series of bands separated by about 320cm^{-1} superimposed on the unresolved emission. On rare occasions, the intensity of the bands was

much greater than that of the unresolved emission as shown in Figure 7b. The bands and "continuum" are indeed distinct features corresponding to different emitters. Although both varied linearly with the incident laser fluence, each had a different time dependence. The bands showed a finite risetime of about 1 μs followed by a decay over 20 to 30 μs. The extrapolated zero-pressure limited of the lifetime of the bands was found to be 48 μs. The unresolved emission also had a 1 μs risetime, but decayed much more rapidly. The zero pressure lifetime for this emitter was determined to be about 4 μs.

Photolysis of NCl_3 at 308nm produced the emission whose spectrum is shown in Figure 7c. Here, again, we find the band system overlying the unresolved emission, but the bands are more intense than in 7a, and their maximum shifted to shorter wavelength. The band positions and the band separation, 320 $\pm 30 cm^{-1}$, are the same in the spectra of Figures 7a, 7b, and 7c. The time profile of the banded emission produced by 308nm photolysis was distinctly different from that found for 248nm photolysis. The rise time of the emission was much shorter, being limited by the time response of the data collection electronics. The decay time was also considerably shorter, on the order of a few μs.

Auto-decomposition of NCl_3 vapor, as when the gas is expanded through an orifice, produces an easily visible red flame. This emission is readily identified as the $B^3\Pi o_u^+ \rightarrow X^1\Sigma_g^+$ transition in Cl_2. The emission found from the photodissociation, shown in Figure 7, is clearly not from excited Cl_2. The band positions and separations do not correspond to known transitions in Cl_2. From the mass spectrum of the generator effluent, the species likely to be present in the cell subsequent to the photolysis are Cl_2, NCl, NCl_2, and NCl_3. The emission from the photodissociation clearly

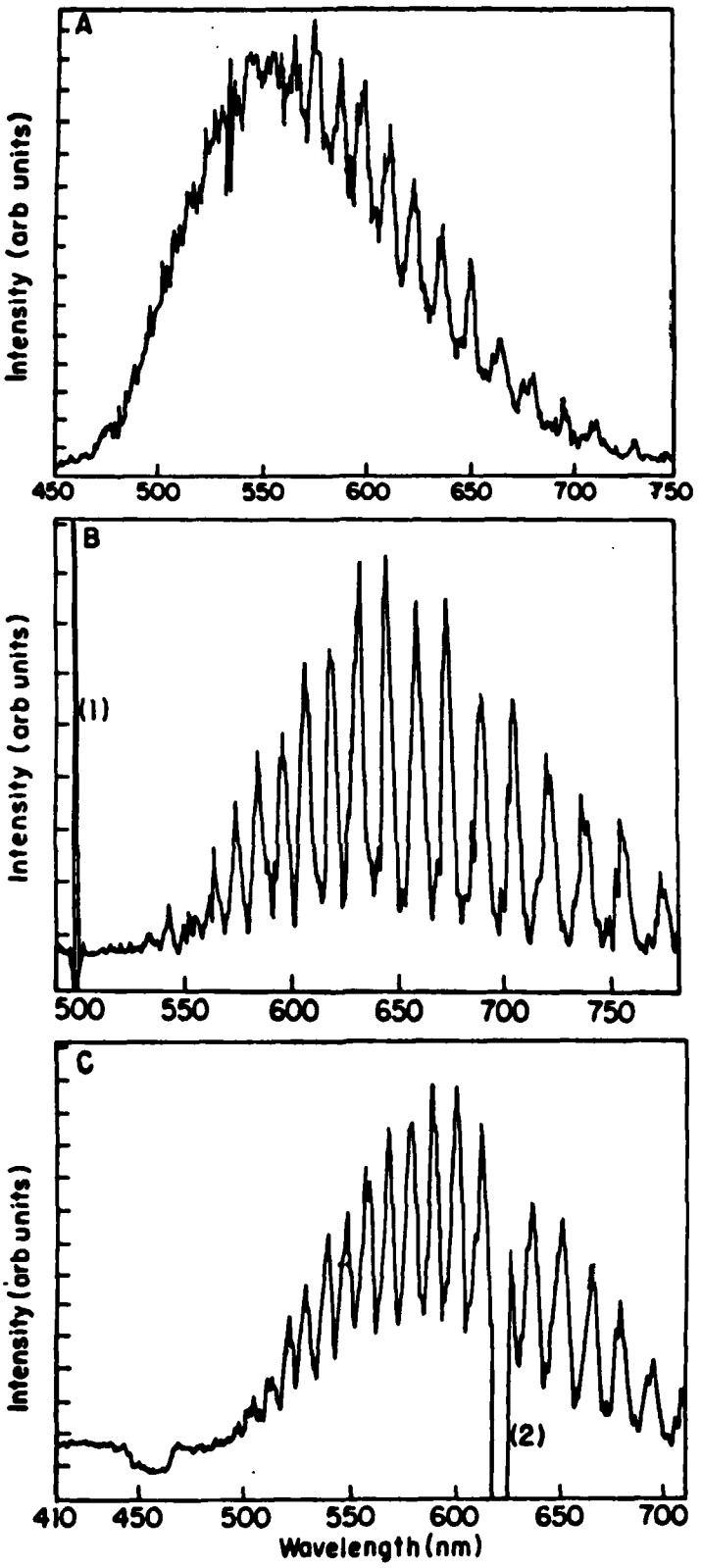

Figure 7. a-b. Spectra of emission produced by 249 nm photolysis od NCl_3. c. Spectrum of emission from 308 nm photolysis of NCl_3.

does not correspond to transitions in Cl_2 or NCl. Almost nothing is known about the spectroscopy of NCl_3 or NCl_2. Consideration of the analogous molecules NH_3 and NH_2 offers some insight. Excited $NH_2(^2A_1)$ produced by photodissociation of NH_3 at 193nm emits with a very complex spectrum throughout the visible.[33] For vibrationally excited $NH_2(A)$, the emission spectrum recorded under low resolution can look much like the unresolved component of our emission shown in Figure 7. On the other hand, the X-A absorption spectrum of NH_3 shows a very harmonic vibrational progression in the ν_2 out of plane symmetric bending mode (i.e., the umbrella mode). The fact that this mode is active in the $A \leftarrow X$ transition is consistent with the large change in the H-N-H angle between the X and the A states (the ground state of NH_3 is pyramidal, whereas all of the known excited states are planar). The $A \leftarrow X$ absorption spectrum in NH_3 is in fact strikingly similar in appearance to the banded emission we find from NCl_3, being an extremely harmonic single progression. No $A \rightarrow X$ emission has been observed for NH_3 but the corresponding emission has been seen[35] in ND_3. This emission also consists of a progression in the umbrella mode, superimposed on 0, 1, or 2 quanta in the ν_1" symmetric stretch. The corresponding umbrella frequency in NCl_3 is $347cm^{-1}$, determined[36] from NCl_3 solution in CCl_4. This value is within the experimental error of our band spacing, $320 \pm 30cm^{-1}$.

On the basis of these considerations, we tentatively assign the banded features in our spectrum to NCl_3, and the unresolved emission to NCl_2. Figure 8 shows a model for the photochemistry based on these assignments. Photolysis at 248nm excites NCl_3 to excited state C, which has a lifetime of 1 μs (corresponding to the risetime observed for the banded and unresolved emissions). State C relaxes to state A, the emitter of the banded emission, or dissociates to excited NCl_2, the emitter of the

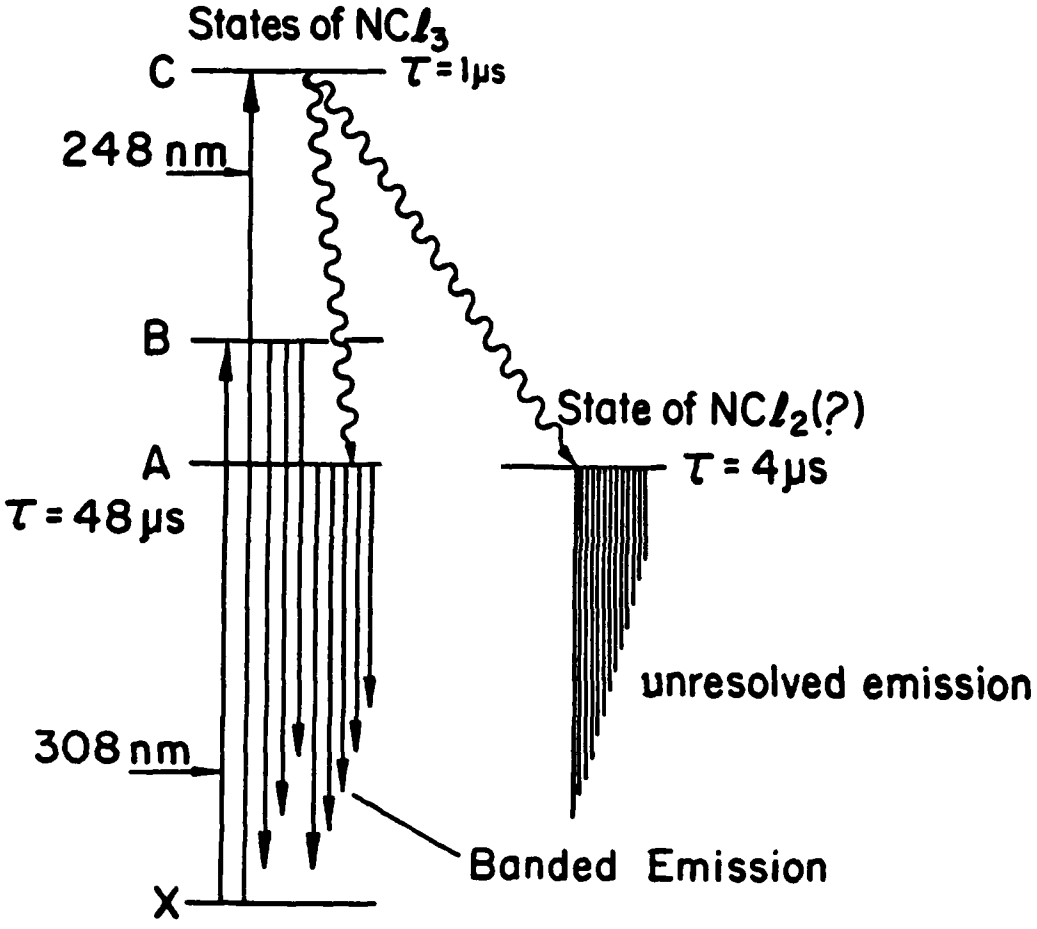

Figure 8. Model for the photochemistry of NCl_3.

unresolved emission. State A has a lifetime of 4 μs. Photolysis at 308nm excites NCl_3 to state B, which emits to vibrational levels of the ground state as state A does. The intensity maximum in the bands is shifted to shorter wavelength because excited state B is at higher energy than state A.

Clearly, this model can be tested by further experiments, in particular measurement of the UV excitation spectrum of NCl_3. These experiments are to begin in our laboratory shortly. These data represent the first information obtained regarding the excited state chemistry of NCl_3, although the molecule has been known since 1811. The experiments suggest that a wealth of similar information can be obtained for a variety of halogen amines.

III. RADIATIVE AND COLLISIONAL RELAXATION OF EXCITED HALOGEN NITRENES

The photodissociation of halogen azides (XN_3) produces excited singlet states of the halogen nitrenes (NX) via dissociation channel 1a described above.[4-7] The quantum yield for production of NX($b^1\Sigma^+$), the second excited singlet state, appears to be on the order of 10%. Although quantum yields for NX($a^1\Delta$) production are unknown, it seems logical that allowed dissociation to this lower-lying singlet state, which has a greater degeneracy than $b^1\Sigma^+$, would also be significant. These results are important since these metastables may play a role in subsequent chain mechanisms which remove the azide parent. In addition, they show that pulsed photodissociation of XN_3 is an excellent source of excited singlet NX which can be used for real time measurements of the kinetics of radiative and collisional relaxation of these states.

Previous to this program, Pritt and Coombe used photodissociation of ClN_3 to measure the radiative lifetime of NCl($b^1\Sigma^+$) and rate constants for its quenching by collisions with a variety of chaperone species.[4,8] The lifetime[8] of NCl(b), 630 μs, is significantly less than that of NF(b),[37] 22 ms, as expected from the greater spin-orbit coupling in NCl. Before the data described below was obtained, lifetimes of the $^1\Delta$ states were unknown except for NF, for which the lifetime[38] is 5 sec. In the work described below, we used the photodissociation method to measure lifetimes and quenching kinetics for the $b^1\Sigma^+$ state of NBr and the $a^1\Delta$ states of NBr and NCl. In addition, the mechanism of radiation on the $b^1\Sigma^+ \rightarrow X^3\Sigma^-$ and $a^1\Delta \rightarrow X^3\Sigma^-$ transitions was investigated by a first order theoretical treatment.

Radiative and Collisional Decay of NBr ($b^1\Sigma^+, v$)

1. Preparation of BrN_3 and Data Collection.

Flows of gaseous BrN_3 were generated by a procedure in which Br_2, carried in an inert diluent, was passed over solid NaN_3 suspended on glass wool at 273 K. This method and the apparatus employed have been described in detail in the literature.[1] The BrN_3/ diluent stream, typically about 8% BrN_3, was passed through a stainless steel photolysis cell prior to movement through a pump with a vented exhaust. Pressures in the photolysis cell (typically a few Torr) were measured with a capacitance manometer. The gaseous BrN_3 was photolyzed with the 193nm output of a pulsed excimer laser. Fluorescence produced subsequent to the photolysis cell was detected at 90° to the axis of the laser beam by a 0.25m monochromator/cooled GaAs photomultiplier assembly. To record spectra of the pulsed emission, the amplified response of the PMT was sent to a dual-channel gated integrator and boxcar averager (Stanford Research Systems). To record to time behavior of particular spectral features, the PMT response was digitized and averaged with a Nicolet 1270 pulsed data acquisition system. Both the signal averager and gated integrator were interfaced to an IBM PC which acted as an intermediate data storage station and terminal for a VAX 780.

2. BrN_3 photodissociation at 193nm.

Figure 9 shows the spectrum of emission produced by 193nm photolysis of BrN_3, within the first 900 ns after the excimer laser pulse. The spectrum consists largely of NBr $b^1\Sigma^+ \rightarrow X^3\Sigma^-$ bands assigned as shown. Population of the $b^1\Sigma^+$ state in vibrational levels as high as v=10 is evident. The initial vibrational population distribution was determined

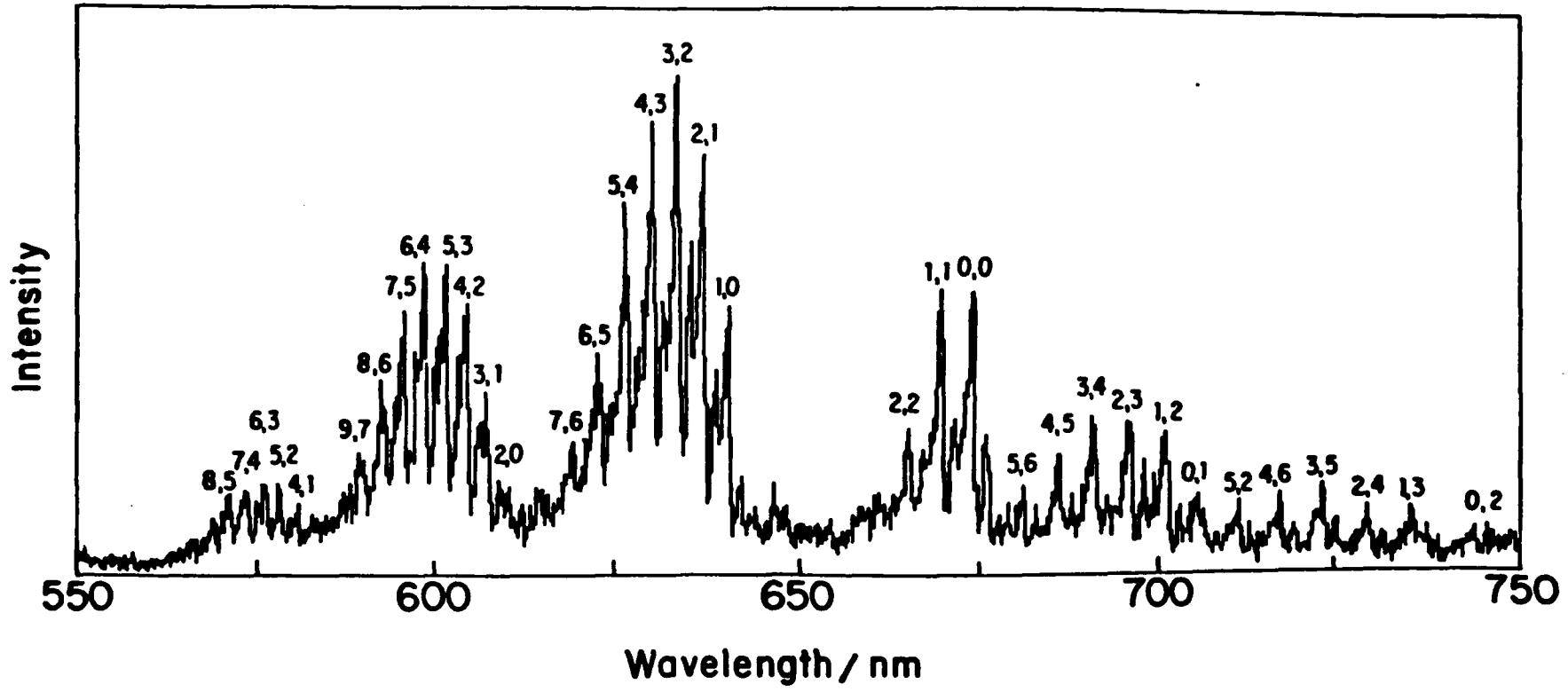

Figure 9. Spectrum of emission from the photolysis of BrN_3 at 193 nm. Bands of the $b^1\Sigma^+ \rightarrow X^3\Sigma^-$ transition in NBr are indicated.

from these data by integration of the emission from various v levels, and the result is shown in Figure 10. The distribution is clearly inverted, peaking near v=2. The vibrational excitation of NBr(b) can be explained as in the production of NCO(A) from photodissociation of BrNCO and the production of NCl(b) from ClN_3. The origin of the vibrational excitation lies in the extension of the weak N-Br bond in ground state BrN_3; excitation by a vertical transition to the dissociative state leads to production of NBr(b) with an extended bond.

Figure 11 shows the time evolution of the visible emission produced by the photodissociation. Two trends are evident in the figure. First, the vibrational distribution in NBr(b) tends rapidly toward lower v' levels, indicating either fast vibrational relaxation in this state or selective reaction of the higher v levels. A second trend is the growth in intensity of the N_2 first positive ($B^3\Pi_g \rightarrow A^3\Sigma_u^+$) emission, which becomes dominant after 20 μs. This emission offers evidence of a reaction mechanism occurring subsequent to the laser pulse which produces excited N_2. As discussed in Part IV below, we have found that BrN_3 can decompose via a chain mechanism in which Br atoms, N_3 radicals, and excited N_2 metastables act as chain carriers. The chain produces vibrationally cold NBr(b) and $N_2(B^3\Pi_g)$. The observation of these products at relatively long times after the photolysis pulse in the present experiments suggests the operation of the chain in this system.

The quantum yield of NBr $b \rightarrow X$ emission was measured by using the photolysis of NH_3 vapor at 193nm as an actinometer. This technique has been used previously in our laboratory[5] for determination of the $N_2(A^3\Sigma_u^+)$ quantum yield from photodissociation of ClN_3. It relies on a determination of the absolute yield of $NH_2\ ^2A_1 \rightarrow\ ^2B_1$ photons from photodissociation of NH_3

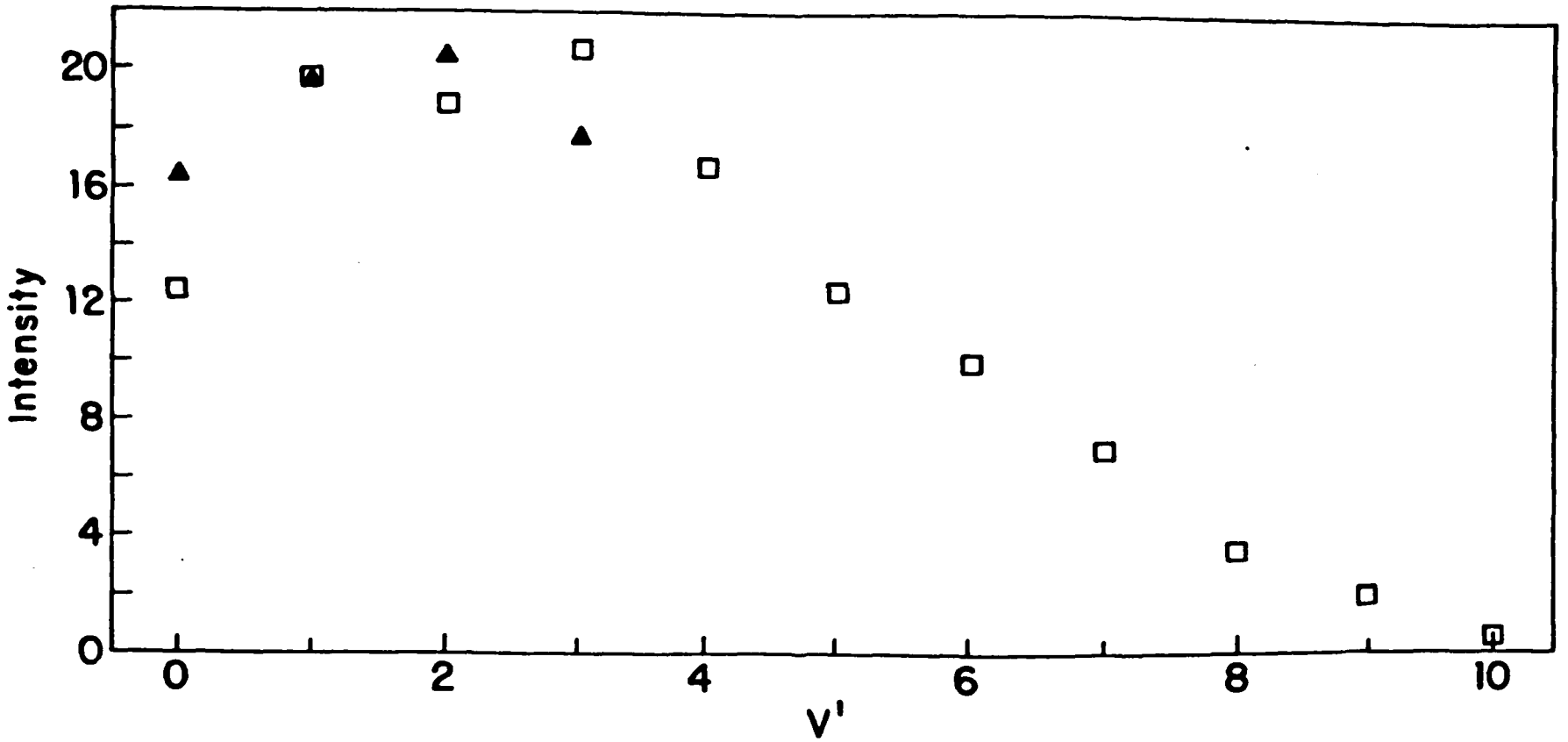

Figure 10. Vibrational distribution in NBr(b) produced by 193 nm photolysis of BrN_3. Open squares, data from experimental intensities. Closed triangles, data from intensities and published Franck-Condon factors.

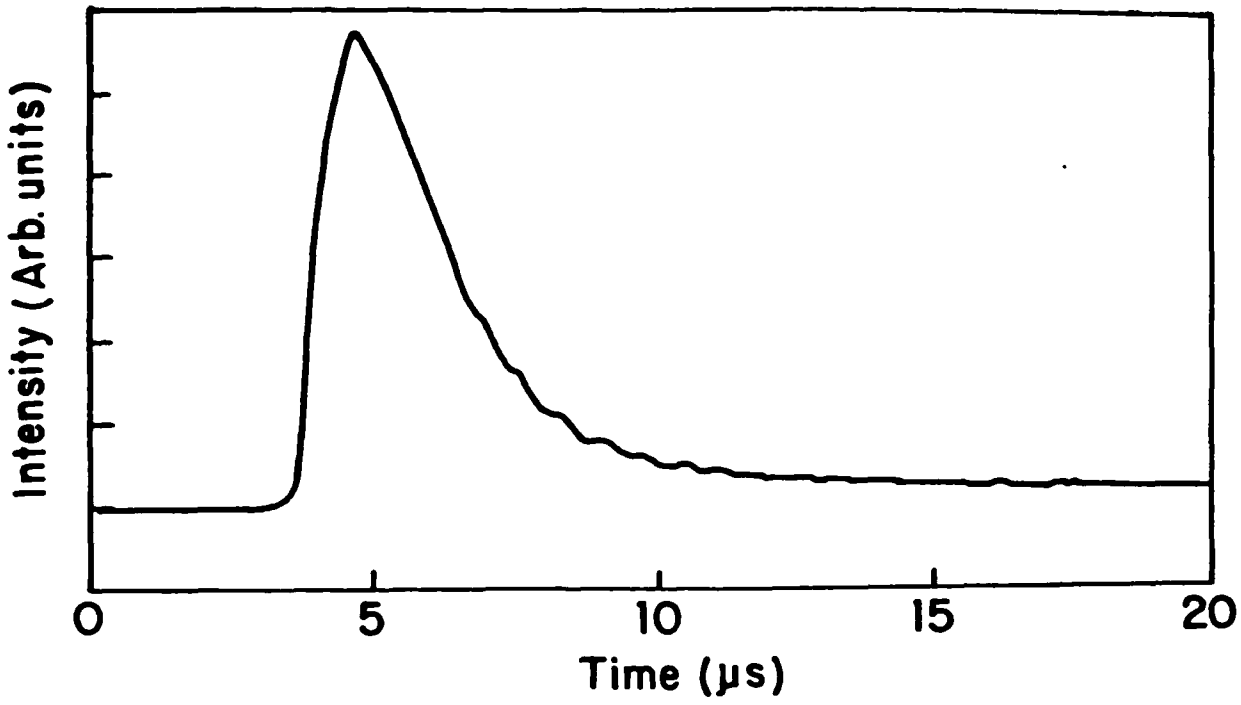

Figure 11. Time profile of NBr b→X emission produced from 193 nm photolysis of BrN_3.

reported by Donnelly and co-workers.[33] In brief, the intensities of NBr b $\rightarrow$X emission from photodissociation of BrN_3 and NH_2 A $\rightarrow$B emission from photodissociation of NH_3 were compared, and the data deconvoluted through known absorption coefficients, radiative rates, and collisional relaxation rates. This procedure yielded a quantum yield of 12% for production of $NBr(b^1\Sigma^+)$. This value is in reasonable accord with that determined by Benard and co-workers[6] for $NF(b^1\Sigma^+)$ production from photodissociation of FN_3.

3. Kinetics of $NBr(b^1\Sigma^+,v)$ Relaxation

The data shown above indicate that NBr(b) is produced with up to ten quanta of vibrational excitation by the photodissociation of BrN_3 at 193nm. Rate constants for radiative and collisional decay of excited NBr were measured for the v=0,2, and 5 levels. In each case, the time profile of the b $\rightarrow$X emission exhibited a rise limited by the detection electronics followed by a double exponential decay. Decay rates were determined by fitting the data to a sum of two exponential terms as follows:

$$I=I_0e^{-t/\tau}+I_0'e^{-t/\tau'} \qquad (7)$$

The initial intensity of the slowly decaying component of the emission, I_0', was at most 10% of I_0. For higher v levels, this percentage was much smaller. As noted above, these data lead us to identify the fast decay component with the NBr(b) initially produced by the photodissociation, and the slower decay component with vibrationally colder NBr(b) produced by subsequent collisional processes.

Figure 12 shows a plot of the exponential decay rate (s^{-1}) of the fast component of the NBr b $\rightarrow$X emission from v=0 vs. the BrN_3 density in the system. The intercept of the linear least squares fit to these data

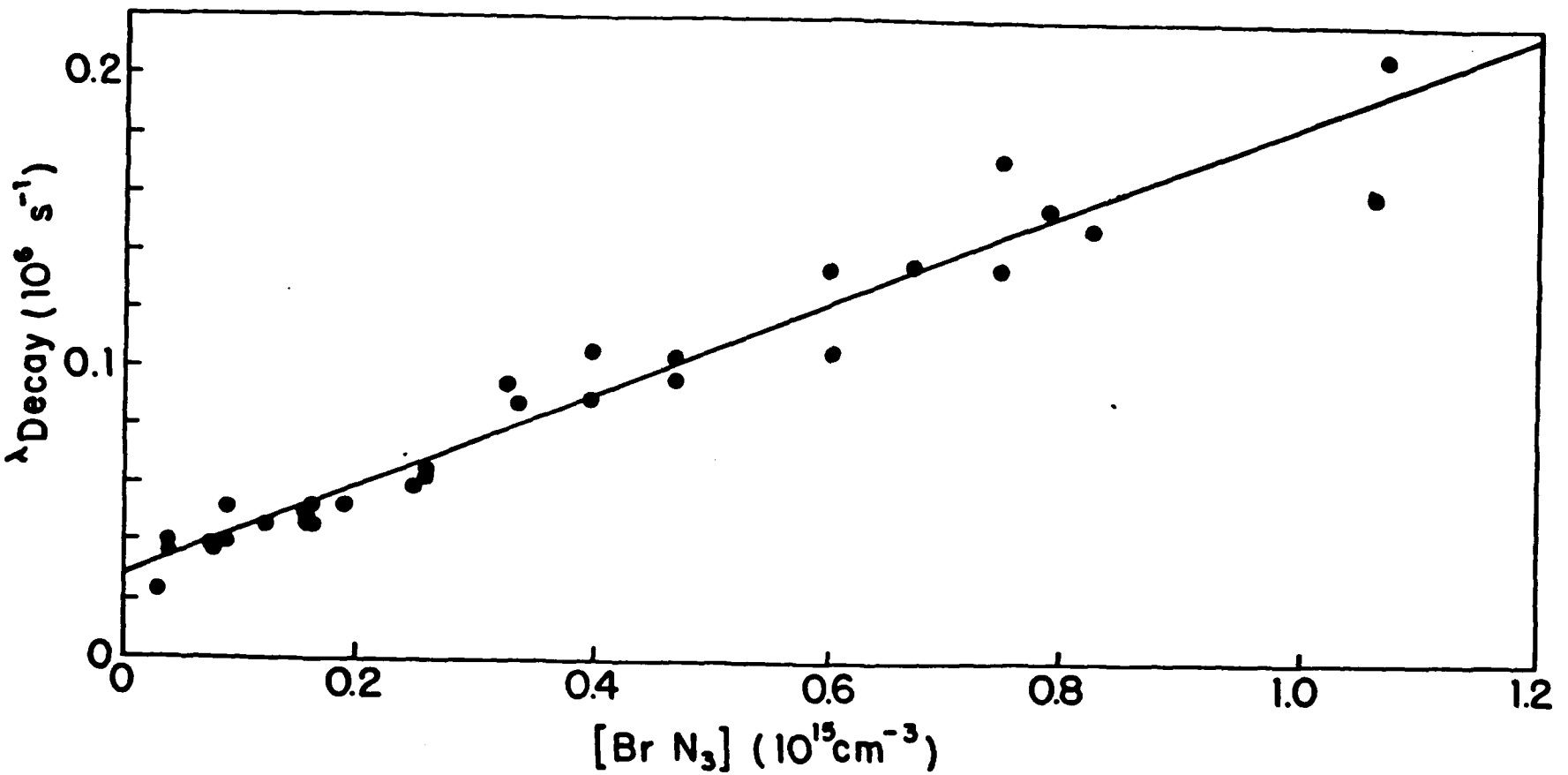

Figure 12. Exponential decay rate of the fast component of the NBr b→X emission from v=0 vs. the BrN_3 density.

represents $k_r+k_{N_2}[N_2]$, where k_r is the radiative rate of the $b \rightarrow X$ transition and k_{N_2} is the rate constant for NBr(b,v=0) quenching by N_2. The slope represents the rate constant for quenching by BrN_3, determined to be $k_{BrN_3}=1.57 \pm 0.06 \times 10^{-10} cm^3 s^{-1}$. In order to determine k_r explicitely, it was necessary to measure k_{N_2}. For this purpose, additional N_2 was added to the BrN_3/N_2 flow and the time decays remeasured. These measurements indicated that k_{N_2} is certainly less than $10^{-14} cm^3 s^{-1}$. Hence, from the data in Figure 12, k_r is determined to be $2.8 \pm 0.5 \times 10^4$ sec^{-1}, corresponding to a radiative lifetime of 36 ± 6 μs. Similar measurements for v=2 and v=5 of the NBr(b) state yielded k_r values of $2.6 \pm 0.8 \times 10^4 s^{-1}$(v=2) and $2.2 \pm 0.5 \times 10^4 s^{-1}$(v=5).

The radiative rate determined for NBr(b,v=0) agrees very well with that reported by Miller and Andrews[39] from laser-induced fluorescence of NBr trapped in a low temperature matrix. Apparently, the argon matrix used in those experiments had a negligible effect on the electronic structure of the trapped NBr. Our experiments indicate very little change in the radiative rate with increasing v', however, contrary to results from the matrix work. Miller and Andrews observed a lifetime of 25 μs from v=1 (relative to 40 μs from v=0), interpreted as the result of radiationless vibrational relaxation in the matrix. The present data appear to confirm this interpretation.

Relaxation of the $a^1\Delta$ States of NCl and NBr

Chemiluminescence from the $a^1\Delta \rightarrow X^3\Sigma^-$ transitions of NCl and NBr was first observed by Pritt, Patel, and Coombe from Cl or Br reactions with N_3 some years ago.[45] The 0, 0 bands of these transitions in both NCl and NBr lie near 1.08 μm in the near infrared. In these experiments, pulsed

emission from these a → X transitions was observed subsequent to photodissociation of ClN_3 and BrN_3, and the kinetics of relaxation processes inferred from the time profiles of the emission.

The halogen azides were prepared as previously described in the literature,[1] by passing the halogens over solid NaN_3. Photodissociation was accomplished by using excimer laser sources at 308nm for BrN_3 and 249nm for ClN_3. Near IR emission produced by the photodissociation was dispersed by a 0.25m monochromator equipped with a grating blazed at 1.0 μm, and detected by a cooled intrinsic Ge detector. The time constant of the response of the detector was several tens of μs, much faster than the time decay of the infrared emissions observed. Time decays were digitized and signal averaged with the Nicolet 1270 system described above.

Spectra of near infrared emissions from the photodissociation of ClN_3 or BrN_3 were obtained using a gated integration system. Data for the ClN_3 system in the region from 1.05 μm to 1.16 μm is shown in Figure 13. These data were taken with a gate extending from 6 μs to 100 μs after the laser pulse. The $\Delta v=0$ sequence of the NCl a → X transition, peaked at the 0,0 band near 1.076 μm is clearly identified. The 4.0nm resolution of the monochromator is just sufficient to indicate the 1,1 band as a shoulder near 1.069 μm. Positions of bands of the $B^3\Pi g \rightarrow A^3\Sigma u^+$ (first positive) transition in N_2 are also shown in the figure. Although the feature at 1.07nm overlaps the position of the 4,5 band of N_2(B → A), the absence of other nearby N_2 bands supports the assignment of the feature to NCl a → X. A similar spectrum was obtained for the a → X transition in NBr subsequent to 308nm photolysis of BrN_3. The signal was much weaker in that case, however.

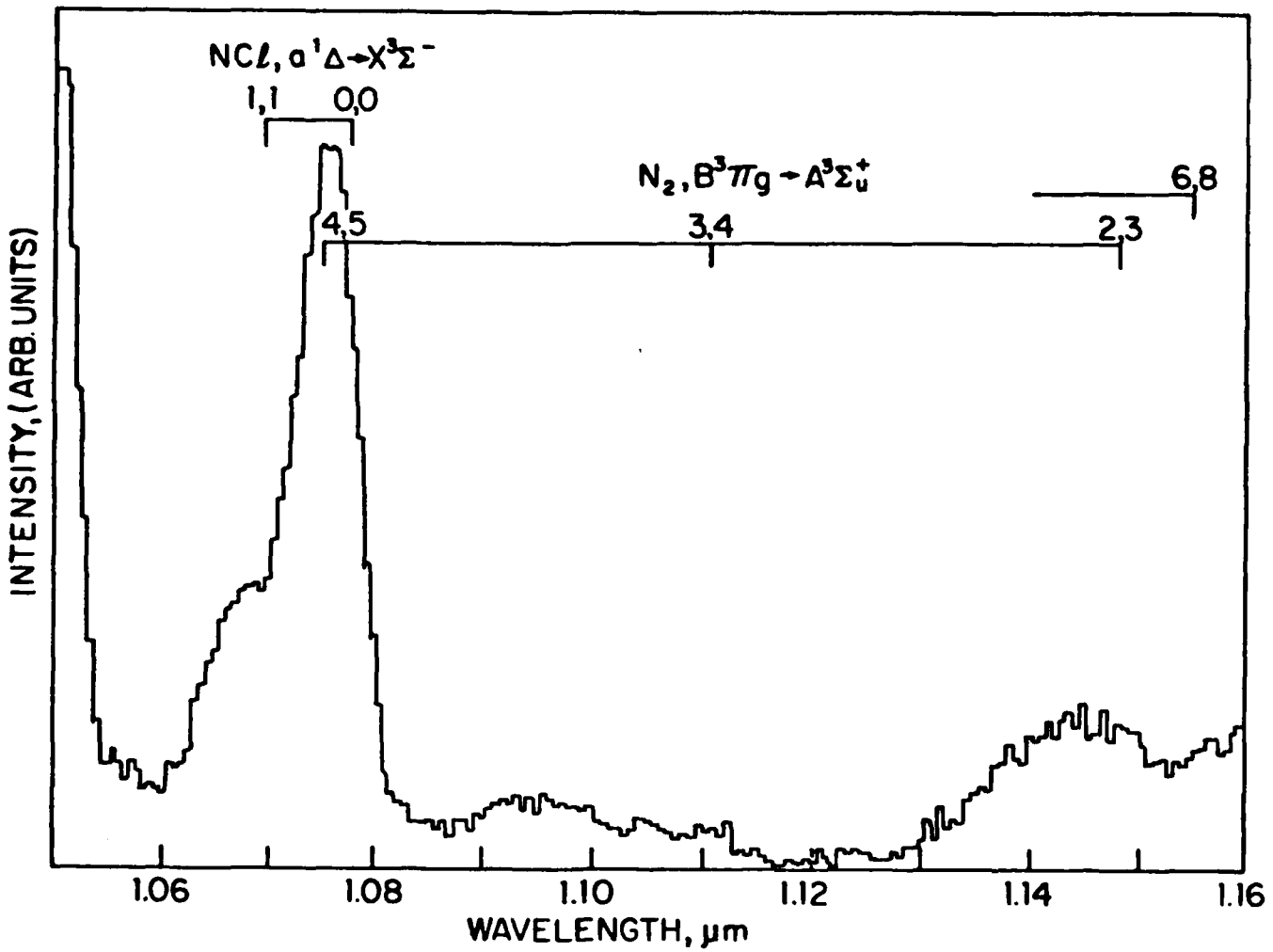

Figure 13. Spectrum od near-IR emission from the photolysis of ClN_3 at 249 nm.

Initial studies of the temporal behavior of the a→X transitions in NCl and NBr were performed by measuring the decay of the emission for various densities of the parent azides at a constant total pressure (XN_3+N_2 diluent) of approximately 5.0 Torr. Time decays were typically averaged over 50 to 100 laser pulses. For the large majority of azide densities, the decays were well described by a single exponential function, and the decay rate (s^{-1}) increased with increasing XN_3 flow. For the conditions of these experiments, the decay rate is given by the following expression:

$$\lambda_{decay}=A_{NX}+\lambda_{diff}+k_{XN_3}[XN_3]+k_{N_2}[N_2] \quad , \qquad (8)$$

where A_{NX} is the a→X radiative decay rate, λ_{diff} is the rate of diffusion out of the observation zone, and k_{XN_3} and k_{N_2} are rate constants for collisional quenching. Hence, a plot of λ_{decay} vs. $[XN_3]$ at constant pressure (i.e., approximately constant $[N_2]$) should yield a line whose slope gives k_{XN_3} and whose intercept is $A_{NX}+\lambda_{diff}+k_{N_2}[N_2]$ These plots for the NCl and NBr systems are shown in Figures 14a and 14b. From the slopes of the plots, $k_{ClN_3}=1.09 \pm 0.11X10^{-13}cm^3s^{-1}$, and $k_{BrN_3}=1.76 \pm 0.04X10^{-11}cm^3s^{-1}$.

From experience with other systems under similar conditions,[4] it is expected that λ_{diff} and k_{N_2} are both negligible under the conditions of these experiments. An experimental test of this expectation was made by measuring λ_{decay} for various total pressures at a fixed XN_3/N_2 ratio. In this case, the slope of a plot of λ_{decay} vs. pressure should yield the rate constant for quenching by the XN_3/N_2 mixture, and the intercept should yield A_{NX}. The effect of diffusion should be evident in the low density region, if it is a factor. Plots of these data for NCl(a→X) and NBr(a→X) are shown in figures 15a and 15b. From a comparison between Figures 14 and 15, k_{N_2} is found to be negligibly small (on the order of $10^{-16}cm^3s^{-1}$).

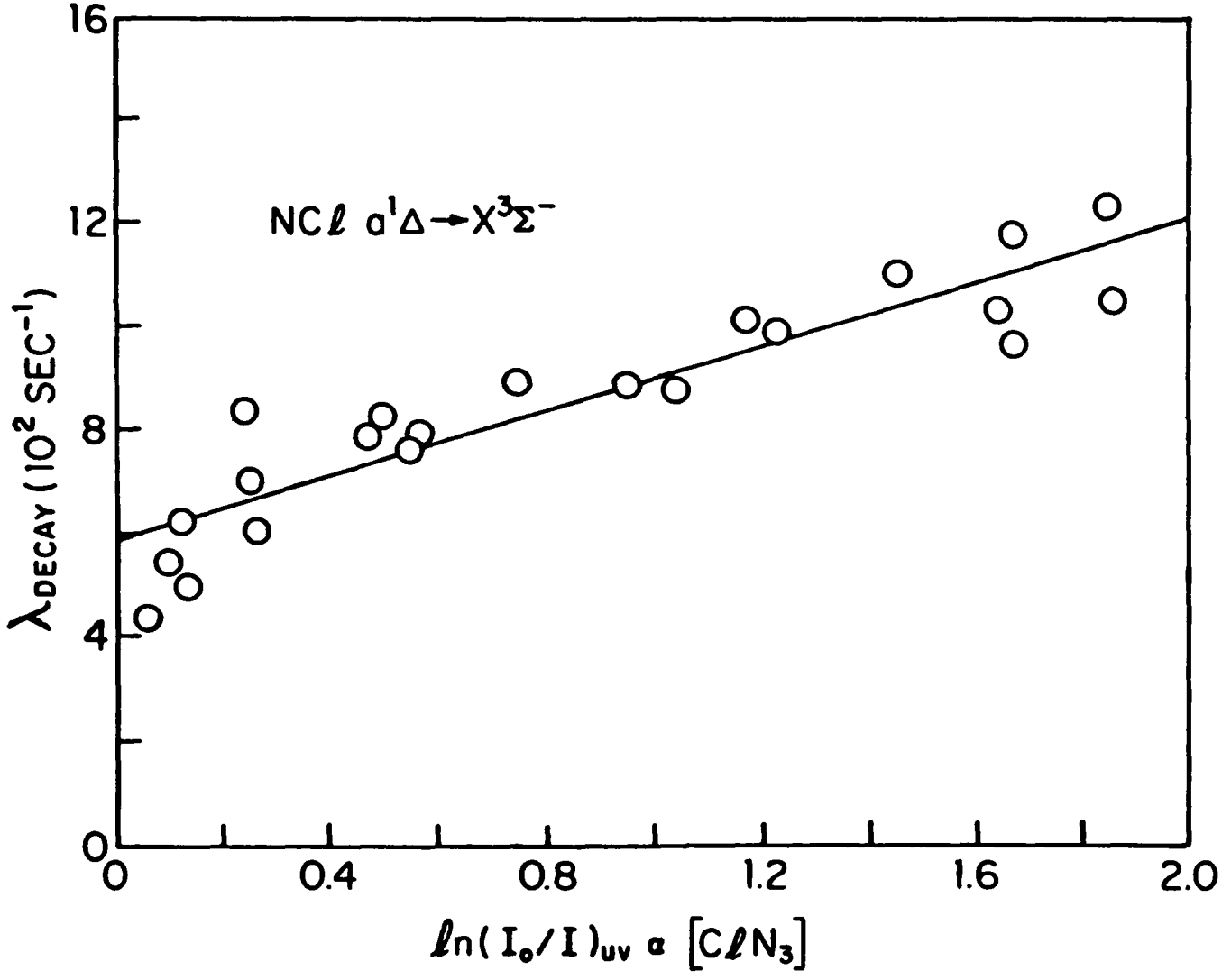

Figure 14a. Exponential decay rate of NCl a→X emission from photolysis of ClN_3 vs. a factor proportional to the ClN_3 density.

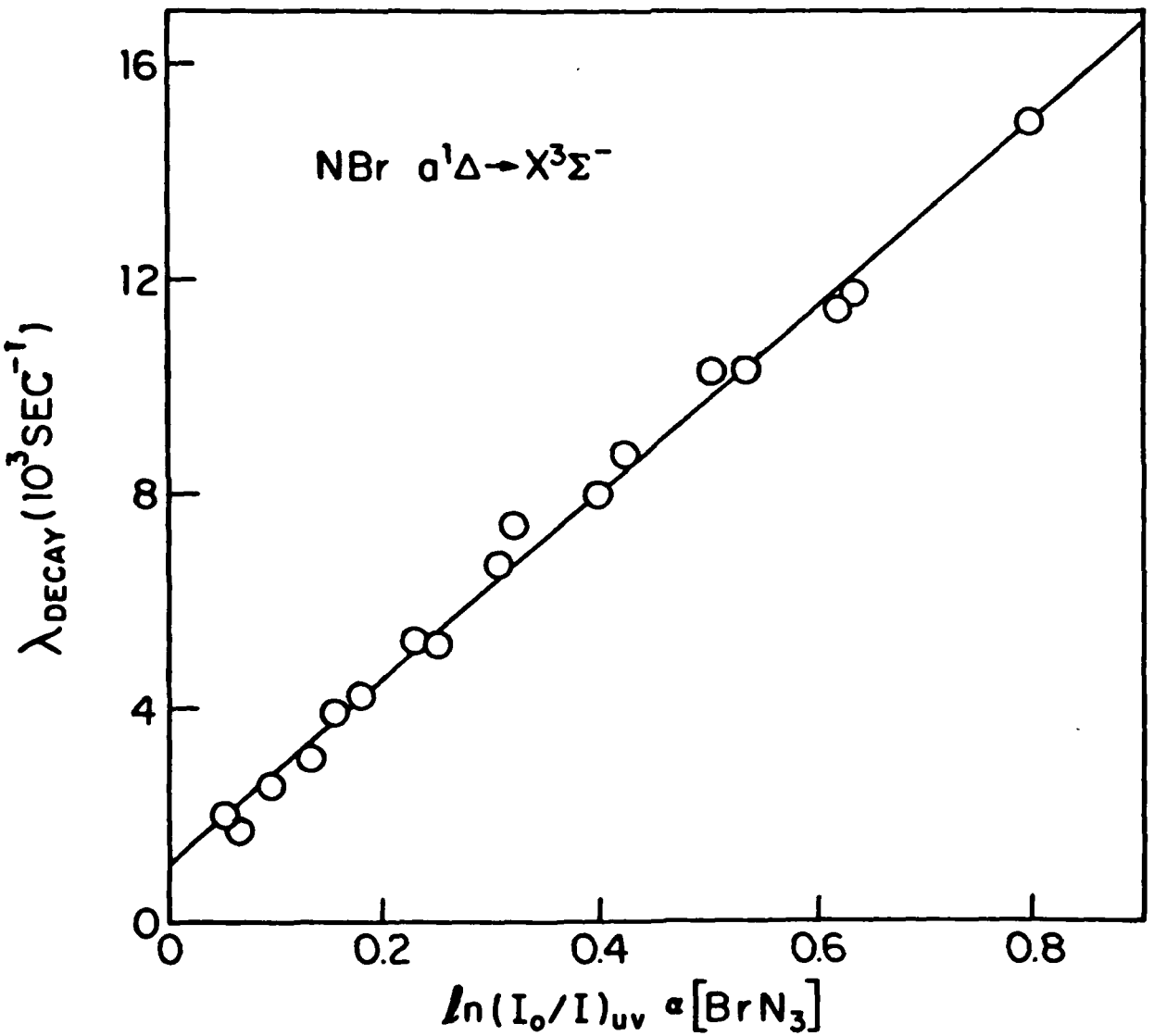

Figure 14b. Exponential decay rate of NBr a→X emission from photolysis of BrN_3 vs. a factor proportional to the BrN_3 density.

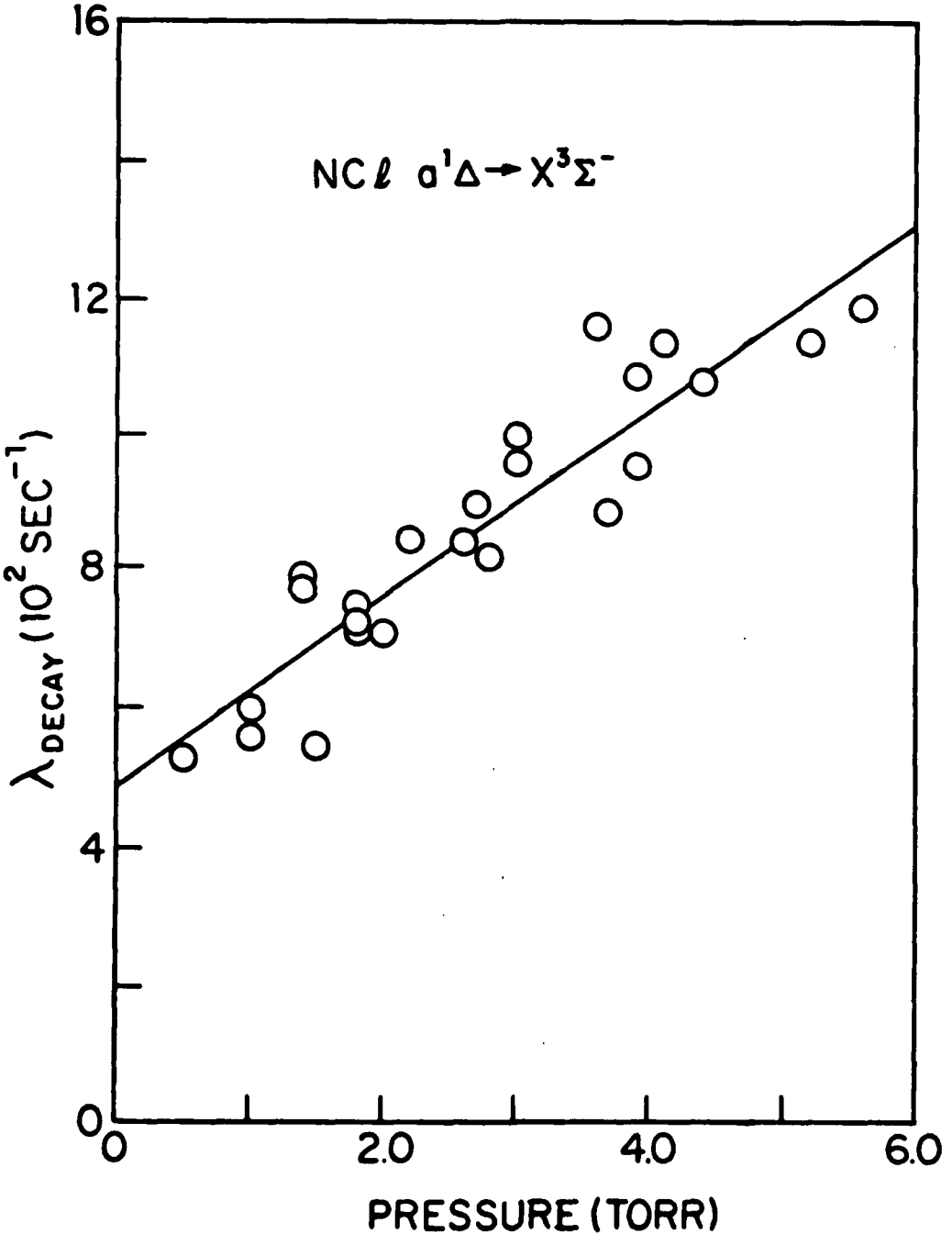

Figure 15a. Exponential decay rate of NCl a→X emission from photolysis of ClN_3 vs. the total pressure.

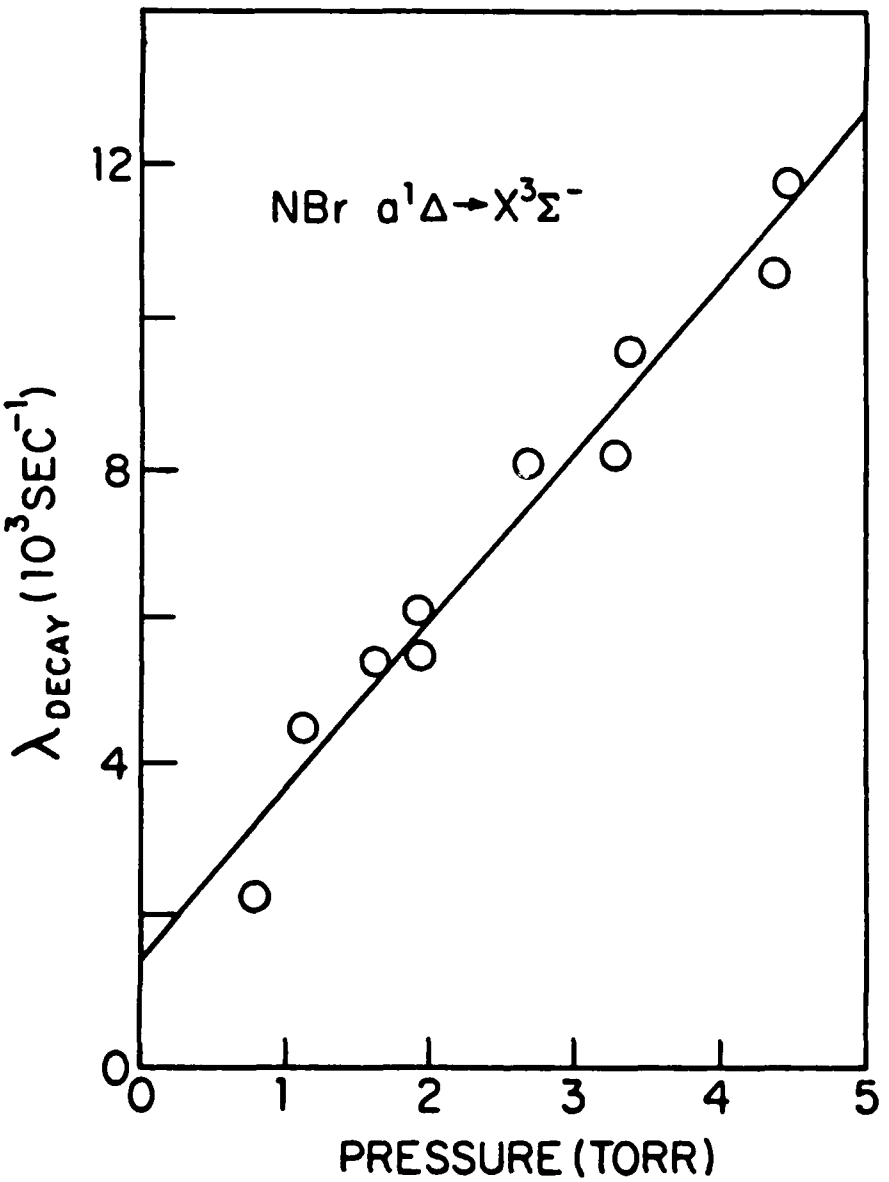

Figure 15b. Exponential decay rate of NBr a→X emission from photolysis of BrN_3 vs. the total pressure.

Further, there is no evidence of the effect of diffusion losses, although some of the data were taken at total pressures as low as 0.8 Torr. Given these results, the intercepts in the figures should correspond to A_{NCl} and A_{NBr}, and indeed the two experiments agree well with one another in this regard. A_{NCl} and A_{NBr} are determined to be $4.87 \pm 0.37 \times 10^{2} s^{-1}$ and $1.24 \pm 0.34 \times 10^{3} s^{-1}$, respectively.

Recently, Becker and co-workers[40] have determined radiative rates for the a→X transitions in NCl and NBr from studies in which laser-induced fluorescence from these diatomics trapped in low temperaturematrices was measured. These experiments suggested that A_{NCl} and A_{NBr} are in fact many times smaller than the values determined from our data. No explanation for this discrepancy is as yet at hand. Since our data were taken with great care and obvious problems with measurement of slow rates (e.g., diffusion) taken explicitely into account, any error in our data would have to result from interpretation of the observed decays as NCl(a) and NBr(a) decay rates; i.e., the decays might correspond to the rate of some collisional formation process, the true decay being buried under the finite time response (a few tens of μs) of the detector. For example, excited NX(a) might be produced by $X+N_3$ reactions, if X and N_3 were somehow produced by the photodissociation of XN_3. This seems unlikely, though, since such reactions would have to compete with the fairly rapid reactions of the halogen atoms (X) with the parent XN_3. The observed decays are far too slow for this to be the case.

Theoretical Discussion of NX Radiative Rates

Table III shows a summary of the energies of the $a^1\Delta$ and $b^1\Sigma^+$ states of NF, NCl, and NBr, and the radiative rates of the b→X and a→X

transitions as determined from data obtained in this program and work done by other researchers. For each transition, the rates increase in the series NF<NCl<NBr. This trend is expected from the increasing spin-orbit coupling in the series, which serves to mix the X, a, and b states with states of other configurations. A similar phenomenon has been well documented for the case of halogenated organic molecules, for which the triplet-singlet radiative rate is observed to scale linearly with the square of the spin-orbit coupling constant (ζ_{np}) in the halogen atom.[41] The a →X and b →X radiative rates in the nitrogen halides do not appear to follow such a simple pattern, however. For example, the b→ X rate increases by more than a factor of twenty in going from NF to NCl, whereas $\zeta_{Cl,3p}$ is only about twice the magnitude of $\zeta_{F,2p}$.

Table III. Radiative Rates of the a →X and b→ X Transitions in Nitrogen Halides

Molecule	$T_e(a^1\Delta)$, cm^{-1}	$T_e(b^1\Sigma^+)$, cm^{-1}	A, $a^1\Delta \rightarrow X^3\Sigma^-$, (s^{-1})	A, $b^1\Sigma^+ \rightarrow X^3\Sigma^-$, s^{-1}
NF	11435.16 (a)	18877.15 (b)	0.2 (c)	44.5 ± 3.4 (d)
NCL	9260 (e)	14984.6 (f)	$4.87 \pm 0.37 \times 10^2$ (g) 6.87×10^{-1} (e)	$1.59 \pm 0.16 \times 10^3$ (h)
NBr	9226 (e)	14787.3 (i)	$1.24 \pm 0.34 \times 10^3$ (g) 2.0 (l)	$\leq 2.5 \times 10^4$ (j) $2.8 \pm 0.5 \times 10^4$ (k)

a) W.E. Jones, Can. J. Phys., 45, 21 (1967)
b) A.E. Douglas and W.E. Jones, Can. J. Phys. 44, 2251 (1966).
c) R.J. Malins and D.W. Setser, J. Phys. Chem., 85, 1342 (1981).
d) P.H. Tennyson, A. Fontijn, and M.A.A. Clyne, Chem. Phys., 62, 171 (1981).
e) A.T. Pritt, Jr., D. Patel, and R.D. Coombe, J. Mol. Spectrosc., 87401 (1981).
f) R. Colin and W.E. Jones, Can. J. Phys., 45, 301 (1967).
g) R.D. Coombe and M.H. Van Benthem, J. Chem. Phys., 81, 2984 (1984).
h) A.T. Pritt, Jr., D. Patel, and R.D. Coombe, J. Chem. Phys., 75, 5720 (1981).
i) E.R.V. Milton, H.B. Dunford, and A.E. Douglas, J. Chem. Phys., 35, 1202 (1961).
j) J.C. Miller and L. Andrews, J. Chem. Phys., 71, 5276 (1979).
k) M.A. MacDonald, S.J. David, and R.D. Coombe, J. Chem. Phys., 84, 5513 (1986).
1) A.C. Becker, J. Langen, H.M. Oberhoffer, and U. Schuarath, J. Chem. Phys., 84, 2907 (1986).

Striking differences between the transitions in NF, NCl, and NBr are also apparent in the rotational fine structure of the spectra for those cases which have been studied under high resolution. The movement from Hund's case a toward case c is evident in the increasing magnitude of the spin-spin splitting of the ground $^3\Sigma^-$ state.[42-44] This splitting is observable under moderate resolution in the NBr $b \rightarrow X$ spectrum.[45] Five branches are possible for each band in the $b \rightarrow X$ transitions. For these transitions in NCl and NBr, no ^QQ branch is observed, and the four remaining branches (^OP, ^SR, ^QP, ^QR) have roughly equal strength.[42-44] From rotational intensity relationships derived by Watson,[46] whis result indicates that these $b \rightarrow X$ transitions are strongly parallel, with $\mu_{||}$ (the parallel component of the transition moment) being much greater than $\mu_\perp$, which is near zero. All five branches are present in the $b \rightarrow X$ transition in NF, and Watson reported that $\mu_\perp : \mu_{||} = 7:1$ for this case. A recent review of these calculations by Yarkony,[47] however, has indicated that $\mu_\perp$ is in fact greater than $\mu_\perp$ for NF $b \rightarrow X$, the ratio being $\mu_{||} : \mu_\perp \approx 3.8$.

This kinetic and spectroscopic information suggests the contributions of different basis sets to the $X^3\Sigma^-$, $a^1\Delta$, and $b^1\Sigma^+$ wavefunctions in NF, NCl, and NBr. It would seem reasonable that these differences would be apparent from a first order perturbation treatment of the wavefunctions in which the mixing coefficients are given by spin-orbit matrix elements divided by the energy separations between the mixed states. Approximate values of the matrix elements in question can be determined from a consideration of one-electron interactions in the molecular orbitals and estimated values of the spin-orbit coupling strength in these orbitals. The states most likely to be involved in mixing are those arising from the lowest energy excited electronic configurations $\pi^3\pi^{*3}$ and $\pi^4\pi^*\sigma^*$. The

$\pi^3 \pi^{*3}$ configuration gives rise to states $^1\Sigma^+$, $^1\Sigma^-$, $^3\Sigma^+$, $^3\Sigma^-$, $^1\Delta$, and $^3\Delta$. The $^3\Sigma^-$ state of this configuration is well known for the group VIA diatomics O_2,[48] S_2,[49] SO,[50] and SeO.[51] The $\pi^4 \pi^* \sigma^*$ configuration gives rise to $^1\Pi$ and $^3\Pi$ states. The $^3\Pi$ states of this configuration are known for SO,[52] S_2,[53] PF,[54] and for the isoconfigurational molecule NH.[55] The $^1\Pi$ state has been observed in PF[54] and NH. None of these excited states have been experimentally observed for any of the nitrogen halides, however. Considering these states and the selection rules for spin-orbit mixing, only a few possible interactions might lend appreciable probability to the a $\rightarrow$X and b$\rightarrow$ X transitions observed. First, the $(\pi^4 \pi^* \sigma^*)\ ^1\Pi$ state could mix with the Ω=1 component of the $X^3\Sigma^-$ ground state, affecting both the a$\rightarrow$X and b$\rightarrow$ X radiation rates. The Ω=2 multiplet of the $(\pi^4 \pi^* \sigma^*)^3\Pi$ state could mix with the $a^1\Delta$ state, allowing transitions to the pure $X^3\Sigma^-$ ground state. Similarly, the $^3\Pi_0$ multiplet might mix with the $b^1\Sigma^+$ state. A fourth possibility involves mixing of the $(\pi^3 \pi^{*3})^3\Sigma^-$ state with the $b^1\Sigma^+$ state. It is also possible that the $b^1\Sigma^+$ state could mix with the Ω=0 component of the $X^3\Sigma^-$ ground state, although both arise from the same configuration. It is questionable how much this latter interaction would affect the b$\rightarrow$X radiation rate, however, since the $b^1\Sigma^+$ state would acquire the character of a vibrational level of the ground state. Presumably, the observed radiation rates reflect some combination of all these individual interactions.

The wavefunctions of the states may be designated as combinations of spin-orbitals in the following manner, where m_l=1, m_s=1/2 for $\pi\alpha$ and m_l=-1, m_s=-1/2 for $\bar{\pi}\beta$:

$(\pi^4\pi^{*2})\ |^3\Sigma_1^-\rangle$: $\pi^*\alpha\,\bar{\pi}^*\alpha$

$(\pi^4\pi^{*2})\ |^3\Sigma_0^-\rangle$: $2^{-1/2}(\pi^*\alpha\,\bar{\pi}^*\beta + \pi^*\beta\,\bar{\pi}^*\alpha)$

$(\pi^4\pi^{*2})\ |^1\Delta_2\rangle$: $\pi^*\alpha\,\pi^*\beta$

$(\pi^4\pi^{*2})\ |^1\Sigma_0^+\rangle$: $2^{-1/2}(\pi^*\alpha\,\bar{\pi}^*\beta - \pi^*\beta\,\bar{\pi}^*\alpha)$

$(\pi^3\pi^{*3})\ |^3\Sigma_0^-\rangle$: $2^{-1}(\pi\alpha\bar{\pi}^*\beta + \pi\beta\bar{\pi}^*\alpha - \bar{\pi}\alpha\pi^*\beta - \bar{\pi}\beta\pi^*\alpha)$

$(\pi^4\pi^*\sigma^*)\ |^1\Pi_1\rangle$: $2^{-1/2}(\pi^*\alpha\,\sigma^*\beta - \pi^*\beta\,\sigma^*\alpha)$

$(\pi^4\pi^*\sigma^*)\ |^3\Pi_0\rangle$: $2^{-1/2}(\pi^*\beta\,\sigma^*\beta - \bar{\pi}^*\alpha\,\sigma^*\alpha)$

$(\pi^4\pi^*\sigma^*)\ |^3\Pi_2\rangle$: $\pi^*\alpha\,\sigma^*\alpha$

The Hamiltonian operator for spin-orbit coupling is given by $\hat{H}_{so} = a_i l_i \cdot s_i$ where l_i and s_i are individual one electron orbital and spin angular momentum operators. The terms a_i contain the r dependent portion of $\hat{H}_{so}$; the expectation value of the operator $\hat{a}_i$ is the spin-orbit coupling constant ζ_i. As an example, consider mixing of the $(\pi^4\pi^*\sigma^*)\ ^1\Pi_1$ state into $(\pi^4\pi^{*2})\ ^3\Sigma_1^-$. For this case, the matrix element of the spin-orbit operator is written as follows:

$$\langle {}^3\Sigma_1^- | \hat{H}_{so} | {}^1\Pi_1 \rangle = 2^{-1/2} \langle \pi^*\alpha\,\bar{\pi}^*\alpha | \hat{H}_{so} | \pi^*\alpha\,\sigma^*\beta - \pi^*\beta\,\sigma^*\alpha \rangle . \quad (9)$$

If only one electron interactions are considered, this expression reduces to

$$\langle {}^3\Sigma_1^- | \hat{H}_{so} | {}^1\Pi_1 \rangle = 2^{-1/2} \langle \bar{\pi}^*\alpha | \hat{H}_{so} | \sigma^*\beta \rangle . \quad (10)$$

If the spin orbit operator is written as $H_{so} = \hat{a}(l_z s_z + 1/2\ l^+ s^- + 1/2\ l^- s^+)$, the matrix element can be written as

$$\begin{aligned} \langle {}^3\Sigma_1^- | \hat{H}_{so} | {}^1\Pi_1 \rangle &= (2^{-1/2})(1/2) \langle \pi^*\alpha | \hat{a} l^- s^+ | \sigma^*\beta \rangle \quad (11) \\ &= 1/2 \langle \bar{\pi}^* | \hat{a} | \bar{\pi}^* \rangle \\ &= 1/2\, \zeta_{\bar{\pi}^*} , \end{aligned}$$

where $\zeta_{\bar{\pi}^*}$ is the spin-orbit coupling strength in the $\bar{\pi}^*$ molecular orbital.

The values of $\zeta_{\pi^*} = \zeta_{\pi^*}$ may be estimated from the spin-orbit coupling constants in the nitrogen and halogen atoms. If the molecule in question, say NCl, were covalent, then $\zeta_{\pi^*} = 1/2\ (\zeta_{N,2p} + \zeta_{Cl,3p}) = 330\ cm^{-1}$. From consideration of the ionization potentials and electron affinities of the atoms, NCl and NBr are expected to be covalent or slightly polarized toward the nitrogen atom. For the ionic molecule N^-Cl^+, $\zeta_{\pi^*} = 1/2\ (\zeta_{N^-,2p} + \zeta_{Cl^+,3p}) = 365\ cm^{-1}$, very similar to the result for the covalent case. Hence in these two molecules, ζ_{π^*} is expected to be near the covalent value. Table IV shows a collection of spin-orbit matrix elements calculated in the manner described above, assuming covalent values for ζ_{π^*} in NCl and NBr. In NF, the direction of the dipole should be inverted with the fluorine atom bearing a partial negative charge. For N^+F^-, $\zeta_{\pi^*} = 1/2\ (87.5 + 0) = 44.3\ cm^{-1}$, whereas ζ_{π^*} for covalent NF is calculated to be $173\ cm^{-1}$. Hence if NF were significantly ionic, the matrix elements could be much smaller than calculated for the covalent case.

Table IV. Spin-Orbit Matrix Elements for interactions in NCl and NBr[a]

Matrix Element	NCl (cm^{-1})	NBr (cm^{-1})
$\langle X^3\Sigma_1^-(\pi^4\pi^{*2}) \lvert \hat{H}_{so} \rvert {}^1\Pi, (\pi^4\pi^*\sigma^*)\rangle$	165	633
$\langle a^1\Delta_2(\pi^4\pi^{*2}) \lvert \hat{H}_{so} \rvert {}^3\Pi_2(\pi^4\pi^*\sigma^*)\rangle$	233	896
$\langle b^1\Sigma_0^+(\pi^4\pi^{*2}) \lvert \hat{H}_{so} \rvert {}^3\Pi_0(\pi^4\pi^*\sigma^*)\rangle$	233	986
$\langle b^1\Sigma_0^+(\pi^4\pi^{*2}) \lvert \hat{H}_{so} \rvert {}^3\Sigma_0^-(\pi^3\pi^{*3})\rangle$	0	0

(a) Calculated assuming the molecules to be covalent.

The calculated matrix elements can be related to measured radiation rates by using first order perturbation theory. The perturbed wavefunction of a state $|n_o\rangle$ is written as

$$|n\rangle = |n_o\rangle + \sum_{\ell} \left(\frac{\langle n_o | \hat{H}_{so} | \ell \rangle}{\Delta E} \right) |\ell\rangle \qquad (12)$$

where $|n_o\rangle$ is the wavefunction of the unperturbed stated and ΔE is the energy separation between $|n_o\rangle$ and $|\ell\rangle$. Since radiation from the pure state $|n_o\rangle$ to a lower energy state $|m\rangle$ is strictly forbidden for the $a \rightarrow X$ and $b \rightarrow X$ transitions under consideration, the spontaneous emission rate is given by

$$A_{nm} = \left(\frac{64 \pi^4 \bar{\nu}^3}{3h} \right) \sum_{\ell} \left(\frac{\langle n_o | \hat{H}_{so} | \ell \rangle}{\Delta E} \right)^2 |R_e|^2_{\ell m} \qquad (13)$$

where $|R_e|^2_{\ell m}$ is the square of the electric dipole transition moment between states $|\ell\rangle$ and $|m\rangle$. It is assumed that the electric dipole moment is independent of the r-centroid such that $\bar{\nu}^3 = \sum \bar{\nu}^3_{v'v''} q_{v'v''}$, where $q_{v'v''}$ are the Franck-Condon factors for individual bands.

Among the possible mixing schemes considered, the $a \rightarrow X$ radiation rate is affected only by mixing of the $^1\Pi_1$ state into $X^3\Sigma_1^-$ or by mixing of the $^3\Pi_2$ state into $a^1\Delta_2$. Since the calculated matrix element is smaller and the energy separation larger for the $^1\Pi_1 - {}^3\Sigma_1^-$ perturbation, it is reasonable to assume that the $^3\Pi_2 - {}^1\Delta_2$ interaction dominates the radiation rate. Since $\Delta\Omega = 1$ for the $^3\Pi - {}^3\Sigma^-$ transition, this perturbation should give rise to a strong perpendicular component in the $a \rightarrow X$ transition, as is found in NF. For the case where perturbation by one state dominates the wavefunction, the energy separation between the mixed states may be calculated from the measured value of A_{nm}, (Table III), the spin-orbit matrix element (Table IV), and the electric dipole transition moment $|R_e|_{1m}$.

The latter quantity has not been measured for the nitrogen halides (since the $^3\Pi$ states have not been observed), but calculated values of $^3\Pi - ^3\Sigma^-$ transition dipole moments have been reported by Wayne and Colbourn[56] in an ab initio study of open shell diatomics. Using the transition moment reported by these authors, the $^3\Pi_2 - ^1\Delta_2$ energy separation in NCl is calculated to approximately 9500 cm^{-1}, placing the $^3\Pi_2$ state about 18,800 cm^{-1} above the ground state. Assuming this state to dissociate to ground state atoms, it would be bound by about 6000 cm^{-1}. This result seems quite reasonable in light of the binding energies of the $^3\Pi$ states of S_2, SO, and PF.[52-54] Wayne and Colbourn do not report a $^3\Pi - ^3\Sigma^-$ transition moment for NBr. If the $^3\Pi - ^1\Delta$ energy separation in NBr were near that calculated for NCl, however, the data in Tables III and IV would suggest a $^3\Pi - ^3\Sigma^-$ transition moment about one half that reported for NCl. A similar calculation for NF, using the spin-orbit matrix element for covalent bonding, results in a $^3\Pi - ^1\Delta_2$ energy separation on the order of 10^5 cm^{-1}. It would seem that, if the $^3\Pi - ^3\Sigma^-$ transition moment reported by Wayne and Colbourn is correct, the spin-orbit matrix element coupling the $^3\Pi_2$ and $^1\Delta_2$ states in NF must be very small indeed, suggesting a strong ionic contribution to the bond.

A fundamental problem brought out by these calculations is that if the $^3\Pi_2$ state is strongly coupled to the $^1\Delta_2$ state in NCl and NBr, so must the $^3\Pi_0$ state be coupled to $b^1\Sigma_0^+$ since the spin-orbit matrix elements for these two interactions are the same. If mixing with the $^3\Pi$ states were to dominate both the $a \rightarrow X$ and $b \rightarrow X$ radiation rates, then the ratio of these rates would be given by

$$\frac{A_{b\to X}}{A_{a\to X}} = \frac{\left(\bar{\nu}_{b\to X}\right)^3}{\left(\bar{\nu}_{a\to X}\right)^3} \times \left(\frac{\Delta E\ {}^1\Delta - {}^3\Pi}{\Delta E\ {}^1\Sigma^+ - {}^3\Pi}\right)^2 \qquad (14)$$

where the ${}^3\Pi_0 - {}^3\pi_2$ energy separation is assumed to be small. In this case, the $a \to X$ radiative rate in NCl would suggest a $b \to X$ rate significantly larger than the measured value, unless the ${}^3\Pi$ states were to lie between the $a^1\Delta_2$ and $b^1\Sigma_0^+$ states, an unlikely prospect. In any case, the ${}^3\Pi_0$ states cannot be strongly mixed into the $b^1\Sigma^+$ states of NCl and NBr, since this interaction would give rise to a strong perpendicular component in the transition moment. Interaction of the ${}^1\Pi_1$ state with the $X^3\Sigma^-$ ground state cannot contribute to the $b \to X$ transition moment for the same reason. As noted above, $\mu_\perp$ is thought to be near zero in these transitions. The calculated matrix elements would suggest that the $a \to X$ radiation rate in NCl would have to be more than 18 times smaller than our experimental result in order that the ${}^3\Pi_0 - {}^1\Sigma_0^+$ interaction contribute less than 10% of the measured $b \to X$ radiation rate. this would, of course, be possible if the radiative rates reported by Becker, et al,[40] were correct.

The parallel nature of the $b \to X$ transitions in NCl and NBr indicates that the wavefunctions in question are perturbed only by other Σ states. Two such interactions are possible among those considered above. First, the $b^1\Sigma_0^+$ state can mix with the ${}^3\Sigma_0^-$ state of the $\pi\,{}^3\pi^{*3}$ configuration. The one electron calculations suggest the spin-orbit matrix element for this interaction to be zero, however. A second possibility is mixing of the $b^1\Sigma^+_0$ state with the ground $X^3\Sigma^-_0$ state of the same configuration. In this case, the $b^1\Sigma^+$ state would acquire the character of a vibration-rotation level in the $X^3\Sigma^-$ state. Franck-Condon factors would strongly

favor mixing between like vibrational levels in the b and X states, producing an intense $\Delta v=0$ sequence in the emission spectrum, as is actually observed. For this mechanism, the transition dipole moment would reduce to a spin-orbit mixing coefficient multiplied by the difference between the permanent dipole moments of the b and X states.[56] Calculations similar to those described above yield a matrix element $H_{so}=330\ cm^{-1}$ for this interaction in NCl. Experimental values for the dipole moments of the b and X states of this molecule are unknown, but Wayne and Colbourn[56] report calculated values for these parameters. Using these values, a $b \rightarrow X$ radiative rate $A=44\ sec^{-1}$ is calculated for this mixing scheme, many times smaller than the actual value $A=1590\ sec^{-1}$. In order for this mechanism to account for the observed rate, H_{so} would have to be about $1982\ cm^{-1}$, six times greater than the calculated value.

Although these simplified one electron calculations of the matrix elements serve to indicate, in a qualitative way, the contributions of various states to the $a \rightarrow X$ and $b \rightarrow X$ radiation rates, it is apparent that they cannot quantitatively account for the experimental results. It is gratifying to observe that recent, more detailed calculations on these systems by Yarkony[47] and by Peyerimhoff[57] have begun to unravel some of these issues.

IV. Collisional Decomposition of Halogen Azides

Halogen azides are metastable molecules capable of releasing substantial amounts of energy upon photolysis or reaction with various atomic species. These processes tend to produce excited metastable fragments or products which may subsequently react with the parent azide. Hence, it is expected that chain decomposition mechanisms might readily occur in halogen azide systems, and indeed qualitative evidence of such chains has been reported. Piper and co-workers,[58] in studies of the photochemistry of ClN_3 and HN_3, found that near UV photolysis of a small portion of a sample of ClN_3 resulted in dissociation of the entire sample, whereas similar experiments with HN_3 showed no such effect. Combourieu and co-workers[18] discussed the possible operation of chain processes in reactions of ClN_3 studied with a discharge-flow system. Recently, Setser and co-workers[59] have determined the rate constant for $N_2(A)$ quenching by HN_3 to be 8.5×10^{-11} cm^3s^{-1}. This result is in contrast to the rate constant for $N_2(A)$ quenching by BrN_3 inferred from earlier BrN_3 photolysis experiments,[1] 1.2×10^{-12} cm^3s^{-1}. It seems most unlikely that $N_2(A)$ quenching by BrN_3, a molecule much more fragile than HN_3, would be nearly 50 times slower than quenching by HN_3. Hence, the time decay of $N_2(A)$ in the BrN_3 system may well reflect the influence of chemical processes regenerating these metastables, rather than direct pseudo-first order relaxation in collisions with the azide. The work described in this section has sought to examine the mechanisms of such collision processes, with particular interest in the role of metastable excited species.

Generation and Quenching of $N_2(A\ ^3\Sigma_u^+)$ in ClN_3 Photolysis

It has been shown previously that photolysis of ClN_3 at 193nm or 249nm produces either $NCl(b^1\Sigma^+)$ by a process analogous to 1a above, or $N_2(A^3\Sigma_u^+)$ by a process analogous to 1c. Based on these results, we performed a number of experiments in which the time decay of the $N_2(A)$ produced by photodissociation was monitored subsequent to the laser pulse. This was accomplished by adding a trace amount of NO to the ClN_3 flow, such that the intensity of the NO γ bands $(A^2\Sigma^+ \rightarrow X^2\Pi)$ reflected the density of the N_2 metastables. A typical $N_2(A)$ time profile measured in this manner is shown in Figure 16. The decay clearly exhibits both a fast and a slow component. For fixed ClN_3 flow, variation of the laser fluence had no observable effect on the $N_2(A)$ time decay, suggesting that pseudo-first order processes involving the parent azide are dominant.

In order to study these processes in the absence of NO, N_2 second positive $(C^3\Pi_u \rightarrow B^3\Pi_g)$ emission present in the system was monitored. Previous experiments[4] have shown that this emission is produced by $N_2(A)$ energy pooling, and its intensity varies as the square of the $N_2(A)$ density. Pseudo-first order $N_2(A)$ decay rates were obtained from logarithmic plots of the square root of the second positive intensity vs. time. These plots were quite linear in the time frame of the fast component of the decay. Decay rates were determined from the slopes of such plots for a number of ClN_3 densities, and the results are shown in Figure 17. From the linearity of the plot and its intercept near the origin, and the insensitivity of the decay to laser fluence as noted above, the fast component of the decay is assigned to $N_2(A)$ quenching by the parent ClN_3. From the slope of the plot, the rate constant of the process is determined to be $5.1 \pm 0.3 \times 10^{-11}$ cm^3s^{-1}.

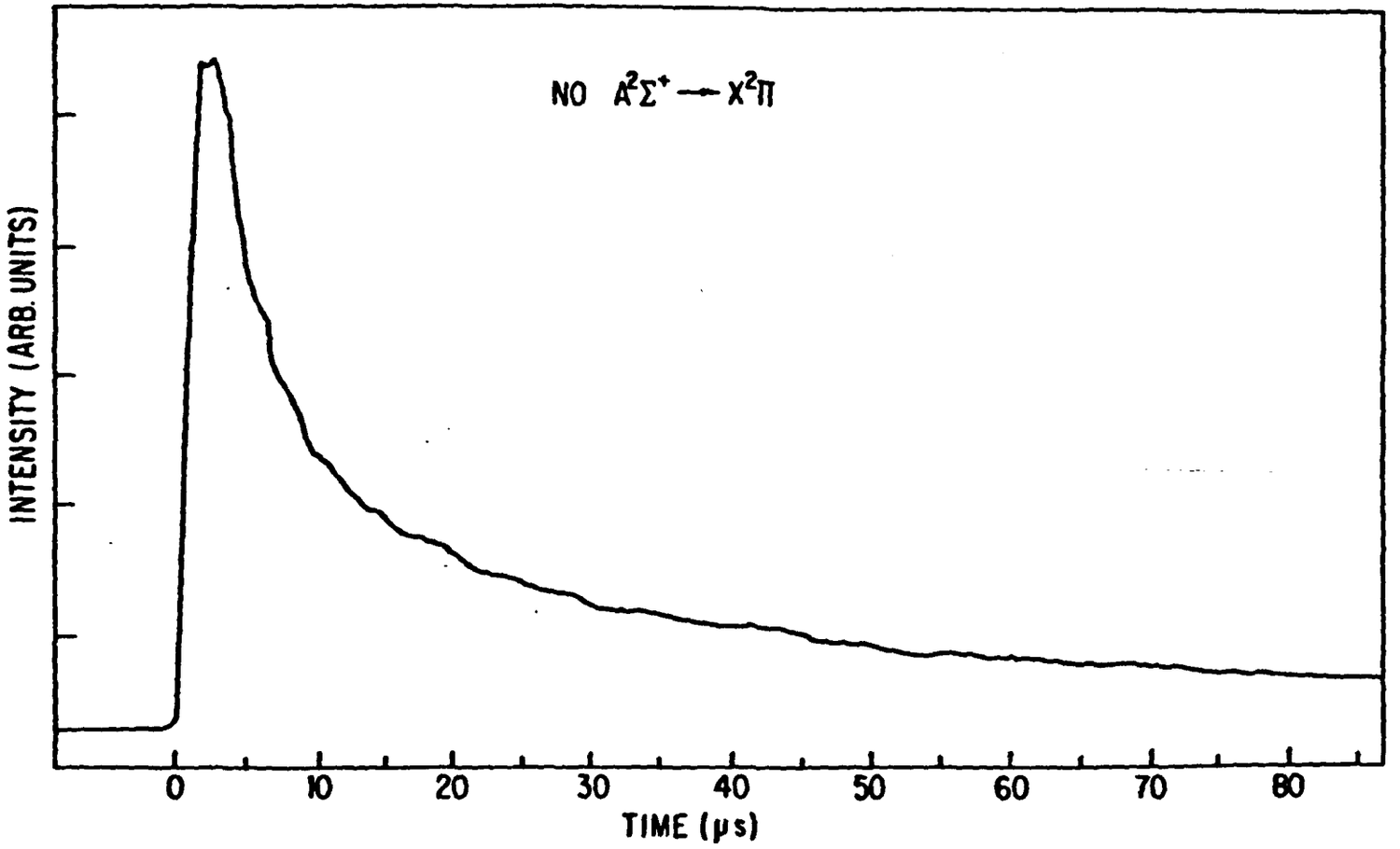

Figure 16. Time profile of $N_2(A)$ density (tracked by NO γ band emission) produced by 193 nm photolysis of ClN_3.

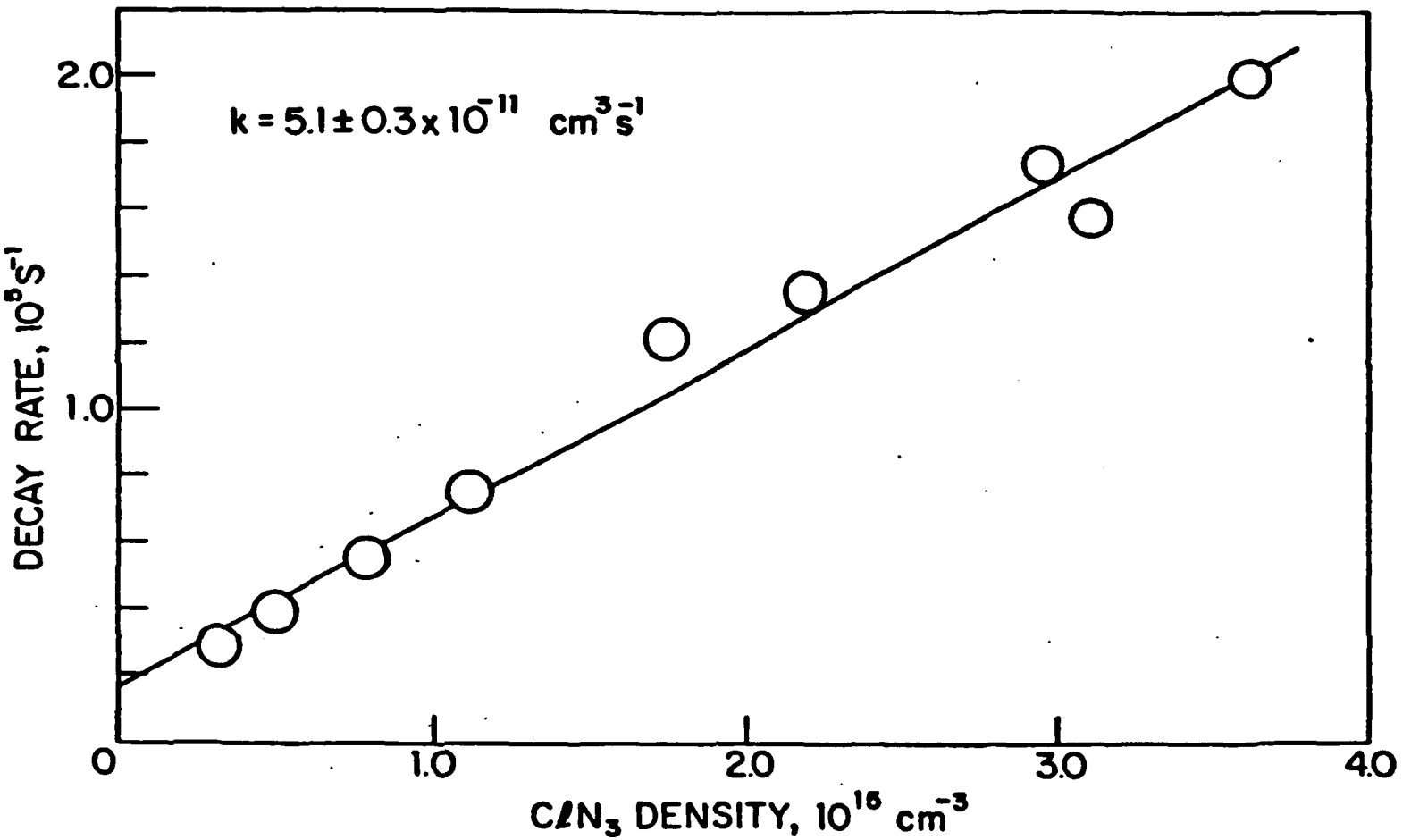

Figure 17. Plot of the decay rate of the $N_2(A)$ density produced from photodissociation of ClN_3 (monitored from the square root of the N_2 C→B emission) vs. the ClN_3 density.

In order to verify the assignment of the fast component to quenching in ClN_3, a series of experiments were performed in which the rate constant for this process was independently measured using a continuous discharge-flow apparatus. The flow reactor was a 2.54 cm inner diameter pyrex tube pumped by a 500 l min^{-1} mechanical pump. $N_2(A)$ was produced in a sidearm by admission of N_2 to a flow of Ar ($^3P_{0,2}$) metastables, which were generated by passage of argon through a low-current dc discharge. The density of $N_2(A)$ downstream of the discharge was monitored by admission of trace quantities of NO just upstream of a fixed observation port, where a solar-blind PMT detected NO γ band emission. The ClN_3/N_2 mixture entered the flow through a sliding injector. $N_2(A)$ time decays were determined from the NO γ band intensity (linear with the $N_2(A)$ density) vs. the position of the azide injector. The $N_2(A)$ decay times were such that formation of a parabolic flow profile from quenching of the metastables at the reactor walls was not a factor. The measured decays were found to be exponential, the decay rates (s^{-1}) varying linearly with the ClN_3 flow. Figure 18 shows a plot of the data. From the slope of the plot, the rate constant for $N_2(A)$ quenching by ClN_3 is determined to be $6.2 \pm 0.4 \times 10^{-11}$ $cm^3 s^{-1}$, in very good agreement with the value determined from pulsed photolysis of ClN_3 (Figure 17). Similar experiments were performed to determine the rate constant for $N_2(A)$ quenching by HN_3. These data yielded a value $k_{HN_3} = 7.3 \pm 0.2 \times 10^{-11}$ $cm^3 s^{-1}$, in good agreement with that recently reported by Setser and co-workers[59] this process. The mechanism for $N_2(A)$ quenching by HN_3 is well known. HN_3 is dissociated via a spin-allowed route to produce excited $NH(A^3\Pi)$:

$$N^2(A^3\Sigma_u^+) + HN_3(X^1A') \rightarrow 2N_2(X^1\Sigma_g^+) + NH(A^3\Pi) \quad . \qquad (15)$$

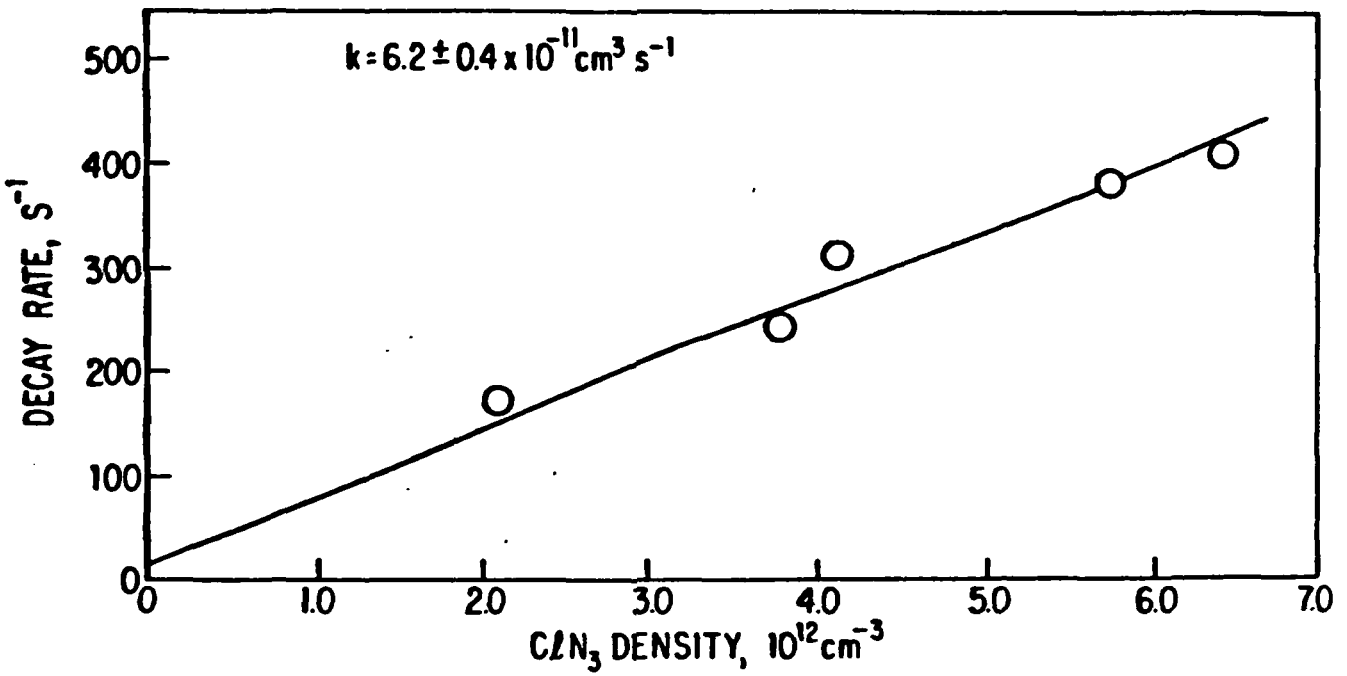

Figure 18. Rate of decay of $N_2(A)$ produced in a discharge-flow system vs. the density of added ClN_3.

This process generates intense NH A→X emission near 336nm. In contrast, no UV or visible emission was observed from $N_2(A)$ quenching by ClN_3, suggesting that exceited triplet states of NCl generated by a process analogous to (15) may be repulsive.

The agreement between the discharge-flow and pulsed data for $N_2(A)$ quenching by ClN_3 indicates that our assignment of the fast decay component in Figure 16 to pseudo-first order quenching by ClN_3 is correct. The presence of the slow component of the decay indicates that pseudo-first order quenching of the initial $N_2(A)$ density does not remove all the metastables. It would seem that some process generating $N_2(A)$ is operative after the laser pulse. This process may well be chain decomposition of the azide. We infer also that the slow decay of the $N_2(A)$ density after photolysis of BrN_3 at 222nm (as described in ref. 1) likely represents some collisional formation process rather than pseudo-first order quenching by BrN_3. It seems most unlikely that $N_2(A)$ quenching by BrN_3 would be 47 times slower than quenching by ClN_3.

Collisional Decomposition of Bromine Azide

Within the context of the results noted above, the mechanism and kinetics of the collisional decomposition of BrN_3, stimulated by reaction or photolysis, was investigated. Data were obtained from several different kinds of discharge-flow experiments, and the results synthesized into a unified kinetic model for the decomposition mechanism.

1. $N_2(A^3\Sigma_u^+)$ Quenching by Bromine Azide

The time decay of $N_2(A)$ in the presence of excess flows of BrN_3 was measured using the NO tracer method as described above. The $N_2(A)$-BrN_3 interaction produced no emission visible to the eye. The $N_2(A)$ decay

profiles showed two distinct components, however, as shown in Figure 19. This behavior is similar to that observed from ClN_3 photolysis and shown in Figure 16. By analogy, it is expected that the initial rapid decay in Figure 19 corresponds to pseudo-first order quenching of $N_2(A)$, and the subsequent slow decay corresponds to regeneration of the metastable. Determination of the rate constant for pseudo-first order quenching by BrN_3 from such data is complicated by the presence of a substantial Br_2 impurity in the flow. This impurity arises from the finite efficiency of the BrN_3 generator and decomposition of BrN_3 during transport to the flow reactor. Hence, a series of separate experiments were performed in which the rate constant for $N_2(A)$ quenching by added Br_2 was determined. These data yielded a value $k_{Br_2}=1.0 \pm 0.2 \times 10^{-10}$ $cm^3 s^{-1}$, in good agreement with results recently reported by Cao and Setser.[60]

For experiments in which the rapid component of the $N_2(A)$ decay in the presence of BrN_3/Br_2 was observed, the data were correlated to a rate expression

$$\lambda = k'[BrN_3]+k[Br_2] \qquad (16)$$

where k' is the rate constant for quenching by BrN_3 and k is the rate constant for quenching by Br_2. The BrN_3 density was determined by on-line measurement of the UV and IR absorption spectra of the azide generator effluent, and the Br_2 density was taken as the difference between that corresponding to the initial Br_2 flow entering the generator and the measured BrN_3 density. Figure 20 shows a plot of $\lambda - k[Br_2]$ vs. $[BrN_3]$. Although the data exhibit considerable scatter (reflecting the deconvolution procedure), a linear correlation is apparent. The slope of the least-squares line drawn through the data yields a value

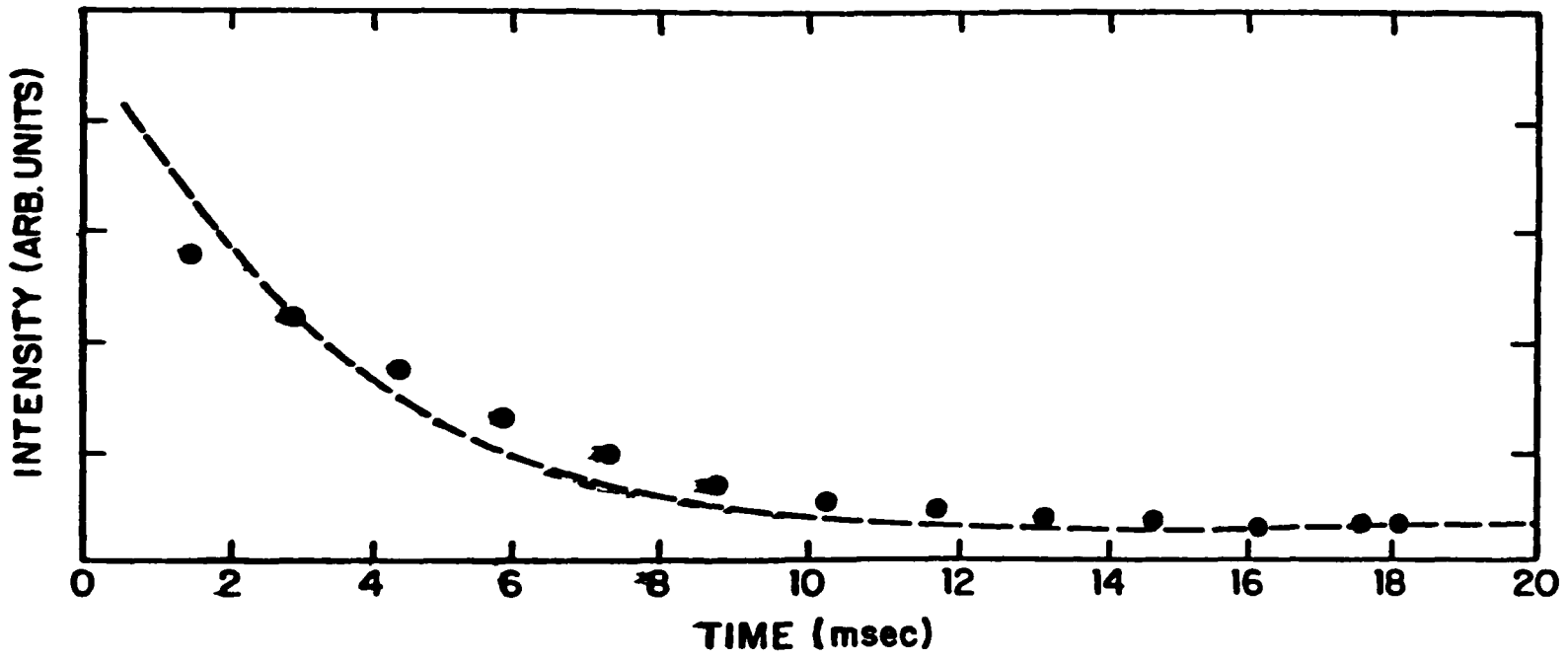

Figure 19. Time decay of $N_2(A)$ (produced in a discharge-flow system) in the presence of BrN_3. Broken line is a fit to the data with a kinetic model described in the text.

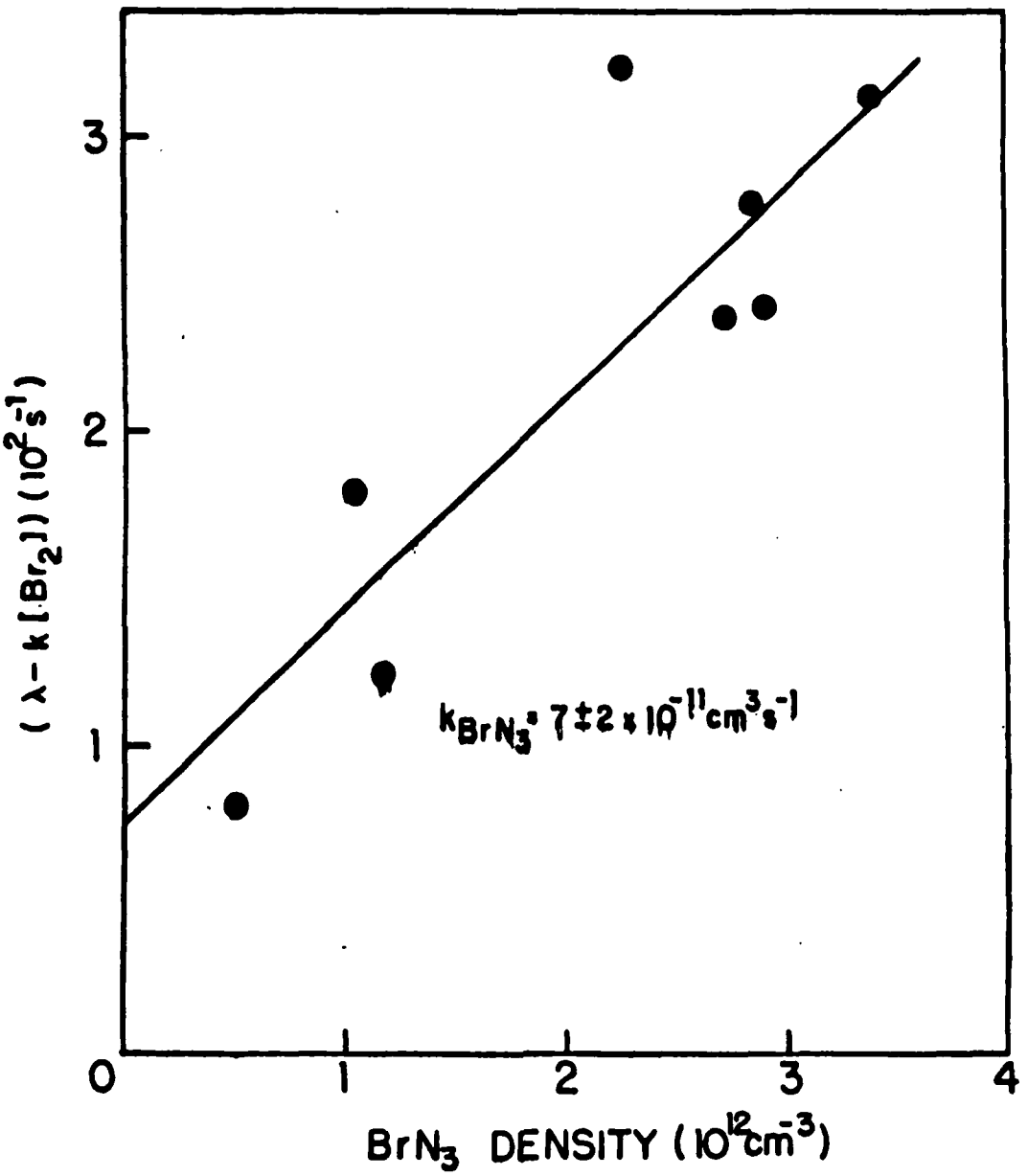

Figure 20. Rate of decay of $N_2(A)$, corrected for quenching by Br_2, vs. the density of BrN_3.

$k'=7 \pm 2X10^{-11}$ cm^3s^{-1}. This value is very similar to those noted above for $N_2(A)$ quenching by ClN_3 and HN_3.

2. Chemiluminescent Reactions of BrN_3

The reaction of BrN_3 with excess N atoms was studied with a standard discharge-flow apparatus. Nitrogen atoms were produced by passage of N_2, diluted in Ar, through a 100 W microwave discharge cavity. The density of N atoms in the stream, typically greater than 10^{13} cm^{-3}, was determined by titration with NO. Admission of small flows of BrN_3 (initial density $<10^{12}cm^{-3}$) to this stream produced a bright orange flame, whose spectrum identified the emission as bands of the first positive ($B^3\Pi_g \rightarrow A^3\Sigma_u^+$) transition in N_2. An analysis of the intensities of the various bands indicated a vibrational distribution favoring the lower v levels of the $B^3\Pi_g$ state. The vibrational distribution was reasonably well fit by an equilibrium (thermal) distribution corresponding to $T_{vib} \approx 10,000K$. This distribution (and consequently the visual appearance of the flame) is quite similar to that observed in previous experiments with the $N+N_3$ chemiluminescent reaction.[12] The absolute yield of N_2 $B \rightarrow A$ photons from this system was determined by calibrating the efficiency of the detection system with the O+NO chemiluminescent reaction. This procedure has been described in detail previously.[2] The average photon yield obtained from several measurements was $\Phi \approx 30\%$. As with all such measurements, the uncertainty in this result is a minimum of 50% of the stated yield. Nonetheless, the data clearly indicate that the photon yield is in fact quite large and is on the order of that previously determined[12] for the $N+N_3$ reaction (20%).

A typical time profile of the N_2 emission is shown by the data in Figure 21. The profile exhibits a rise over a few ms followed by a very

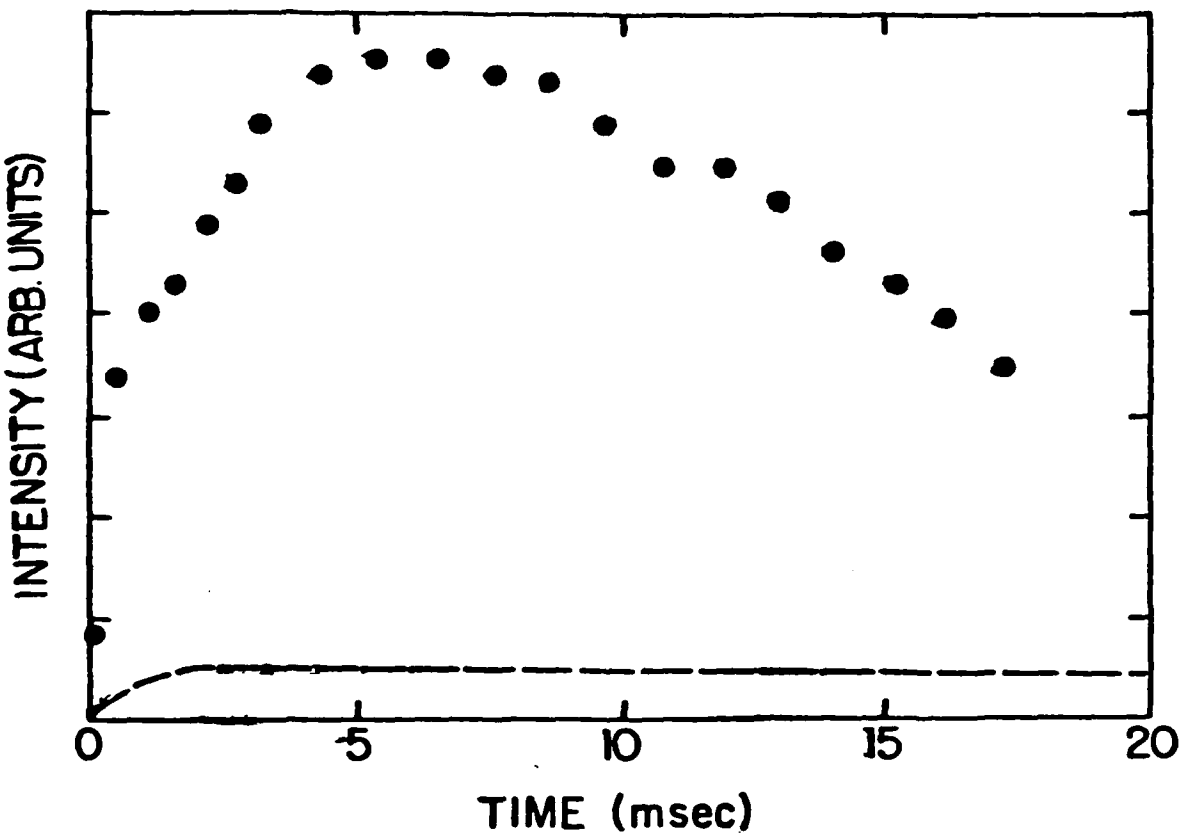

Figure 21. Time profile of N_2 B A chemiluminescence produced by the interaction of BrN_3 with active nitrogen (closed circles). Broken line is the best fit obtained with a kinetic model described in the text.

long decay (several ms). Since the radiative lifetime of $N_2(B)$ is about 6 μs, the time profile is tracking the density of an intermediate in the production mechanism. From the information above, it seems plausible that this intermediate is N_3.

The reaction of bromine atoms with BrN_3 was studied by replacing the active N_2 flow in the experiments described above by a flow of Br_2/Ar which had been passed through the microwave discharge. For these experiments, the flow reactor was coated with halocarbon wax to reduce the loss of Br atoms at the reactor walls. The Br/BrN_3 reaction produced a visible emission whose spectrum is shown in Figure 22. The spectrum shows bands from two systems, which are the $b^1\Sigma^+ \rightarrow X^3\Sigma^-$ transition of NBr and the $B^3\Pi_g \rightarrow A^3\Sigma_u^+$ transition in N_2. As the flow of Br_2 (and hence Br atoms) was reduced, the NBr features diminished in intensity relative to the N_2 features. The N_2 first positive bands dominated at very low Br_2 flows. These data also suggest the action of N_3 radicals, since the Br+N_3 reaction is known to produce NBr($b^1\Sigma^+$). The data indicate a competition between Br and N atoms present in the flow (the latter from decomposition of the azide) for available N_3 radicals.

3. Reactions of N Atoms with Molecular Azides

These experiments made use of a flow reactor equipped with an apparatus for detecting relative densities of N atoms in the flow via vacuum UV resonance fluorescence on the $^4S-^4P$ transition near 120nm. The resonance fluorescence apparatus was fixed at the end of the flow reactor and detected N atoms produced by a microwave discharge in N_2 heavily diluted in Ar. Molecular azides were added to the flow through a sliding injector which could be moved along the axis of the flow reactor. Experiments were performed in which N atom removal by BrN_3, ClN_3, and HN_3

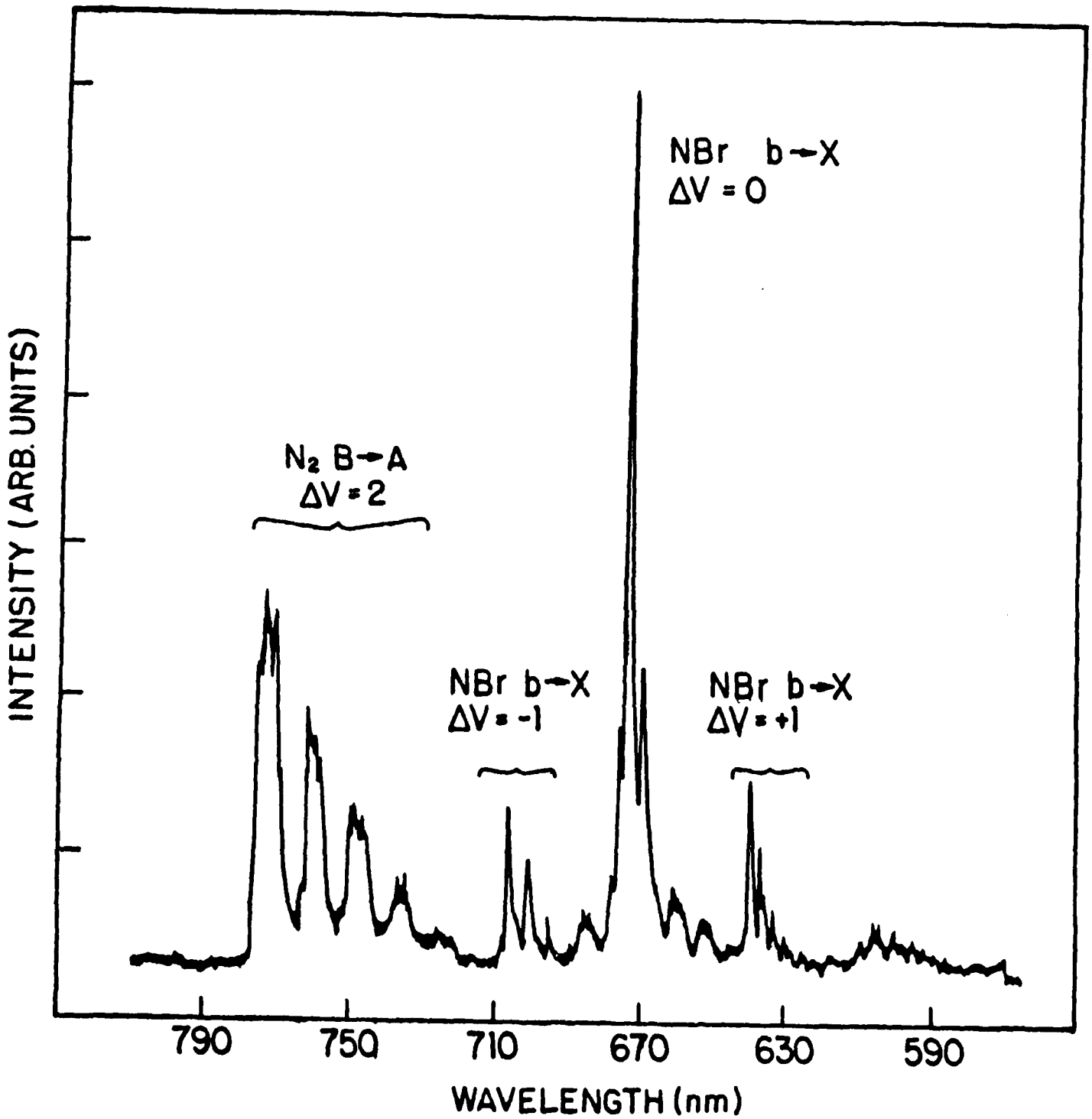

Figure 22. Spectrum of visible emission from the reaction of BrN_3 with Br atoms in a discharge-flow system.

was measured. In each case, the N atom density was found to decay a maximum of 20% over the length of the flow reactor (~50cm) for the highest azide flows. From these data, rate constants for reaction of $N(^4S)$ atoms with these species would appear to be no greater than $1.5X10^{13}cm^3s^{-1}$.

During the course of the $N+BrN_3$ experiments, emission spectra recorded around 150nm were found to exhibit a number of distinct features attributable to excited states of bromine atoms. These same features were found when Br_2 was added to the N atom stream. From the time profile of this emission, the generation of the excited Br atoms is much more rapid than the loss of N atoms from the system. From such observations, it seems that the chemistry in the $N+BrN_3$ system may well occur at a much faster rate than is implied by the apparent loss of N atoms. It is possible that the $N+BrN_3$ reaction regenerates the atoms, by a process such as

$$N+BrN_3 \rightarrow NBr+N+N_2 \qquad (17)$$

Excited bromine atoms might then be generated by a mechanism such as that suggested by Phillips:

$$N+NBr \rightarrow N_2^*+Br \qquad (18)$$

$$N_2^*+Br \rightarrow N_2+Br^* \qquad (19)$$

where N_2^* and Br^* are electronically excited species.

4. Model for the Decomposition Mechanism

As noted above, the time profile of the N_2 first positive emission generated by the interaction of BrN_3 with active nitrogen suggests the action of an intermediate, rather than direct production of the excited N_2 by reaction of BrN_3 with nitrogen atoms. From a number of observations, it would appear likely that reactions of free N_3 radicals are responsible for the excited species observed in these discharge-flow experiments. For

example, the N_2 first positive emission produced by the BrN_3-active nitrogen system is very similar to that produced by the $N+N_3$ reaction. The emission from $Br+BrN_3$ resembles that from the isolated $Br+N_3$ reaction. Hence, it would seem likely that N_3 is an important intermediate in BrN_3 decomposition. Further, it is apparent from the $N_2(A)$ quenching data that interaction of these metastables with BrN_3 or ClN_3 initiates chemical processes which regenerate the $N_2(A)$ subsequent to its initial relaxation. Given that the $N+N_3$ reaction is known to produce a high yield of $N_2(B)$ (and hence $N_2(A)$), azide radicals may also be important in these experiments.

Based on these observations, we propose the following general model for the decomposition of BrN_3:

$N_2(A)+BrN_3 \rightarrow 2N_2(X)+Br+N$	$k=7X10^{-11}cm^3s^{-1}$	(20)
$N_2(A)+Br_2 \rightarrow N_2(X)+2Br$	$k=1.0X10^{-10}cm^3s^{-1}$	(21)
$Br+BrN_3 \rightarrow Br_2+N_3$	$k=3.0X10^{-11}cm^3s^{-1}$	(22)
$N+N_3 \rightarrow N_2(B)+N_2$	$k=1.4X10^{-10}cm^3s^{-1}$	(23)
$N_2(B) \rightarrow N_2(A)+h\nu$	$k=1.6X10^{5}s^{-1}$	(24)
$Br+N_3 \rightarrow NBr\ (a,b)+N_2$	$k=8.0X10^{-12}cm^3s^{-1}$	(25)
$N_2(A)+N \rightarrow N_2(X)+N$	$k=3.0X10^{-11}cm^3s^{-1}$	(26)
$M+N_3 \rightarrow$ Products	k=Variable	(27)

These processes describe a chain carried by $N_2(A)$ metastables, Br atoms, N atoms, and N_3 radicals. In order to gauge the adequacy of the model, calculations were performed in which the coupled differential equations corresponding to reactions (20 through (27) were numerically integrated by using a fourth-order Runge-Kutta routine. The results of these calculations are shown as broken lines in Figures 19 and 21, experimental time profiles for $N_2(A)$ quenching by BrN_3 and N_2 emission from BrN_3+ active nitrogen. The agreement with the $N_2(A)$ quenching data is reasonably good,

with the calculations showing both the pseudo-first order and "chain" components of the decay. The model clearly fails to predict the time behavior of the BrN_3/active nitrogen system, however. The chain processes described by the model are far too slow to account for the rapid rise of the first positive emission found in these experiments. It still seems quite probable, however, that the excited nitrogen in the system is produced by $N+N_3$. This could be the case if there were a mechanism operative which rapidly produced bromine atoms, such that N_3 would be generated by $Br+BrN_3$. The azide radicals would then rapidly react with the large excess of N atoms in the flow to generate $N_2(B)$. Although our VUV resonance fluorescence experiments showed $N+BrN_3$ and $N+Br_2$ to be slow, recall that the emission from excited bromine atoms suggested the occurrence of a more rapid process. Such a process, for example, interaction of Br_2 or BrN_3 with highly vibrationally excited N_2, could lead to the production of bromine atoms on the required time scale.

The model may be applied to consideration of the N_2 first positive emission observed previously from the pulsed photodissociation of BrN_3.[1] The experiments suggested a rate constant for $N_2(A)$ quenching by BrN_3 of $1.2X10^{-12}cm^3s^{-1}$, about 58 times smaller than the value determined in the experiments described above. In the pulsed experiments, a KrCl laser (222nm) was used to photolyze a flow containing BrN_3 at densities between 10^{15} and $10^{16}cm^{-3}$. About 4% of the azide was dissociated by each pulse. No NBr $b \rightarrow X$ emission was found subsequent to the photolysis pulse, but evidence for the production of $N_2(A)$ as an initial photoproduct was obtained. Hence, the chemistry of the system may be described by eqns. (20)-(24) above. For a BrN_3 density of $5X10^{15}cm^{-3}$, the initial $N_2(A)$ photoproduct would be quenched by BrN_3 in about 3 μs, producing Br atoms

and N atoms. Br atoms would also be produced by $N_2(A)$ collisions with any Br_2 present. The Br atoms would be removed by the parent BrN_3 in about 6 μs, producing N_3 radicals. These radicals could then react with N atoms according to reaction (23) to produce $N_2(B)$. Since reactions (20), (21), and (22) occur rapidly, the initial densities of the products N and N_3 are given approximately by the initial density of $N_2(A)$ produced by the photodissociation. In practice, N atoms are likely to be in large excess over N_3 because of the fragility of the azide radicals. Hence, subsequent production of $N_2(B)$ by $N+N_3$ would appear to be pseudo-first order as was observed. For an $N_2(A)$ quantum yield of, say, 10%, the N_3 density would be $2X10^{13}cm^{-3}$ such that the time constant of the subsequent $N+N_3$ reaction would be 350 μs, on the order of the N_2 first positive decay time observed in the pulsed experiments. In fact, the apparent rate constant inferred for $N_2(A)$ quenching by BrN_3 in the pulsed experiments ($1.2X10^{-12}cm^3s^{-1}$) can be used to estimate the photodissociation quantum yield for $N_2(A)$, assuming that one $N_2(A)$ metastable produces one N atom. The $N_2(A)$ quantum yield is given by

$$\Phi = \left(\frac{1.2X10^{-12}}{k_{23}}\right)\left(\frac{100\%}{0.04}\right) = 21\% \qquad (28)$$

This yield is close to that observed by Benard and co-workers[6] from the photolysis of FN_3 at 193nm. It is much higher than the yield of $N_2(A)$ from 193nm photolysis[5] of ClN_3, but then no visible N_2 first positive emission was observed in that case.

V. Azide Chemistry for the Production ofExcited IF($B^3\Pi_o^+$).

Recent work performed in our laboratory [12,13] has shown that $N_2(A^3\Sigma_u^+)$ metastables are produced rapidly and efficiently by the reaction of N atoms with N_3 radicals:

$$N(^4S_u)+N_3(^2\Pi_g) \rightarrow N_2(B^3\Pi_g)+N_2(X^1\Sigma_g^+) \quad (29)$$

$$N_2(B^3\Pi_g) \rightarrow N_2(A^3\Sigma_u^+) + h\nu \quad (30)$$

The radiative process (30) occurs at a rate $1.6X10^5 s^{-1}$, such that the overall rate of production of $N_2(A)$ is typically limited by the rate of reaction (29), which has a rate constant[13] $k=1.4\pm0.4X10^{-10}$ cm^3s^{-1}. Within the last two years, considerable interest has been directed toward the use of $N_2(A)$ metastables in pumping IF, NO, or other laser candidate molecules to excited electronic states. For example, Piper and co-workers[61] have found that the process

$$N_2(A) + IF(X) \rightarrow N_2(X) + IF(B^3\Pi_o^+) \quad (31)$$

occurs with a rate constant near $1.0X10^{-10}$ cm^3s^{-1}. The rate constant for overall quenching of $N_2(A)$ by IF is $2.0X10^{-10}$ cm^3s^{-1}. IF is a molecule which has spectroscopic characteristics appropriate for supporting lasing in the visible, as has been shown by the demonstration of both pulsed[62] and CW[63] optically pumped lasers operating on the $B^3\Pi_o^+ \rightarrow X^1\Sigma^+$ transition of this species.

The work described in this section was directed toward the coupling of the chemical production of $N_2(A)$ metastables by reactions (29) and (30) above to the collisional pumping of IF to its B state as in (81) above. This work was supported in part by this AFOSR grant and in part by contract No. AFWL - F29601-84-C-0094 with the Air Force Weapons Laboratory.

Chemical Production of IF($B^3\Pi_{0^+}$)

In principle, the chemical pumping of IF(B) can be accomplished since both N_3 radicals and IF are typically produced by reactions of fluorine atoms. Azide radicals have been produced[16] by the rapid reaction of F atoms with HN_3:

$$F+HN_3 \rightarrow HF(v \geq 5)+N_3 \qquad (32)$$

This process has a rate constant[12] $k=1.6\pm0.4X10^{-10}$ cm^3s^{-1}. IF can be produced by the reaction of F atoms with CF_3I:

$$F+CF_3I \rightarrow CF_3+IF \qquad (33)$$

Reaction (33) has a rate constant reported to be $k=1.6X10^{-10}$ cm^3s^{-1}. Hence, excited IF should be produced by mixing F atoms, N atoms, HN_3, and CF_3I in a continuous flow.

Continuous flow experiments were performed by using a standard discharge-flow apparatus. The flow reactor was fabricated from 3.5 cm i.d. teflon pipe, and had one sidearm equipped with a 100W microwave discharge. Two reagent inlets made from 0.6 cm o.d. teflon tubing entered the reactor at one end and could be independently moved along its axis. One of these inlets was used to admit gases which had passed through a second microwave discharge. The reactor had a single observation port located 50cm downstream of the sidearm.

In order to generate the chemical system described above, HN_3 and CF_3I must be admitted to a medium containing both nitrogen and fluorine atoms. In these experiments, the F atoms were produced by passage of either CF_4/Ar or F_2/Ar mixtures through the microwave discharge located on the sidearm of the reactor. N atoms were produced by passage of N_2/Ar through the discharge located on the movable inlet. The F and N atom densities were determined by standard chemiluminescent titrations, and were both typically

on the order of 10^{13} cm^{-3}. Under these conditions, the familiar yellow-orange N_2 afterglow was readily visible downstream of the N atom orifice. Admission of HN_3 to this flow via the other movable injector produced a bright orange N_2 first positive flame about two orders of magnitude more intense than the nitrogen afterglow. This behavior has been observed before[12] and is indicative of the occurrence of reactions (32), (29), and (30) above.

In order to generate IF, a metered flow of CF_3I was pre-mixed with the HN_3 flow such that both species entered to the F/N/Ar stream through the same inlet. The initial density of CF_3I was on the order of $10^{13}cm^{-3}$. The addition of CF_3I dramatically changed the visual appearance of the flame, from orange to yellow-green. The spectrum of the yellow-green flame is shown in Figure 23, and is readily identified as bands of the IF B→ X transition. Although some N_2 first positive emission is still evident at longer wavelengths, the intensity of the individual IF bands is much greater than that of the N_2 features. By comparison of the total intensity of the IF emission (integrated from the recorded spectrum) to the total intensity of the nitrogen first positive emission with no CF_3I flow, it was determined that the total IF B →X intensity was ≈25% of the original N_2 intensity. The N_2 intensity was corrected for the portion emitted in the infrared beyond the cutoff of the detection system (about 50% of the total). In view of the possibility of the efficient loss of $N_2(A)$ by collisions with other species and the reactor walls, this substantial fraction testifies to the efficiency of the $N_2(A)$-IF energy transfer process in this system.

The azide-IF reaction mechanism can be initiated by the introduction of fluorine atoms into a system containing HN_3, CF_3I, and N atoms. since

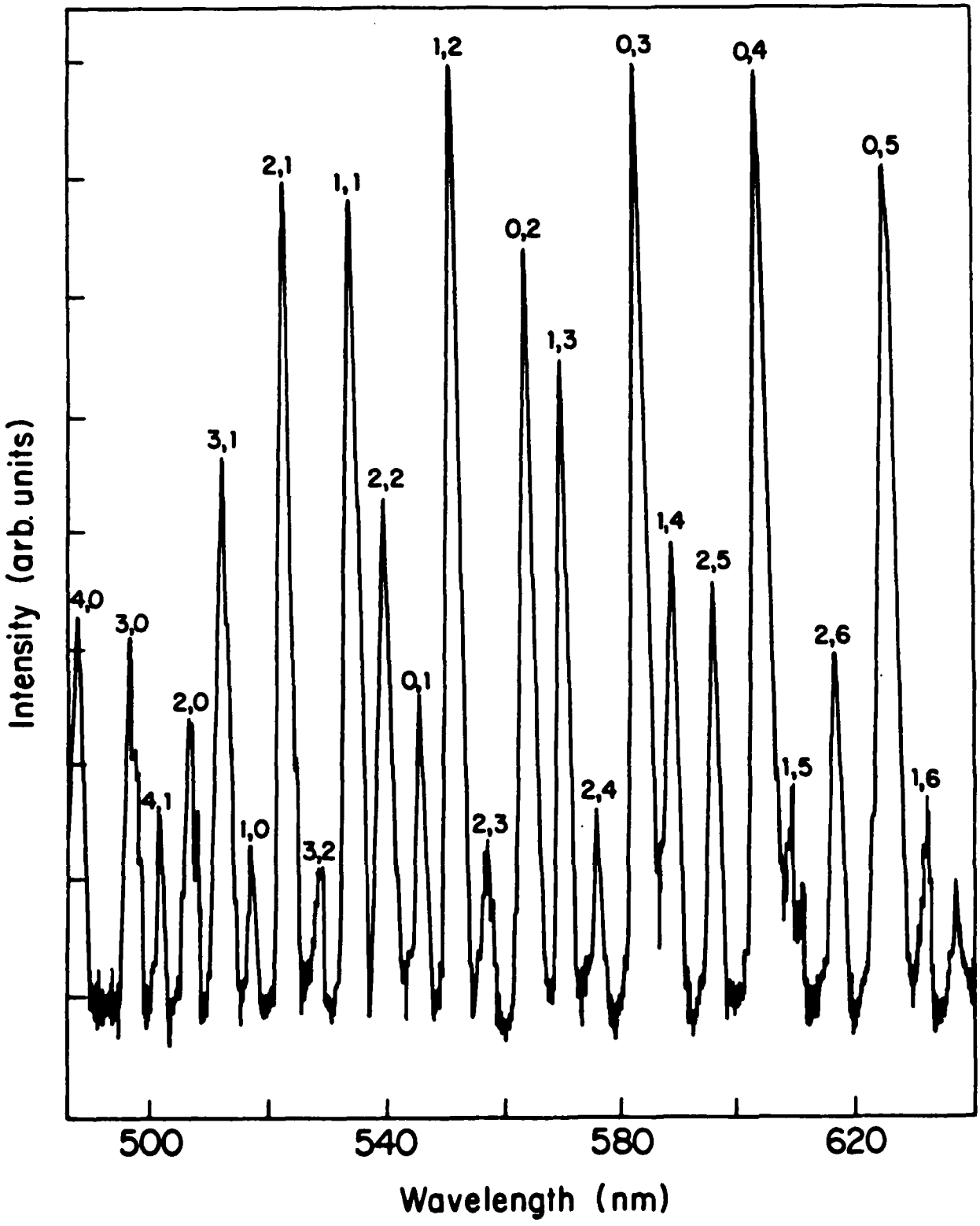

Figure 23. Chemiluminescence generated by admission of HN_3 and CF_3I to a stream of F and N atoms. IF B→X bands are labeled.

the latter three species can be pre-mixed without appreciable reaction, the mechanism can be operated in a pulse by inclusion of an inert species from which F atoms can be generated by some pulsed means such as photolysis. Both CF_3I and HN_3 are strong absorbers in the UV, such that UV photolysis of a fluorinated species would likely lead to complex chemistry. In order to avoid this complexity, infrared multi-photon dissociation of SF_6 was used to produce fluorine atoms in the present experiments. SF_6 is an effectively inert species which does not react with CF_3I, HN_3, or N atoms, and it is also a very inefficient quencher of IF(B).[61] Neither HN_3 nor CF_3I have appreciable absorptions[65,66] at 10.6 μm, the frequency used to dissociate SF_6. The CO_2 laser used to produce the 10.6 μm pulse in the present experiments was a Lumonics 103 which routinely delivered ~8J in an area of ~10 cm^2. The laser beam was focussed into the center of a flow reactor through which a stream containing N, CF_3I, HN_3, and Ar was passed. The reactor ends were closed with KCl windows to prevent transmission of the laser beam. Photolysis of a flowing mixture including SF_6, HN_3, and N atoms at densities $5X10^{14}$, $1X10^{14}$, and $7X10^{13}$ cm^{-3}, respectively, at a total pressure of 1.8 Torr produced a bright orange flame readily visible to the eye. The flame was produced along the entire pathlength of the laser beam in the reactor, although the fluence was <3 J cm^{-2} over most of the path. The spectrum of this pulsed emission is shown in Figure 24, and is readily identified as bands of the N_2 first positive transition. The intensity distribution among the bands is quite similar to that observed from the continuous $N+N_3$ flame,[12] as expected. A much less intense pulse of N_2 first positive emission was produced by pulsed photolysis of mixtures including SF_6 and N atoms only, i.e., when <u>no</u> HN_3 was present. This phenomenon appears to be similar to that observed in discharge-flow

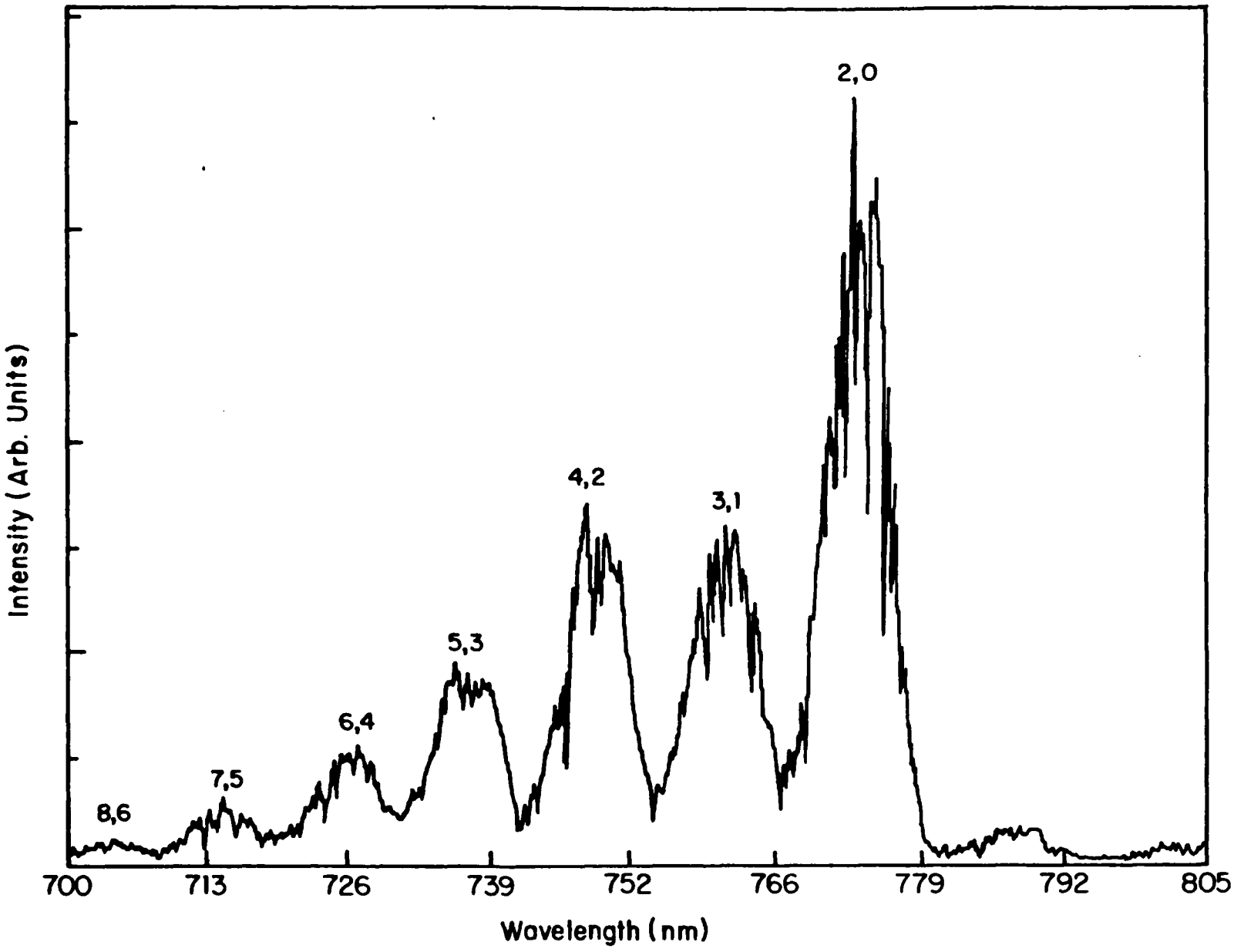

Figure 24. N_2 B→A emission from pulsed 10.6μm photolysis of $SF_6/HN_3/N$.

experiments, where addition of F atoms to a stream of "active nitrogen" was found to substantially enhance the visible emission from the nitrogen afterglow.

The time profile of the pulsed N_2 emission exhibited a rise to a peak over a fraction of a ms followed by a slower decay over about 2ms. A typical time profile is shown in Figure 25a. In principle, the rise and decay of the emission should reflect the rates of the $N+N_3$ and $F+HN_3$ reactions, or vice versa. From the initial densities of N atoms and HN_3 ($5X10^{13}$ and $7X10^{13}$, respectively) and the known rate constants[12,13] for these reactions (both of which exceed $10^{-10}cm^3s^{-1}$), both the rise and the decay time of the emission should be much shorter than 1 ms. The slow decay evident in Figure 25a indicates that the density of one of these reagents has been substantially reduced in the flow stream prior to the photolysis. The most likely scenario is loss of HN_3 in the active nitrogen flow, such that its actual density is much less than that calculated from the measured flow rates. Further support for this contention was found from the observation that the intensity of the emission was sensitive to the flow rates of both HN_3 and SF_6 but was insensitive to the N_2 flow through the microwave. Hence, N atoms are indeed present in large excess (i.e., the intensity is limited by the rate of production of N_3 rather than by competition of $N+N_3$ with other N_3 loss routes). Consequently, the rise of the emission in Figure 25a is identified as the $N+N_3$ rate, the decay as the $F+HN_3$ rate. Figure 25b shows a time profile measured with a much greater flow of SF_6. Clearly, the decay of the emission is much more rapid, in accord with this model. The rise rate also increased somewhat, probably because of more efficient production of N atoms in the discharge at the higher pressure.

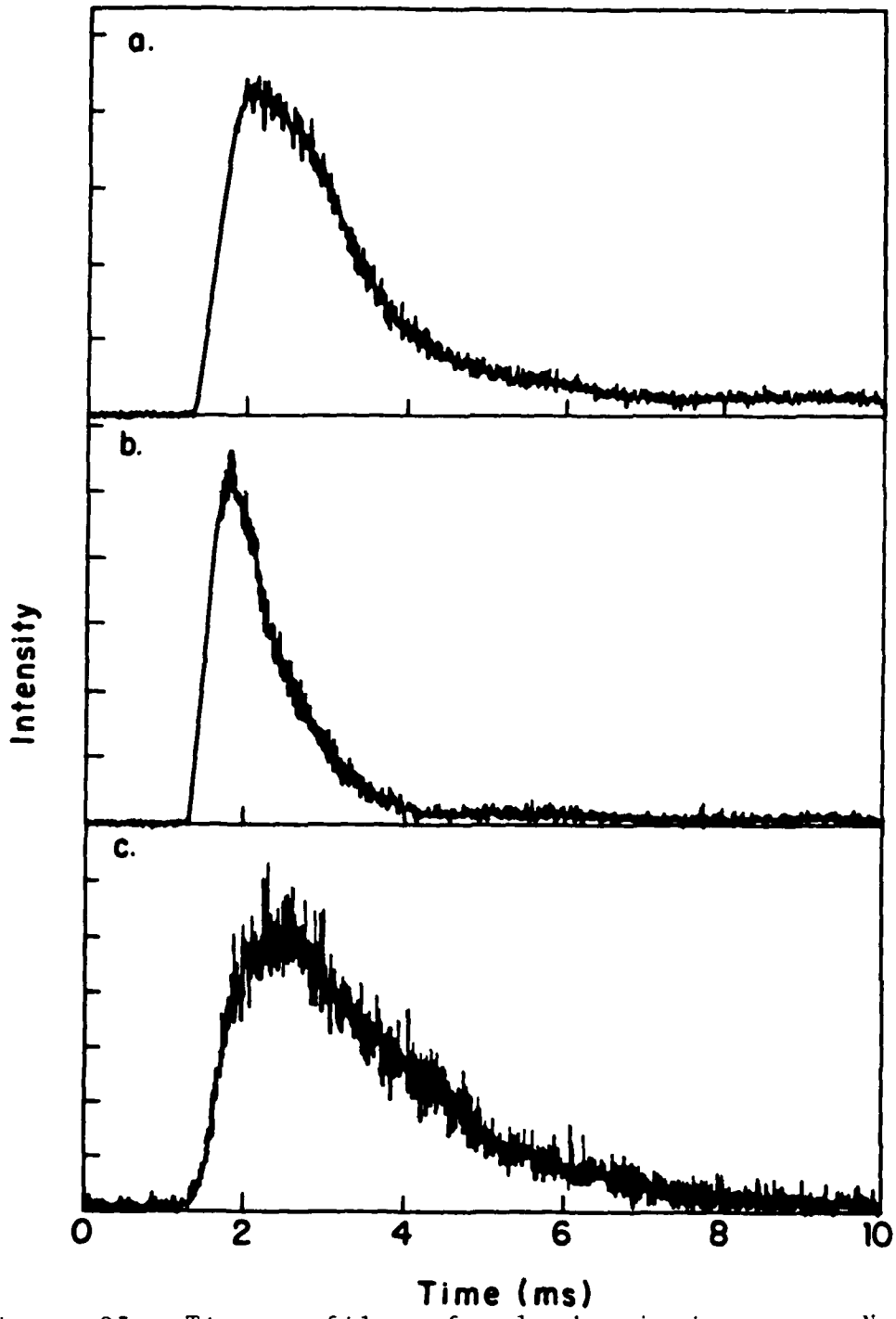

Figure 25. Time profiles of pulsed emissions. a. N_2 B→A emission from photolysis of $SF_6/HN_3/N$. b. N_2 emission as in (a), with added SF_6. c. IF B→X emission from photolysis of $SF_6/HN_3/N/CF_3I$.

Addition of CF_3I to the $SF_6/N/HN_3$ stream produced a marked change in the pulsed emission. The orange N_2 flame was replaced by a yellow-green emission, which extended for 10 to 15cm on either side of the focus of the laser beam. The spectrum of this emission is shown in Figure 26. The major features are readily identified as IF B X bands, as indicated in the figure. Some N_2 first positive emission was apparent at longer wavelengths. When compared to the spectrum of continuous emission shown in Figure 23, it would appear that the pulsed IF emission is vibrationally colder, with most of the intensity in bands from v'=0 or v'=1. This result suggests the influence of collisional relaxation of IF(B) in the pulsed system, which was operated at a higher pressure (a considerable fraction of which was SF_6). The time profile of the IF emission is shown in Figure 25c. As expected, it follows the general pattern of th N_2 emission (Fig. 25a) but has a somewhat slower rise, since the production of IF is limited not by the $N+N_3$ rate, but by the rate of $N_2(A)$-IF energy transfer.

These results serve to demonstrate the ready coupling of the azide mechanism for production of N_2 metastables to the IF B X system, and clearly indicate the potential utility of this system as a pulsed or cw chemical laser.

Interaction of Trifluorohalomethanes with Active Nitrogen

During the course of the experiments described above, a number of interesting observations regarding the interaction of CF_3I with active nitrogen were made. These observations led us to investigate similar interactions of CF_3Br and CF_3Cl with active nitrogen, and to measure rate constants for $N_2(A)$ quenching by these species.

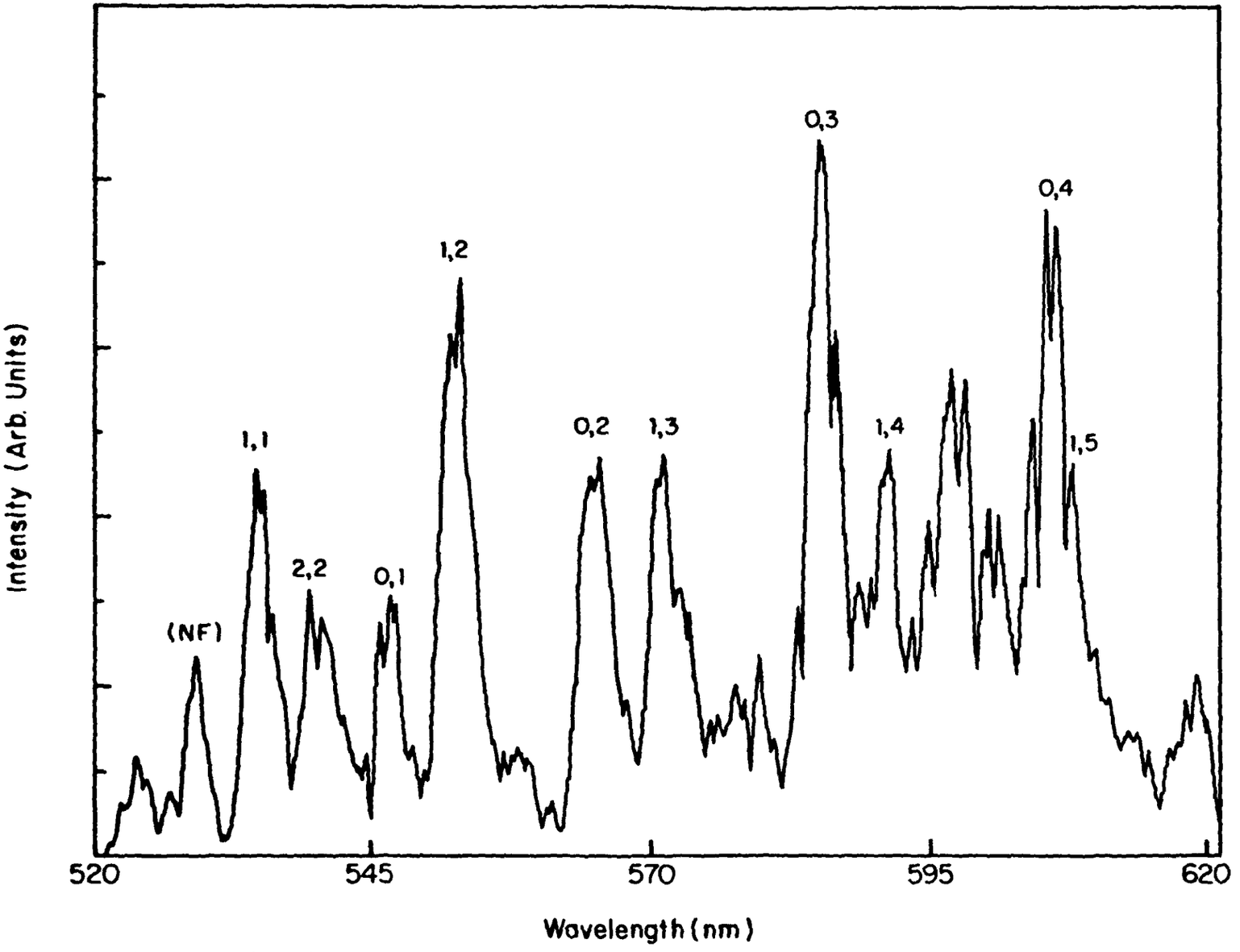

Figure 26. Spectrum of emission from pulsed 10.6μm photolysis of $SF_6/HN_3/N/CF_3I$. IF B→X bands are indicated.

Admission of a small flow of CF_3I to a flow of active nitrogen produced a bright yellow-green flame which extended down the full length of the flow reactor and into the pumping system. The spectrum of this flame is shown in Figure 27. All of the banded features shown in the spectrum are attributable to the $B^3\pi_o^+ \rightarrow X^1\Sigma^+$ transition in IF. Emissions from vibrational levels as high as v'=4 of the IF(B) state are evident. In view of the efficiency with which IF is pumped to its $B^3\Pi_o^+$ state by collisions with $N_2(A)$ metastables, it is expected that this is the primary excitation mechanism operative in the system. Indeed, the slow production of $N_2(A)$ by N atom recombination in the active nitrogen flow would account in part for the very long duration of the IF flame. Since IF disproportionates rapidly on the pyrex walls of the flow reactor, however, it seems likely that it too must be continually produced during the time period of the flame. The primary issue is the mechanism by which IF is originally formed in the flow; presumably this mechanism involves interaction of CF_3I with excited species present in the active nitrogen. At least two collisional dissociation mechanisms are energetically feasible:

A	$N_2^* + CF_3I \rightarrow N_2(X) + CF_2 + I + F$	(34)
	$F + CF_3I \rightarrow CF_3 + IF$	(33)
	$IF + N_2^*(A) \rightarrow IF^*(B) + N_2(X)$	(31)
B	$N_2^* + CF_3I \rightarrow N_2(X) + CF_2 + IF(X)$	(35)
	$IF(X) + N_2^*(A) \rightarrow IF^*(B) + N_2(X)$	(31)

where N_2^* represents a metastable excited species. The rate constants for reactions (33) and (31) are $1.6X10^{-10}$ and $1.0X10^{-10}$ cm^3s^{-1}, respectively. Mechanism B, in which IF is produced by collisional dissociation of CF_3I, was eliminated by an experiment in which H_2 was added to the flow to

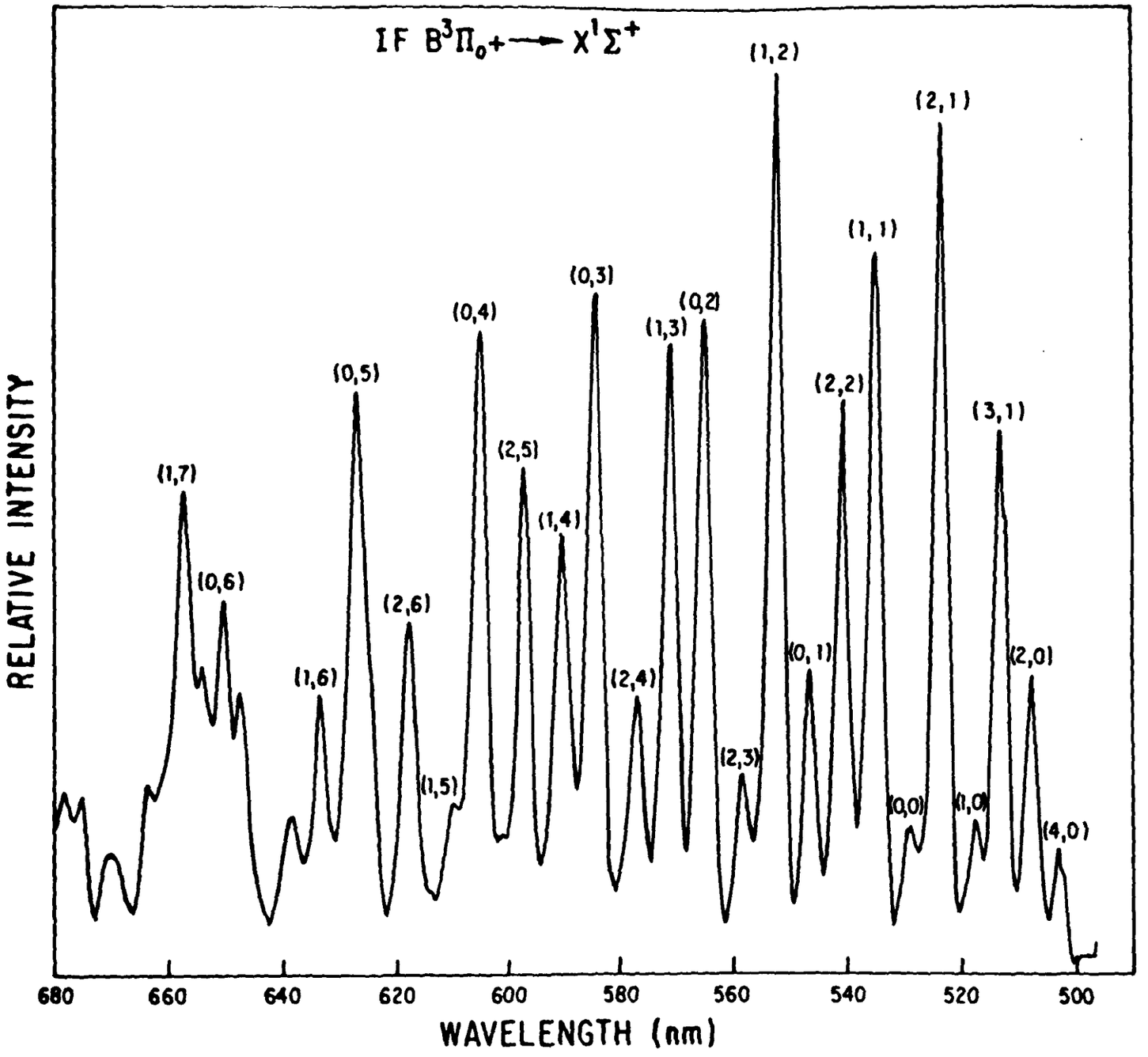

Figure 27. IF B→X emission produced by admission of CF_3I to active N_2.

scavenge fluorine atoms. Admission of a flow of H_2 corresponding to a density of $5X10^{13}$ cm^{-3} effectively titrated the IF flame, suggesting that this density of fluorine atoms is eventually produced by the dissociation of CF_3I (at an initial density of $2.5X10^{14}$ cm^{-3}) via mechanism A above. Hence, it would appear that the dissociation to fluorine atoms (reacton (34)) is a reasonably efficient process.

The choice of N_2 metastables (produced by N atom recombination) as the energy carrier responsible for the dissociation of CF_3I is based largely on the very long duration of the flame, which argues against the action of excited species created in the microwave discharge (e.g., $N(^2D)$ atoms). This point was specifically tested by an experiment in which a glass wool plug was inserted in the flow reactor downstream of the discharge zone, but upstream of the CF_3I injector. The plug, which should effectively remove $N(^2D)$ from the flow, had no observable effect on the production of the IF flame when CF_3I was admitted to the system.

It is well known that photolysis of CF_3I in the continium near 260nm produces CF_3 radicals and excited $I(5^2P_{1/2})$ atoms.[67] It is also known, however, that CF_3I photolysis in the region between 160 and 180nm where the molecule has diffuse banded absorptions produces fluorine atoms.[68] Hence, the present data suggest that reaction (34) may result from excitation of CF_3I to these same pre-dissociated states (C and D) by collisions with N_2* metastables. From the energies of these states (164 kcal $mole^{-1}$ for C and 179 kcal $mole^{-1}$ for D), they cannot be accessed directly by collisions with vibrationally cold $N_2(A^3\Sigma_u^+)$ metastables. Hence, the energy carrier must be another metastable state produced by N atom recombination. Since CF_3I was present in the flow at densities on the order of $10^{14}cm^{-3}$, and the dissociation was reasonably efficient, we infer that the lifetime of the

metastable energy carrier must be at least 100 μs. A number of excited states of N_2 satisfy both of these energy and lifetime criteria.

The admission of a flow of CF_3Br to a stream of active nitrogen produced a markedly different result. A bright red flame was generated in the mixing zone, extending for ~5ms downstream. Figure 28 shows a spectrum of this emission, which is readily identified as NBr $b^1\Sigma^+ \rightarrow X^3\Sigma^-$ transitions. Downstream of the red emission, a dull yellow flame was found, extending down the length of the reactor. The spectrum of this emission exhibited a regular series of bands, identified as the $A^2\Pi \rightarrow X^2\Sigma^+$ transition in CN.

These results for CF_3Br suggest a mechanism quite different from that postulated for the CF_3I case. In view of the short duration of the NBr $b \rightarrow X$ emission downstream of the discharge, an experiment with a glass wool plug (analogous to that described above) was performed to ascertain the role of short-lived discharge products. With the plug in place, the NBr emission was completely quenched. This behavior suggests the following reaction as the source of excited NBr:

$$N(^2D) + CF_3Br \rightarrow NBr(b^1\Sigma^+) + CF_3 \qquad (36)$$

This reaction is feasible both energetically and from the point of view of angular momentum correlations, as $NBr(b^1\Sigma^+)$ correlates adiabatically to $N(^2D) + Br(^2P)$. The absence of NI $b \rightarrow X$ emission when CF_3I was added to active nitorgen, along with the observation that the glass wool plug had no effect, argues that a reaction analogous to (36) is not important in that system. CN emission has been observed from the addition of several different kinds of halomethanes to active nitrogen.[69,70] The mechanism in such cases is thought to involve initial formation of CN by reaction of

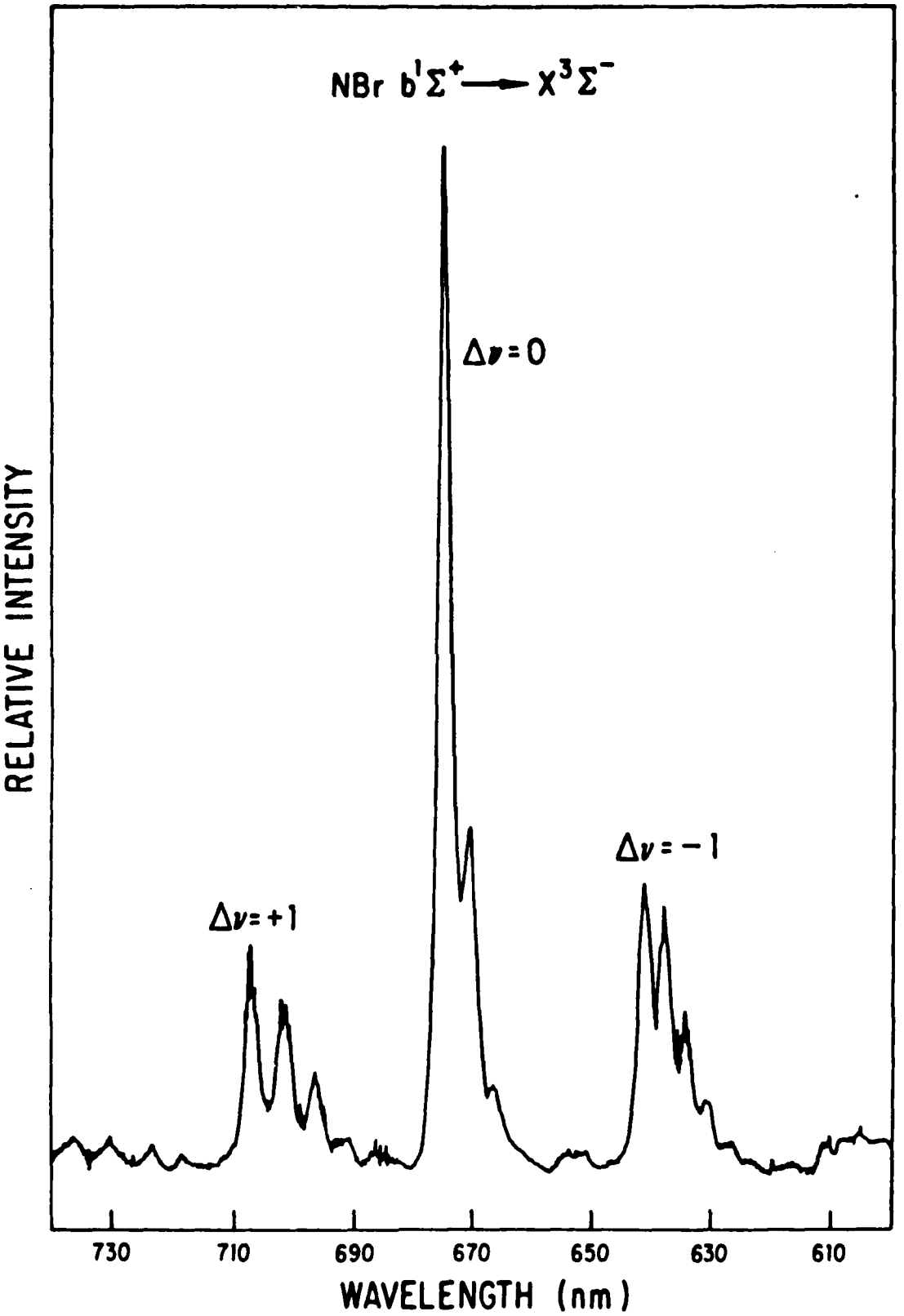

Figure 28. NBr b→X emission produced by admission of CF_3Br to active nitrogen.

$N(^2D)$ atoms with halomethyl or halomethylene radicals, followed by excitation to the $A^2\Pi$ state by collisions with N_2 metastables.

Admission of a flow of CF_3Cl to active nitrogen produced no new emission, nor did it perceptibly diminish the visible emission from the N_2 afterglow.

As a second part of this work, rate constants were determined for the quenching of $N_2(A^3\Sigma_u^+)$ metastables by collisions with CF_3I, CF_3Br, and CF_3Cl. For this purpose, $N_2(A)$ metastables were produced by energy transfer from $Ar(^3P_{0,2})$ and were detected by energy transfer to NO as described above. For CF_3I and CF_3Br, the decay of the $N_2(A)$ density was measured as a function of time for a number of different pseudo-first order densities of these quenchers. Rate constants were determined from the slopes of plots of decay rate vs. density. Quenching by CF_3Cl was found to be so slow as to preclude measurements of actual time decays, so the quenching rate constant was determined by using the "fixed point method" wherein the decline in the $N_2(A)$ density was measured for a single time interval Δt, for large flows of added CF_3Cl. Table V shows the measured quenching rates along with the literature values for quenching by CF_4 and CF_3I. CF_3Cl likely behaves much like CF_4; i.e., it acts only as a vibrational quencher of $N_2(A, v)$. The rate constants for quenching by CF_3I and CF_3Br are orders of magnitude greater than those for quenching by CF_3Cl and CF_4, indicating the accessibility of new channels for the energy transfer process. Given the discussion above, these channels are not likely to be those which produce fluorine atoms, but rather may be those which lead to dissociation to iodine or bromine atoms, respectively. No emission from IF, NBr, or CN was detected in the quenching experiments. Clark and Setser[71] have measured rate constants for $N_2(A)$ quenching by CH_3X

species (X=halogen). These values are approximately four times greater than those from the present work shown in Table V. The relative values of rate constants within the two series CH_3X and CF_3X are quite similar, however, suggesting analogous mechanisms.

Table V. $N_2(A^3\Sigma_u^+)$ Quenching by Trifluorohalomethanes

Quencher	Rate Constant (cm^3S^{-1})	Reference
CF_3I	$1.2 \pm 0.2 \times 10^{-10}$ 2.0×10^{-10}	This work (23)
CF_3Br	$5.0 \pm 0.8 \times 10^{-11}$	This work
CF_3Cl	5×10^{-14}	This work
CF_4	3×19^{-13}	(23)

VI. Publications Arising From This Program

1. R.D. Coombe and M.H. Van Benthem, "Radiative Rates of Singlet-Triplet Transitions in Nitrogen Halide Diatomics", J. Chem. Phys., 81, 2984 (1984).

2. D.D. Bell and R.D. Coombe, "Photodissociation of Chlorine Isocyanate", J. Chem. Phys., 82, 1317 (1985).

3. R.D. coombe, S.J. David, T.L. Henshaw, and D.J. May, "Generation and Quenching of $N_2(A)^3\Sigma_u^+$) in the Photodissociation of ClN_3", Chem. Phys. Lett., 120, 433 (1985).

4. M.A. MacDonald, S.J. David, and R.D. Coombe, "Radiative and Collisional Decay of NBr($b^1\Sigma^+$,v')", J. Chem. Phys., 84, 5513 (1986).

5. T.L. Henshaw, S.J. David, M.A. MacDonald, J.V. Gilbert, D.H. Stedman, and R.D. Coombe, "Collisional Decomposition of Bromine Azide", J. Phys. Chem., in press (1987).

6. J.V. Gilbert, X. Wu, D.H. Stedman, and R.D. Coombe, "Photolysis of Nitrogen Trichloride", J. Phys. Chem., in press (1987).

7. S.J. David, A.P. Ongstad, M.A. MacDonald, and R.D. Coombe, "Chemical Generation of Excited IF($B^3\Pi_{0+}$)", Chem. Phys. Lett., in press (1987).

8. A.P. Ongstad, S.J. David, and R.D. Coombe, "Interaction of Trifluorohalomethanes with Active Nitrogen", Chem. Phys. Lett., in press (1987).

9. X. Liu, J.V. Gilbert, and R.D. Coombe, "Photodissociation of Bromine Isocyanate", in preparation for submission to J. Phys. Chem.

VII. Personnel

Principal Investigator:	Robert D. Coombe
Senior Research Personnel (Faculty and post-doctoral research associates):	Donald H. Stedman Shelle J. David* Michael A. MacDonald** Andrew P. Ongstad Julanna V. Gilbert
Graduate Research Assistants:	Donald J. May‡ Thomas L. Henshaw‡‡ Xu Liu Xian-Liang Wu Debe D. Bell

* Present address: Los Alamos National Laboratory
Los Alamos, NM

** Present Address: Department of Chemistry
University of Edinborough
Edinborough, Scotland, U.K.

‡ M.S. to be awarded, August 1987

‡‡ Ph.D. to be awarded, August 1987

VIII. REFERENCES

1. R.D.Coombe, J. Chem. Phys., 79, 254 (1983).

2. R.D. Coombe and C.H.-T. Lam, J. Chem. Phys., 79, 3746 (1983).

3. T.C. Clark and M.A.A. Clyne, Trans. Faraday Soc., 66, 877 (1970).

4. R.D. Coombe, D. Patel, A.T. Pritt, Jr., and F.J. Wodarczyk, J. Chem. Phys., 75, 2177 (1981).

5. R.D. Coombe, S.J. David, T.L. Henshaw, and D.J. May, Chem. Phys. Lett., 120, 433 (1985).

6. D. Patel, A.T. Pritt, Jr., and D.J. Benard, J. Phys. Chem., 90, 1931 (1986).

7. M.A. MacDonald, S.J. David, and R.D. Coombe, J. Chem. Phys., 84, 5513 (1986).

8. A.T. Pritt, Jr., D.Patel, and R.D. Coombe, J. Chem. Phys., 75, 5720 (1981).

9. R.D. Coombe and M.H. Van Benthem, J. Chem. Phys., 81, 2984 (1984).

10. W.D. Woolley and R.A. Back, Can. J. Chem., 46, 295 (1968).

11. D.D. Bell and R.D. Coombe, J. Chem. Phys., 82, 1317 (1985).

12. S.J. David and R.D. Coombe, J. Phys. Chem., 89, 5206 (1985).

13. S.J. David and R.D. Coombe, J. Phys. Chem., 90, 3260 (1986).

14. R.D. Coombe and co-workers; unpublished data.

15. L.G. Piper, R.H. Krech, and R.L. Taylor, J. Chem. Phys., 71, 2099 (1979).

16. R.D. Coombe and A.T. Pritt, Jr., Chem. Phys. Lett., 58, 606 (1978).

17. T.L. Henshaw, M.A. MacDonald, D.H. Stedman, and R.D. Coombe, J. Phys. Chem., in press (1987).

18. J.L. Jourdain, G. Le Bras, G. Poulet, and J. Combourieu, Combust. Flame, 34, 13 (1979).

19. A.T. Pritt, Jr., D. Patel, and R.D. Coombe, Int. J. Chem. Kinetics, 16, 977 (1984).

20. T.L. Henshaw, S.J. David, M.A. MacDonald, J.V. Gilbert, D.H. Stedman, and R.D. Coombe, J. Phys. Chem., in press (1987).

21. See, for example, G.A. West and M.J. Berry, J. Chem. Phys., 61, 4700 (1974).

22. M.D. Burrows, S.L. Baughcum, and R.C. Oldenborg, Appl. Phys. Lett., 46, 22 (1985).

23. L.G. Piper, W.J. Marinelli, W.T. Rawlins, and B.D. Green, J. Chem. Phys., 83, 5602 (1985).

24. J.M. Herbelin and R.A. Klingberg, Int. J. Chem. Kinetics, 16, 849 (1984).

25. S.J. David, A. Ongstad, M.A. MacDonald, and R.D. Coombe, Chem. Phys. Lett., in press (1987).

26. H. Davy, Phil. Trans. Roy. Soc., 103, 1 (1813).

27. D.C. Frost, C.B. MacDonald, C.A. McDowell, and N.P.C. Westwood, Chem. Phys., 47, 111 (1980).

28. T.R. Charlton, T. Okamura, and B.A. Thrush, Chem. Phys. Lett., 89, 98 (1982).

29. K.H. Welge, J. Chem. Phys., 45, 166 (1966); J.M. Herbelin and N. Cohen, Chem. Phys. Lett., 20, 605 (1973); L.C.Lee and M. Suto, J. Chem. Phys., 80, 4718 (1984).

30. H. Okabe, J. Chem. Phys., 53, 2507 (1970).

31. B.J. Sullivan, G.P. Smith, and D.R. Crosley, Chem. Phys. Lett., 96, 307 (1983).

32. "Chemical Production of Excited Nitrogen Atoms for Short Wavelength Chemical Lasers", Hercules, Inc., Subcontract No. 9X25-X1451-5 with the Los Alamos National Laboratory.

33. T.C. Clark and M.A.A. Clyne, Trans. Faraday Soc., 66, 372, (1970).

34. A.D. Walsh and P.A.Wassop, Trans. Faraday Soc., 57, 345 (1961).

35. T.A. Gregory and S. Lipsky, J. Chem. Phys., 65, 5469 (1976).

36. J. Jander and U. Englehardt, in "Developments in Inorganic Chemistry", Vol. 2, C.B. Colburn, Ed.

37. P.H. Tennyson, A. Fontijn, and M.A.A. Clyne, Chem. Phys., 62, 171 (1981).

38. R.J. Malins and D.W. Setser, J. Phys. Chem., 85, 1342 (1981).

39. J.C. Miller and L.Andrews, J. Chem. Phys., 71, 5276 (1979)

40. A.C. Becker, J. Langen, H.M. Oberhoffer, and U. Schurath, J. Chem. Phys., 84, 2907 (1986).

41. J.C. Miller, J.S. Meek, and S.J. Strickler, J. Amer. Chem. Soc., 99, 8175 (1977).

42. A.E. Douglas and W.E. Jones, Can. J. Phys., 44, 2251 (1966).

43. R. Colin and W.E. Jones, Can. J. Phys., 45, 301 (1967).

44. E.R.V. Milton, H.B. Dunford, and A.E. Douglas, J. Chem. Phys., 35, 1202 (1961).

45. A.T. Pritt, Jr., D. Patel, and R.D. Coombe, J. Mol. Spectrosc., 87, 401 (1981).

46. J.K.G. Watson, Can. J. Phys., 46, 1637 (1968).

47. D.R. Yarkony, J. Chem. Phys., 86, 1642 (1987).

48. P.H Krupenie, J. Phys. Chem. Ref. Data, 1, 423 (1972).

49. W.H. Smith, J. Quant. Spectry. Rad. Trans., 9, 1191 (1969).

50. W.H. Smith and H.S. Liszt, J. Quant. Spectry. Rad. Trans., 11, 45 (1971).

51. R.F. Barrow and E.W. Deutsch, Proc. Phys. Soc. London, 82, 548 (1963).

52. M.A.A. Clyne and I.S. McDermid, J. Chem. Soc. Faraday Trans. 2, 75, 905 (1979).

53. K.A. Meyer and D.R. Crosley, J. Chem. Phys., 59, 3153 (1973); also, S.R. Leone and K.G. Kosnik, Appl. Phys. Lett., 30, 346 (1977).

54. A.E. Douglas and M. Frackowiak, Can. J. Phys., 40, 832 (1962).

55. R.N. Dixon, Can. J. Phys., 37, 1171 (1959).

56. F.D. Wayne and E.A.Colbourn, Mol. Phys., 34, 1141 (1977).

57. M. Bettendorff and S.D. Peyerimhoff, Chem. Phys., 99, 55 (1985).

58. L.G. Piper, R.H. Krech, and R.L. Taylor, U.S. DoE Report C00-4223-4; Physical Sciences Inc., Woburn, MA (1978).

59. D.-Z. Cao and D.W. Setser, to be submitted to J. Phys. Chem.

60. D.-Z. Cao and D.W. Setser, Chem. Phys. Lett., 116, 363 (1985).

61. L.G. Piper, W.J. Marinelli, W.T. Rawlins, and B.D. Green, J. Chem. Phys., 83, 5602 (1985).

62. S.J. Davis, L. Hanko, and R.F. Shea, J. Chem. Phys., 78, 172 (1983).

63. S.J. Davis, L. Hanko, and P.J. Wolf, J. Chem. Phys., 82, 4831 (1985).

64. R.S. Iyer and F.S. Rowland, J. Phys. Chem., 85, 2493 (1981).

65. A. Hartford, Jr., Chem. Phys. Lett., 57. 352 (1978).

66. Aa. S. Sudbo, P.A. Schulz, E.R. Grant, Y.R. Shen, and Y.T. Lee, J. Chem. Phys., 68, 1306 (1978).

67. L.H. Sutcliffe and A.D. Walsh, Trans. Faraday Soc., 57, 873 (1961).

68. M.J. Berry, Chem. Phys. Lett., 15, 269 (1972).

69. B.A. Thrush and M.F. Golde in Chemiluminescence and Bioluminescence (Plenum Press, New York, M.J. Cormier, D.M. Hercules, and J. Lee, eds., 1973).

70. V.Saez Rabanos, F. Tabares, and A. Gonzalez Urena, J. Photochem., 18, 301 (1982).

71. W.G. Clark and D.W. Setser, J. Phys. Chem., 84, 2225 (1980).

END

7-87

DTIC